UNIVERSIDADE DE COIMBRA

Faculdade de Ciências e Tecnologia

Departamento de Química

A theoretical study on the HSO_2 molecular system

Maikel Yusat Ballester Furones

COIMBRA
2008

UNIVERSIDADE DE COIMBRA

Faculdade de Ciências e Tecnologia

Departamento de Química

A theoretical study on the HSO_2 molecular system

Dissertation presented for fulfillment of the requirements for the degree of "Doutor em Ciências, especialidade em Química Teórica"

Maikel Yusat Ballester Furones

COIMBRA
2008

Acknowledgments

I would like to thanks my supervisor, Professor A. J. C. Varandas for give me the opportunity of carry my Ph. D. studies at the Coimbra Theoretical & Computational Chemistry group. Financial support, grant SFRH/BD/4777/2001 from Fundação para a Ciência e Tecnologia, Portugal is also acknowledge. All the work here reported and the presentation of results at International Conferences were also thanks to this support.

Abstract

A theoretical study on the HSO_2 molecular system is presented in this thesis: starting from the construction of a global potential energy surface for its ground electronic state, to dynamical studies of collisions taking place on it. The double many-body expansion (DMBE) method is employed in the construction of such six-dimensional function. The topology of the new surface is characterized in detail. A comparison between the properties of the stationary points obtained here with those reported in the literature is given, new structures are also characterized. Three bi-molecular reactions are then studied using quasi-classical trajectories method and the new potential. For the first time these reactions are studied in their full dimensionality. Main attributes of these molecular collisions are discussed and compared with available information in the literature.

Contents

Foreword

Sulfur has been known since the beginning of history. It occurs uncombined in nature, and it is a major global pollutant when oxidized to sulfur dioxide (SO_2). Sulfur compounds are used extensively in the modern industrialized world [1]. Hydrogen sulfide (H_2S) and organic sulfides are found in a variety of feed-stocks and crude oil. Other anthropogenic sources of sulfur include: (i) industrial gas streams (ii) natural and refinery gases which contain sulfur as mercaptans (also named thiols: any organic compound containing the group SH bonded to a carbon atom like thiophene C_4H_4S) and carbonyl sulfide (COS); (iii) synthesis gases ($CO + H_2$) containing sulfur as COS and carbon disulphide (CS_2); and (iv) emissions from vehicle exhausts [1, 2].

There are also substantial natural reserves of sulfur, the most important of which are biogenic sources, sea spray and volcanoes. The biogenic sources originate from bacterial reduction of sediments to H_2S in the sea and release of dimethyl sulfide ($(CH_3)_2S$) from sea organisms. Volcanoes are the main natural source of SO_2 [1].

Other species found in the atmosphere include H_2S, $(CH_3)_2S$, dimethyl disulphide ($(CH_3)_2S_2$), COS and CS_2. H_2S, $(CH_3)_2S$ and $(CH_3)_2S_2$ are rapidly oxidized to SO_2, remaining only a few days in the atmosphere. COS and CS_2 are much longer lived species also found in the troposphere [3]. In the atmosphere, H_2S, COS and CS_2 react with hydroxide radicals to form mercapto radicals (HS) [3]:

$$OH + CS_2 \rightarrow COS + HS \quad (1)$$

$$OH + COS \rightarrow CO_2 + HS \quad (2)$$

$$OH + H_2S \rightarrow H_2O + HS \quad (3)$$

Hydroxyl (OH) radical comes into the atmosphere from different sources [2, 4, 5].

HS may also be formed by photo-dissociation of H_2S in the troposphere [3, 6]. Oxidation of HS radicals take place involving species such as hydroxysulfinyl[1] (HSO_2) [2, 3]. The latter is also associated to reactions taking place during combustion process [7, 8]. There, sulfur molecular systems act as oxidation inhibitors of the fuel. Properties of HSO_2 radicals have been reported in the literature [9–19], while chemical reactions, taking place on its ground state potential energy surface had also been studied [8, 9, 15, 18, 20–26].

In the literature however, a potential energy surface (PES) for the title system, describing all its possible configurations, has not been reported previously. To carry out molecular dynamics studies to get information on the mechanism and properties of the products at the same time, a global potential energy surface is needed [27, 28]. Being a tetratomic system with six internuclear distances, 33 electrons and also containing an element of the third row of the periodic table, *ab initio* calculations of the electronic energies are quite demanding.

The construction of such a PES for further use in modeling molecular collisions is the principal aim of this thesis.

This thesis is organized as follows: Part I deals with potential energy surfaces, presenting a theoretical background in chapter 1 and reporting a global PES of HSO_2 in chapter 2. Part II refers to molecular dynamics, with a theoretical introduction in chapter 3. Three reactions that have been studied using the new PES are presented in chapters 4, 5 and 6. Finally the main achievements are summarized and further possible applications are outlined.

Bibliography

[1] D. Stirling, *The sulfur problem. Cleaning up industrials feed-stockes.* (The Royal Society of Chemistry, 2000).

[2] G. W. vanLoon and S. J. Duffy, *Environmental Chemistry: A Global Perspective* (Oxford University Press, 2005), 2nd edn.

[3] R. P. Wayne, *Chemistry of Atmospheres* (Oxford University Press, 2002).

[1] named after the 2004 IUPAC recommendation

[4] T. Slanger, L. Jusinski, G. Black, and G. E. Gadd, Science **241**, 945 (1988).

[5] A. J. C. Varandas, J. Phys. Chem. A **107**, 3769 (2003).

[6] M.-T. Leu and R. H. Smith, J. Phys. Chem. **86**, 73 (1982).

[7] P. Glarborg, D. Kubel, K. Dam-Johansen, H.-M. Chiang, and J. W. Bozzelli, Int. J. Chem. Kinet. **28**, 773 (1996).

[8] M. U. Alzueta, R. Bilbao, and P. Glarborg, Combust. Flame **127**, 2234 (2001).

[9] A. Goumri, J.-D. R. Rocha, and P. Marshall, J. Phys. Chem. **99**, 10834 (1995).

[10] D. Binns and P. Marshall, J. Chem. Phys. **95**, 4940 (1991).

[11] V. R. Morris and W. M. Jackson, Chem. Phys. Lett. **223**, 445 (1994).

[12] D. Laakso, C. E. Smith, A. Goumri, J.-D. R. Rocha, and P. Marshall, Chem. Phys. Lett. **227**, 377 (1994).

[13] A. J. Frank, M. Sadílek, J. G. Ferrier, and F. Tureček, J. Am. Chem. Soc. **118**, 11321 (1996).

[14] J.-X. Qi, W.-Q. Deng, K.-L. Han, and G.-Z. He, J. Chem. Soc. Faraday Trans. **93**, 25 (1997).

[15] A. J. Frank, M. Sadílek, J. G. Ferrier, and F. Tureček, J. Am. Chem. Soc. **119**, 12343 (1997).

[16] E. Isoniemi, L. Kriadchtchev, J. Lundell, and M. Räsänen, J. Mol. Struct. **563-564**, 261 (2001).

[17] E. Isoniemi, L. Kriadchtchev, J. Lundell, and M. Räsänen, Phys. Chem. Chem. Phys. **4**, 1549 (2002).

[18] A. Goumri, J.-D. R. Rocha, D. Laakso, C. E. Smith, and P. Marshall, J. Phys. Chem. A **103**, 11328 (1999).

[19] P. A. Denis and O. N. Ventura, Chem. Phys. Lett. **344**, 221 (2001).

[20] S. M. Resende and F. R. Ornellas, Phys. Chem. Chem. Phys. **5**, 4617 (2003).

[21] R. W. Fair and B. A. Thrush, Trans. Faraday Soc. **65**, 1557 (1969).

[22] J. W. E. Wilson, Phys. Chem. Ref. Data. **1**, 535 (1972).

[23] K. Schofield, J. Phys. Chem. Ref. Data. **2**, 25 (1973).

[24] J. L. Jourdain, G. L. Bras, and J. Combourieu, Int. J. Chem Kinet. **11**, 569 (1979).

[25] M. A. Blitz, K. W. McKee, and M. J. Pilling, Proceedings of the Combustion Institute **28**, 2491 (2000).

[26] S. P. Sander, R. R. Friedl, D. M. Golden, M. J. Kurylo, G. K. Moorgat, P. H. Wine, A. R. Ravishankara, C. E. Kolb, M. J. Molina, B. J. Finlayson-Pitts, R. E. Huie, and V. L. Orkin, *Chemical kinetics and photochemical data for use in atmospheric modeling.*, Tech. rep., Jet Propulsion Laboratory, NASA (2006).

[27] A. J. C. Varandas, Int. Rev. Phys. Chem. **19**, 199 (2000).

[28] A. J. C. Varandas, *Conical Intersections Electronic Structure, Dynamics and Spectroscopy* (World Scientific, 2004), chap. Modeling and interpolation of global multi-sheeted potential energy surfaces, p. 205.

Part I

Potential energy Surfaces

Chapter 1

Theoretical Framework

The potential energy surface (PES) concept is a cornerstone in theoretical studies of chemical processes [1–4]. Its definition comes from applying quantum mechanics to a molecular system within the Born-Oppenheimer approximation [5]. These functions are needed for any (quantum or classical) dynamical study of molecules, including rate constants of chemical reactions, molecular beam scattering cross sections and ro-vibrational spectroscopy [2, 3]. Detailed discussions on potential energy surfaces may be found elsewhere [1, 4, 6–8]; in the following, main ideas related to molecular PES are briefly reviewed. First the origin of its concept is introduced, and then ideas leading to its construction, representation and characterization will be discussed.

1.1 Born-Oppenheimer Approximation

From a quantum mechanical description of matter [7], motion of atomic particles is governed by the Schrödinger equation, with the stationary form:

$$\hat{H}\Psi = E\Psi \tag{1.1}$$

being $\hat{H}$ the Hamiltonian operator of the studied system, Ψ the wave function and E the energy of the system. Atomic units [9] will be used in this chapter.

For a general molecular system consisting of electrons and nuclei, the Hamiltonian can be written as:

$$\hat{H}(\mathbf{r}, \mathbf{R}) = \hat{T}_{\mathrm{N}}(\mathbf{R}) + \hat{H}_{\mathrm{e}}(\mathbf{r}, \mathbf{R}) \tag{1.2}$$

where $\hat{T}_{\mathrm{N}}$ represents nuclear kinetic operator, $\hat{H}_{\mathrm{e}}$ is the electronic Hamiltonian, $\mathbf{r}$ and $\mathbf{R}$ are the electron and nuclear coordinates respectively. The electronic Hamiltonian, depending also on nuclear coordinates, can be written as:

$$\hat{H}_{\mathrm{e}} = \hat{T}_{\mathrm{e}} + V_{\mathrm{ee}} + V_{\mathrm{eN}} + V_{\mathrm{NN}} \tag{1.3}$$

being $\hat{T}_{\mathrm{e}}$ the electrons kinetic energy operator, V_{ee} includes all the electron-electron interactions, V_{eN} stands for electron-nucleus interactions and V_{NN} includes all nuclei-nuclei interactions. For a system with N nuclei and n_e electrons, the above presented terms are given by:

$$\hat{T}_{\mathrm{N}} = -\sum_{k}^{N} \left(\frac{1}{2M_k}\right) \nabla_k^2,\ \hat{T}_{\mathrm{e}} = -\frac{1}{2}\sum_{i}^{n_e} \nabla_i^2 \tag{1.4}$$

$$V_{\mathrm{ee}} = \frac{1}{2}\sum_{i\neq j}^{n_e} \frac{1}{r_{ij}}, V_{\mathrm{eN}} = -\sum_{k}^{N}\sum_{i}^{n_e} \frac{Z_k}{|\mathbf{R}_k - \mathbf{r}_i|}, V_{\mathrm{NN}} = \frac{1}{2}\sum_{k\neq k'}^{N} \frac{Z_k Z_{k'}}{R_{kk'}} \tag{1.5}$$

where M_k and Z_k are the mass and charge number of the k^{th} nucleus respectively, $r_{ij} = |\mathbf{r}_i - \mathbf{r}_j|$, and $R_{kk'} = |\mathbf{R}_k - \mathbf{R}_{k'}|$

If all nuclei were fixed in the space, the motion of the electrons would be governed by the equation:

$$\hat{H}_{\mathrm{e}}(\mathbf{r};\mathbf{R})\Phi_n(\mathbf{r};\mathbf{R}) = \varepsilon_n(\mathbf{R})\Phi_n(\mathbf{r};\mathbf{R}) \tag{1.6}$$

where $\Phi_n(\mathbf{r};\mathbf{R})$ and $\varepsilon_n(\mathbf{R})$ are the adiabatic eigenfunctions and eigenvalues of the electronic Hamiltonian (1.3) parametrically depending on $\mathbf{R}$, for a given n electronic state. Since adiabatic eigenfunctions are a complete basis set, the molecular wave function $\Psi(\mathbf{r},\mathbf{R})$, fulfilling the whole system stationary Schrödinger equation:

$$\hat{H}(\mathbf{r},\mathbf{R})\Psi(\mathbf{r},\mathbf{R}) = E\Psi(\mathbf{r},\mathbf{R}), \tag{1.7}$$

can be expanded as [10]:

$$\Psi(\mathbf{r},\mathbf{R}) = \sum_{n} \chi_{\mathrm{n}}(\mathbf{R})\Phi_n(\mathbf{r};\mathbf{R}) \tag{1.8}$$

where $\chi_n(\mathbf{R})$ is the nuclear wave function in the adiabatic representation. Substituting (1.8) into (1.7) and integrating over the electronic coordinates, the following coupled equations are obtained:

$$[\hat{T}(\mathbf{R}) + \varepsilon_m(\mathbf{R})]\chi_m(\mathbf{R}) + \sum_n \hat{\Lambda}_{mn}(\mathbf{R})\chi_n(\mathbf{R}) = E\chi_m(\mathbf{R}) \tag{1.9}$$

being $\hat{\Lambda}_{mn}$ the elements of the coupling matrix operator $\hat{\mathbf{\Lambda}}$ given by:

$$\hat{\Lambda}_{mn} = -\sum_{\mathrm{i}} \frac{1}{M_i}\left(A^{(\mathrm{i})}_{mn}\frac{\partial}{\partial R_i} + \frac{1}{2}B^{(\mathrm{i})}_{mn}\right) \tag{1.10}$$

where the elements of matrices $\mathbf{A}^{(\mathrm{i})}$ and $\mathbf{B}^{(\mathrm{i})}$ are:

$$A^{(\mathrm{i})}_{mn} = \int \Phi^*_m \frac{\partial}{\partial R_i}\Phi_n \mathrm{d}^3\mathbf{r},\ B^{(\mathrm{i})}_{mn} = \int \Phi^*_m \frac{\partial^2}{\partial R_i^2}\Phi_n \mathrm{d}^3\mathbf{r} \tag{1.11}$$

In order to solve the coupled equations (1.9), off-diagonal coupling terms $\hat{\Lambda}_{mn}$ ($m \neq n$) are often disregarded. This idea is justified by the fact that nuclear mass is much larger than the mass of the electrons; it is called adiabatic approximation [10].

If non-adiabatic coupling is neglected, which is equivalent to keep only one term in the expansion (1.8), the wave function becomes:

$$\Psi(\mathbf{r}, \mathbf{R}) = \chi_n(\mathbf{R})\Phi_n(\mathbf{r}; \mathbf{R}). \tag{1.12}$$

The adiabatic approximation for nuclear wave function assumes the form:

$$\hat{H}^{\mathrm{ad}}_n \chi_n(\mathbf{R}) = E\chi_n(\mathbf{R}) \tag{1.13}$$

where the nuclear adiabatic Hamiltonian is given by:

$$\hat{H}^{\mathrm{ad}}_n = \hat{T}_{\mathrm{N}} + \varepsilon_n(\mathbf{R}) + \hat{\Lambda}_{nn}(\mathbf{R}) \tag{1.14}$$

In most situations involving molecular species, the dependence of $\hat{\Lambda}_{nn}(\mathbf{R})$ on nuclear coordinates $\mathbf{R}$ is relatively weak compared to that of the adiabatic potential $\varepsilon_n(\mathbf{R})$. Thus, the term $\hat{\Lambda}_{nn}(\mathbf{R})$ is often neglected in the adiabatic approximation and the Born-Oppenheimer approximation (BOA) [5] is then obtained:

$$[\hat{T}_{\mathrm{N}} + V_n(\mathbf{R})]\chi_n(\mathbf{R}) = E\chi_n(\mathbf{R}) \tag{1.15}$$

where $\varepsilon_n(R)$ was replaced by $V_n(R)$, to remark that the electronic energy becomes an interaction potential in the nuclear problem. Hence, in the adiabatic BOA, a complete separation of electronic and nuclear motion is achieved; one first solves the electronic problem getting the eigenvalues $\varepsilon_n(R)$ at a given R and defined electronic state characterized by the quantum number n, then solves the nuclear dynamics using such $V_n(R)$ as the interaction potential for nuclei. Thus, $V_n(R)$ is a potential energy surface on which atomic nuclei of the molecular system move.

1.2 *Ab initio* calculations

For a molecular system consisting of n_e electrons and N nuclei, the electronic Hamiltonian for a fixed nuclear configuration can be written as:

$$\hat{H}_{\mathrm{e}} = \sum_{i}^{n_e} \hat{h}(i) + \frac{1}{2} \sum_{i \neq j} \frac{1}{r_{ij}} \tag{1.16}$$

where the second term represents the electron-electron interaction V_{ee} and the one electron Hamiltonian is given by:

$$\hat{h}(i) = -\frac{1}{2}\nabla_i^2 + \sum_{k}^{N} \frac{Z_{\mathrm{k}}}{\mathcal{R}_{ik}} \tag{1.17}$$

$\mathcal{R}_{ik} = |\mathbf{r}_i - \mathbf{R}_k|$ and r_{ij} have the same meaning as in previous section. Thus, equation (1.6) becomes:

$$\left(\sum_{i}^{n} \hat{h}(i) + \frac{1}{2} \sum_{i \neq j} \frac{1}{r_{ij}} \right) \Phi_n(\mathbf{r}) = \varepsilon_n \Phi_n(\mathbf{r}) \tag{1.18}$$

where dependence of $\hat{h}(i)$, ε_n and Φ_n on $\mathbf{R}$ has been omitted for clarity and nuclear-nuclear interactions have been excluded.

To obtain the eigenvalues and eigenfunctions of the equation (1.18) is usually called *ab initio* calculations. This task is, at present times, exactly feasible only for hydrogen-like systems. Thus, usually further approximations are needed.

1.2.1 Hartree-Fock approximation

When calculating the ground state energy of a molecular system, the use of variational methods is convenient [7]. In that case, the wave function can be

determined by finding the extremal of the functional:

$$J = \int \Phi^* \hat{H} \Phi \mathrm{d}\tau \tag{1.19}$$

where Φ is assumed to be normalized:

$$\int \Phi^* \Phi \mathrm{d}\tau = 1 \tag{1.20}$$

The success of the variational method depends on the choice of the trial function. It is possible to construct the system wave function as the simple product of different electrons wave functions:

$$\Phi = \psi_1(1)\psi_2(2)\cdots\psi_n(n) \tag{1.21}$$

Such a selection correspond to the assumption that electrons move independently. Substituting (1.21) into (1.19), with $\hat{H}$ given by (1.16) it is obtained:

$$J = \sum_i \int \psi_i^* \hat{h}(i) \psi_i \mathrm{d}^3\mathbf{r}_i + \frac{1}{2} \sum_{j \neq i} \int \psi_i^* \psi_j^* (\frac{1}{r_{ij}}) \psi_i \psi_j \mathrm{d}^3\mathbf{r}_i \mathrm{d}^3\mathbf{r}_j \tag{1.22}$$

the wave function of the ground state is then obtained by the solution of the variational problem:

$$\delta J = \delta \int \Phi^* \hat{H} \Phi \mathrm{d}\tau = \sum_i \int \delta\psi_i^* \{\hat{h}(i) + \sum_{j \neq i} \int \psi_j^* (\frac{1}{r_{ij}}) \psi_j \mathrm{d}^3\mathbf{r}_j\} \psi_i \mathrm{d}^3\mathbf{r}_i = 0 \tag{1.23}$$

the orthonormal character of the ψ_i functions allows to introduce the Lagrangian multipliers ϵ_i:

$$\delta J = \sum_i \int \delta\psi_i^* \{\hat{h}(i) + \sum_{j \neq i} \int \psi_j^* (\frac{1}{r_{ij}}) \psi_j \mathrm{d}^3\mathbf{r}_j - \epsilon_i\} \psi_i \mathrm{d}^3\mathbf{r}_i = 0 \tag{1.24}$$

as the $\delta\psi_i$ are linearly independent, it is then obtained:

$$\left[\hat{h}(i) + \sum_{j \neq i} \int \psi_j^* (\frac{1}{r_{ij}}) \psi_j \mathrm{d}^3\mathbf{r}_j - \epsilon_i\right] \psi_i = 0 \quad i = 1, 2, \cdots, N \tag{1.25}$$

The set of equations (1.25) for determination of single electron wave functions ψ_i and energies ϵ_i was first proposed by Hartree [11] on the basis of the average

field produced by the electrons. Fock [12] obtained such equations by using a variational principle as here presented.

To solve equations set (1.25) Hartree applied the method of successive approximations. As zeroth approximation he used the hydrogen-like functions $\psi_i^{(0)}$ and then evaluate the sum:

$$\mathcal{V}_i^{(0)} = \sum_{j \neq i} \int \psi_j^{(0)*} (\frac{1}{r_{ij}}) \psi_j^{(0)} \mathrm{d}^3\mathbf{r}_j \tag{1.26}$$

which is the average Coulomb interaction energy of the i^{th} electron when interacting with all other electrons whose states are given by $\psi_j^{(0)}$. Substituting $\mathcal{V}_i^{(0)}$ in (1.25) is possible to determine the functions $\psi_i^{(1)}$ in the first order approximation:

$$\left[\hat{h}(i) + \mathcal{V}_i^{(0)} - \epsilon_i\right] \psi_i^{(1)} = 0 \tag{1.27}$$

then, assuming each electron in an state given by $\psi_i^{(1)}$ the new potential $\mathcal{V}_i^{(1)}$ is obtained:

$$\mathcal{V}_i^{(1)} = \sum_{j \neq i} \int \psi_j^{(1)*} (\frac{1}{r_{ij}}) \psi_j^{(1)} \mathrm{d}^3\mathbf{r}_j \tag{1.28}$$

which can be used to evaluate the wave function:

$$\left[\hat{h}(i) + \mathcal{V}_i^{(1)} - \epsilon_i\right] \psi_i^{(2)} = 0 \tag{1.29}$$

if the process converges, it can be continued until obtain a potential energy:

$$\mathcal{V}_i = \sum_{j \neq i} \int \psi_j^{*} (\frac{1}{r_{ij}}) \psi_j \mathrm{d}^3\mathbf{r}_j \tag{1.30}$$

which, by substitution in the set of equations:

$$\left[\hat{h}(i) + \mathcal{V}_i - \epsilon_i\right] \psi_i = 0 \tag{1.31}$$

will lead to almost the same wave functions ψ_i than the used to evaluate the potential energy (1.30). The potential energy so obtained is called self consistent Hartree field.

The above approximation is based upon representation of the system's wave function as a product (1.21) of single electron wave functions. However such a choice does not account the fermionic character of the electrons. A proper

wave function of electrons set must be antisymmetric. A self consistent field (SCF) which correctly account the symmetry of the electronic wave function was obtained by Fock [12]. In Fock's method the trial function is constructed by means of the Slater determinant:

$$\Phi = \frac{1}{\sqrt{n!}} \begin{vmatrix} \psi_1(1) & \psi_1(2) & \cdot & \cdot & \cdot & \psi_1(N) \\ \psi_2(1) & \psi_2(2) & \cdot & \cdot & \cdot & \psi_2(N) \\ \cdot & \cdot & \cdot & & & \cdot \\ \cdot & \cdot & & \cdot & & \cdot \\ \cdot & \cdot & & & \cdot & \cdot \\ \psi_N(1) & \psi_N(2) & \cdot & \cdot & \cdot & \psi_N(N) \end{vmatrix} \tag{1.32}$$

which can be expressed as:

$$\Phi = \hat{A}[\psi_1(1)\psi_2(2)\cdots\psi_n(n)], \tag{1.33}$$

where the anti-symmetrization operator $\hat{A}$ is given by:

$$\hat{A} = \frac{1}{\sqrt{n!}} \sum_{k=1}^{n!} (-1)^k \hat{P}$$

where $\hat{P}$ is the bi-particular permutation operator, $\hat{A}$ fulfill the following relationships:

$$\hat{A}^2 = \sqrt{n!}\hat{A},\ \hat{A}^\dagger = \hat{A},\ \hat{A}(\frac{1}{r_{ij}}) = (\frac{1}{r_{ij}})\hat{A},\ \hat{A}\hat{h}(i) = \hat{h}(i)\hat{A} \tag{1.34}$$

with the trial function (1.32) the equation (1.22) becomes:

$$\begin{aligned} J \;=\; & \underbrace{\frac{1}{\sqrt{n!}} \sum_i \int \hat{A}^*[\psi_1(1)\psi_2(2)\cdots\psi_n(n)]^* \hat{h}(i) \hat{A}[\psi_1(1)\psi_2(2)\cdots\psi_n(n)]\mathrm{d}\tau +}_{I_1} \\ & \underbrace{+ \frac{1}{2}\frac{1}{\sqrt{n!}} \sum_{i\neq j} \int \hat{A}^*[\psi_1(1)\psi_2(2)\cdots\psi_n(n)]^* (\frac{1}{r_{ij}}) \hat{A}[\psi_1(1)\psi_2(2)\cdots\psi_n(n)]\mathrm{d}\tau}_{I_2} \end{aligned}$$

using the properties (1.34) and bearing in mind that $\int \psi_i(i)\psi_j(i)\mathrm{d}^3 r_i = \delta_i^j$, I_1 and I_2 becomes:

$$I_1 = \sum_{i=1}^{n_e} \int \psi_i(i)\hat{h}(i)\psi_i(i)\mathrm{d}^3\mathbf{r}_i = \sum_{i=1}^{n_e} \epsilon_i^{\mathrm{HF}} \tag{1.35}$$

$$\begin{aligned} I_2 &= \frac{1}{2}\sum_{i,j}^{n_e}\left[\int \psi_i(i)^*\psi_j(j)^*\frac{1}{r_{ij}}\psi_i(i)\psi_j(j)\mathrm{d}^3\mathbf{r}_i\mathrm{d}^3\mathbf{r}_j - \right. \\ &\quad \left. - \int \psi_i(i)^*\psi_j(j)^*\frac{1}{r_{ij}}\psi_i(j)\psi_j(i)\mathrm{d}^3\mathbf{r}_i\mathrm{d}^3\mathbf{r}_j\right] \\ &= \frac{1}{2}\sum_{i,j}^{n_e}\left[\mathcal{J}_{ij} - \mathcal{K}_{ij}\right] \end{aligned}$$

then, the Hartree-Fock energy becomes:

$$E_{\mathrm{HF}} = \sum_{i=1}^{n_e}\epsilon_i^{\mathrm{HF}} + \frac{1}{2}\sum_{i,j}^{n_e}\left[\mathcal{J}_{ij} - \mathcal{K}_{ij}\right] \tag{1.36}$$

The first term in equation (1.36) is just the sum of the mean values of the mono-particles energies. The second term contains two parts: $\mathcal{J}_{ij}$ represents the electrostatic interaction of two electrons in states i and j, while $\mathcal{K}_{ij}$ is the so called Hartree-Fock exchange energy, having no analogue in the classical physics. It is a consequence of the fermionic character of the electrons. To calculate the Hartree-Fock energy, the wave functions ψ_i (usually called orbitals) are needed, thus, a similar iterative method as previously described for Hartree approximation is used.

1.2.2 Post Hartree-Fock methods

Although HF calculations give very useful and even accurate results for quantities like equilibrium geometries of the molecules, the HF approach is a very approximate method to solve electronic problems [13]. The HF method, essentially, is a mean field approximation in which each electron move under the influence of the mean interaction due to all other electrons. As a result, it neglects the instantaneous or correlated motions of the electrons. It is useful to define the difference between the exact energy (E_{exact}) of the electronic system and the HF as the electronic correlation energy:

$$E_{corr} = E_{exact} - E_{\mathrm{HF}} \tag{1.37}$$

Even when the HF energy represents the major part of the total energy, usually around 95 to 99 %, correlation energy [13] is very significant in most chemical

problems (molecular collisions, properties calculations, etc.): interest is not in the absolute value of the energy but in the differences between values for given configurations. Such a difference (e.g. between two vibrational levels of a diatom) can be of the same order than E_{corr}. Thus, these "small" contributions may be significant [14].

In order to recover the correlation energy it is necessary to go beyond the HF approximation. The general approach for the electronic correlation energy calculation is to include more than one Slater determinant in the expansion of the electronic wave function.

$$\Phi = \sum_k c_k D_k \tag{1.38}$$

where D_0 is the Slater determinant for the ground state wave function, composed of the N lowest molecular orbitals and $D_k (k > 0)$ are Slater determinants with one or more electrons in excited orbitals. This approach is called configuration interaction or CI [14]. Configuration interaction calculations are classified by the number of excitations used to make each determinant. If only one electron has been moved for each determinant, it is called a configuration interaction single-excitation (CIS) [15] calculation. CIS calculations give an approximation to the excited states of the molecule, but do not change the ground state energy. Single-and double-excitation (CISD) [15] calculations yield a ground-state energy that has been corrected for correlation. Triple-excitation (CISDT) [15] and quadruple-excitation (CISDTQ) [15] calculations are done only when very-high-accuracy results are desired. The configuration interaction calculation with all possible excitations is called a full CI (FCI). The full CI calculation using an infinitely large basis set will give an exact quantum mechanical result. However, full CI calculations are very rarely done due to the immense amount of computer power required. Thus, accurate calculation of correlation energy for electrons in a molecular system is a very difficult task and further methods and/or truncation of the CI expansion are needed. Some type of calculations begins with a HF approximation and are then corrected to include electronic correlation.

Some of these methods [16] are Møller-Plesset perturbation theory (MPn, where n is the order of correction), the generalized valence bond (GVB) method, multiconfigurational self-consistent field (MCSCF), and coupled cluster theory

(CC). As a group, these are referred to as correlated calculation methods. In the following some of them will be introduced.

1.2.2.1 Multiconfigurational self consistent field method

The multiconfigurational self consistent field (MCSCF) [15] wave function is a truncation of the CI expansion (1.38) in which both factors of the expansion, the coefficient and the molecular orbitals of the configurations, are variationally optimized. The molecular orbital is optimized by means of the coefficients of the basis set (see section 1.4) in which it is expanded. Simultaneous optimization of orbitals and coefficients is a difficult task, as it is needed to account the two sets of parameters defining the wave function. Then, a compromise appears between generation of a configuration space sufficiently flexible to describe the molecular system and the number of variables to be computationally tractable.

The MCSCF wave function is well suited to study systems involving degenerate or nearly degenerate configurations, where the static correlation is important [15]. These situations are usually encountered in the description of reaction process where chemical bonds are being broken, but also in ground-state molecular systems at the equilibrium geometry.

An approach to select the MCSCF configurations is to partition the molecular orbital space into three subspaces, containing inactive, active and virtual (or unoccupied) orbitals respectively [17]. Typically, the core orbitals of the system are treated as inactive and the valence orbitals as active. Thus, the complete active space (CAS) consists in all configurations obtained by distributing the valence electrons in all possible ways in the active orbitals, keeping the core orbitals doubled occupied in all configurations. This is referred to as full valence complete active space (FVCAS) [17]. FVCAS method is implemented in MOLPRO [18], an *ab initio* package used to study the title molecular system of this work.

Since the configuration expansion that can be managed within the framework of CASSCF theory corresponds to small active spaces, it is in general impossible to recover the dynamical correlation by MCSCF wave functions. For high accuracy and treatment of dynamical correlation, additional calculations must be carried out based on the initial MCSCF description.

1.2.2.2 Perturbation Methods

In order to apply perturbation theory [7] to the calculation of the correlation energy, the unperturbed Hamiltonian must be selected. The most common choice is to take this as a sum over Fock operators [16], leading to Møller Plesset (MP) Perturbation theory [19]. In this way, the electron repulsion is counted twice. This choice is not consistent with the assumption that perturbation should be small when compared with $\hat{H}_0$ [7]. However, it does fulfill the requirement that solutions of the unperturbed Schrödinger equation should be known.

$$\hat{H}_0 = \sum_{i=1}^{n} \hat{F}_i = \sum_{i=1}^{n} \left(\hat{h}_i + \sum_{j=1}^{n} (\hat{J}_{ij} - \hat{K}_{ij}) \right) \tag{1.39}$$

Subtracting the unperturbed Hamiltonian from the total one, the perturbation becomes:

$$\hat{W} = \hat{H} - \hat{H}_0 = \sum_{i=1}^{n} \hat{h}_i + V_{\text{ee}} - \sum_{i=1}^{n} \left(\hat{h}_i + \sum_{j=1}^{n} (\hat{J}_{ij} - \hat{K}_{ij}) \right) = V_{\text{ee}} - 2\langle V_{\text{ee}} \rangle \tag{1.40}$$

Thus, the Hartree-Fock energy (1.36) is recovered only in the first order of the perturbation:

$$\text{MP1} = \text{MP0} + \text{E(MP1)} = \text{E(HF)} \tag{1.41}$$

electron correlation energy starts at order 2 with this choice.

One can go further to higher orders of perturbations MP3, MP4 and so on. In the ideal case the HF, MP2, MP3 and MP4 results show a monotonic convergence towards a limiting value, with the corrections being of the same sign and numerically smaller as the order of the perturbation increases. Unfortunately this is not the typical behavior. Even in systems where the reference is well described by a single determinant, oscillations in a given property as a function of perturbation order are often observed [20].

In practice only low orders of perturbation theory can be carried out and it is often observed that HF and MP2 results differs considerably, the MP3 moves back towards the HF and the MP4 moves away again. In despite of such a behavior MP offers a cheaper method to account the electronic correlation energy, compared with other approximations [16]. Besides, perturbation methods are size extensive *i.e.* the calculated energy of two fragments placed infinitely farther away is the

same than the sum of the energies of each fragment [15], a significant advantage compared to variational methods.

Perturbation methods can also be used with multireference functions. This is the case of CASPTn [15, 21–23] in which perturbation theory calculations (of n^{th}-order) are carried out using CASSCF wave function as zeroth order approximation.

A difficulty of this method is that the CASSCF wave function is not an eigenfunction of the non-perturbed Hamiltonian (1.39). Then, $\hat{H}_0$ must be redefined to restore the eigenfunction property. A solution, first proposed by Andersson *et al.* [22] was to project the $\hat{H}_0$ operator onto the space of configuration interaction functions. This is done with help of projection operators: $\hat{P}_0$ projecting onto the reference wave function space (V_0), $\hat{P}_K$ project onto an space V_K, defined by the orthogonal complement to V_0 in the restricted subspace used to generate the CAS wave function, $\hat{P}_{SD}$ project onto the space V_{SD}, spanned by all single and double replacement states generated from V_0 and $\hat{P}_{TQ}$ projecting onto the space V_{TQ}, the space containing all higher order excitations not included in the previously mentioned spaces. Thus, the unperturbed Hamiltonian can be written:

$$\hat{H}_0^{\mathrm{CASPT}} = \hat{P}_0\hat{F}\hat{P}_0 + \hat{P}_K\hat{F}\hat{P}_K + \hat{P}_{SD}\hat{F}\hat{P}_{SD} + \hat{P}_{TQ}\hat{F}\hat{P}_{TQ} \tag{1.42}$$

where $\hat{F}$ is the CASSCF Fock operator [22]. With this idea and a rather complicated mathematical formalism, a significant part of the correlation energy can be recovered in CASPT2 energy.

The CASPT approach is almost size extensive [15]. For a CASSCF reference wave function dominated by a single determinant, the contributions to the energy from the terms that are not size-extensive is expected to be small, while for a wave function in which several determinants have large weights, larger non-separable contribution is expected.

The importance of CASPT lies in the fact that, it represents the only generally applicable method for the *ab initio* calculation of dynamical correlation effects of open and closed-shell multiconfigurational electronic systems [15].

1.3 Other methods

When studying molecular structure, either to obtain a potential energy surface or to calculate molecular properties, different methods, besides those presented in the previous section are also used. We can hardly select one of them as a better one, in such a case, it would be only to deal with certain problem or system. In the following some of them are very briefly presented.

The **Gaussian theories (Gn)**, developed in the 1980's [24] have shown great utility in calculating accurate energies [25]. In these theories energy is composite, assembled from a variety of different quantum methods, using basis sets of different sophistication to yield effective energies at high level and large basis sets. The means by which this is achieved may be illustrated with the equation:

$$\begin{aligned} E(\mathrm{Gn}) &= E[\mathrm{MP2/SP}] + \Delta E(+) + \Delta E(2df,p) + \Delta E(\mathrm{QCI}) + \\ &\quad + \Delta E(\mathrm{MP2/large}) + E(\mathrm{HLC}) \end{aligned}$$

where each term represents the corresponding contribution to the energy at the specific level, E(HLC) stands for the "higher level correction" depending [24] on the number of α and β (spin up and down) valence electrons.

In Gaussian theories the accuracy can be extremely good for systems similar to those for which they were parametrized, the ground state of organic molecules. However, for other systems, such as transition structures or clusters, these methods often are less accurate than some less computationally intensive *ab initio* methods [13].

The premise behind **Density Functional Theories (DFT)** is that the ground state electronic energy is completely determined by the electron density ρ instead of the wave function [16]. There exists a one-to-one correspondence between the electron density of a system, and the energy. The origin of this theory comes from a theorem by Hohenberg and Kohn [26] proving the above statement. A wave function for an n_e-electron system contains $3n_e$ coordinates, whereas the electron density is the square of the wave-function integrated over $n_e - 1$ electron coordinates and depends just on three coordinates independently on the size of the system. The "only" problem is that although it has been proven that each different density yields a different ground state energy, the functional connecting

these two quantities is not known. The goal of DFT is to design functionals connecting the electron density with energy.

Perdew and Wang [27] reported its PW86, while Becke [28] presents a widely used correction (B88) to this one. Lee, Yang and Parr [29] proposed the LYP functional, also very used in the literature while the Becke's gradient-correlated exchange correlation density functional B3LYP [29, 30] is perhaps, the most popular. Weak interactions due to dispersion (van der Waals type) are poorly described by the so far used functionals [16]. Hydrogen bonding, however, is mainly electrostatic, which is reasonably well accounted by DFT methods. At the present, such methods are not well suited for excited states of the same symmetry as the ground state. The absence of a wave function makes it difficult to ensure orthogonality between the ground and excited states [16].

Multireference Perturbation theory (MRMP2) is another way of accounting electronic correlation using multireference wave functions and the Møller-Plesset Perturbation theory [31, 32]. Basically the idea is similar to picture presented in CASPT methods. The MR-MP2 is based upon applying the generalized Independent electron-pair approximation (IEPA) [33], consisting in approximating the total correlation energy as a sum of pair contributions, independently calculated, to an MCSCF reference function. The use of IEPA for the study of dynamical correlation, warrant a rapid convergence of the perturbation series. However, perturbation series either show very slow convergence or divergence at intermediate and large internuclear distances.

1.4 Basis sets

One of the approximations inherent to all essentially *ab initio* methods is the introduction of a basis set [16]. To expand the unknown function, such as a molecular orbital, in a set of known functions is not an approximation, if the basis set is complete. However, a complete basis means that an infinite number of functions must be used, which is impossible in practical calculations. The smaller the basis set, the poorer the representation. The type of basis functions used has also influence on the accuracy. The better a single basis function is able to reproduce the unknown function, the fewer basis functions are necessary to

achieve a given level of accuracy. In this section brief ideas on the types of basis sets are given.

There are two types of basis functions (also called Atomic Orbitals, AO, even when they are not in general, solutions of the Schrödinger equation) used in electronic structure calculations: Slater Type Orbitals (STOs) and Gaussian type Orbitals (GTOs). Slater type orbitals [34] are the solutions of the Schrödinger equation for the hydrogen atom. The electron integrals of these functions can not be solved analytically. Thus, STOs are only used for atomic and diatomic systems where high accuracy is needed. When using GTOs [35] more functions are needed to represent the orbitals, however, electronic integrals can be analytically performed, which is faster than numerical integration of the STOs.

Once the type of function (STO or GTO) is selected, the next step is to choose of the number of functions to be used. The smallest number of functions possible, to contain all the electrons in a neutral atom, is called minimum basis set. Thus, for hydrogen (and helium) it means a single s-function, for the first row elements of the periodic table it requires two s-functions $(1s, 2s)$ and one set of p-functions $(2p_x, 2p_y, 2p_z)$ and so on. The next improvement is to double all basis functions, producing a double zeta (DZ) type basis. Then, a DZ basis employs two s-functions for hydrogen ($1s$ and $1s'$), four s and two p-functions for the elements on the first row, and so on. One can also go further to Triple Zeta (TZ), Quadruple Zeta (QZ) and Quintuple Zeta (5Z). In actual calculations doubling the number of core orbitals would rarely be considered. Often the valence functions are doubled, producing a VDZ basis set.

The differences in the electron distributions along a bond and in the perpendicular direction, led to the introduction of polarization functions in basis sets. Adding a single set of polarization functions (p-function hydrogen atoms and d-functions on heavy atoms) to the DZ basis, forms a Double Zeta plus Polarization (DZP) basis set.

The fact that many basis sets go into describing the energetically important, but chemically unimportant core electrons is the foundation for contracted basis sets. An energy optimized basis set which gives a good description of the outer part of the wave function is required to be very large. However, contracted basis sets can lead to better description of the outer part with a smaller number of

functions. A contracted basis set is obtained by combining the full basis set functions, known as primitive GTOs, into a smaller set of functions by forming fixed linear combinations. The resulting functions are called contracted GTOs.

An attempt to a better description of the wave function far from the nucleus is done by the introduction of diffuse functions, basis functions with small exponents. Diffuse functions are needed to describe interactions at long distances or whenever loosely bound electrons are present. Basis sets with diffuse functions are called augmented basis sets.

There is a family of correlation consistent basis sets (aug-cc-pVXZ, X=D,T,Q,5) created by Dunning and coworkers [36, 37]. The "aug" denotes an augmented basis. The "cc" denotes that this is a correlation-consistent basis, meaning that the functions were optimized for best performance with correlated calculations. The "p" denotes that polarization functions are included on all atoms. The "VXZ" stands for valence X (double, triple...) zeta. These sets have become popular for high-accuracy correlated calculations.

Commonly, basis sets are implemented in *ab initio* packages for electronic structure calculations. However, when selecting a basis set, some of the above presented details should be accounted for, as well as the accuracy desired for the calculation, bearing in mind the computing power available.

1.5 Representing a Potential Energy Surface

Results from *ab initio* electronic structure calculations are given mostly in form of tables of energy values for special geometries. Even when such a calculations might also provide the first and second derivatives, a full analytic or numerical representation of the potential energy is commonly needed [3, 38].

For spectroscopy studies, only relatively small regions around some particular configurations are needed to be explored. Extended areas, however, are required for dynamical calculations [2]. In both cases one has a given set of data (inter-atomic distances, internal coordinates, etc. and the corresponding potential energy values) wishing to be condensed by fitting into a model describing the potential energy surface that depends on adjustable parameters.

For local approximations, interpolating functions (splines), polynomial or ra-

tional expansions are frequently used. Functional forms that are special and simulate the topography of the PES (*e.g.* Morse functions, many-body expansions) are used for local and global interpolations [38, 39].

In global methods, the function depends upon the entire set of data, whereas in local methods a restricted number of data values is used. The interpolating functions can cover exactly or approximately the given data points. In some applications, the PES is searched only along the intrinsic reaction coordinate, from the transition state to the product and/or to the reactant configuration [39].

A successful representation of a global PES for dynamical calculations should satisfy certain criteria, as discussed by Wright and Gray [40] and remarked by Varandas [3]:

1. "It should accurately characterize the asymptotic reactant and product molecules (or more generally any fragment of the full system)."

2. "It should have correct symmetry properties of the system."

3. "It should represent the true potential energy surface in interaction regions for which experimental or non-empirical theoretical data are available (including, in principle, the very short-range and long-range regions associated with various asymptotic channels [39])"

4. "It should behave in a physically reasonable manner in those parts of the interaction region for which no experimental or theoretical data are available."

5. "It should smoothly connect the asymptotic and interaction region in a physically reasonable way."

6. "The function and its derivatives should have as simple an algebraic form as possible consistent with the desired quality of the fit."

7. "It should require as small a number of data points as possible to achieve an accurate fit."

8. "It should converge to the true surface as more data become available."

9. "It should indicate where it is most meaningful to compute the data points."

10. "It should have a minimal amount of *ad hoc* or 'patched up character'."

Criteria from 1 to 5 must be obeyed in order to obtain reasonable results in subsequent calculations using the function. Criteria from 6 to 10 are desirable for practical reasons. Finding a function that meets these criteria requires skill and experience, and considerable amount of patience [13].

The aim of this thesis is to construct a potential energy surface to be used for dynamical calculations. Thus, a global representation is needed, bearing in mind the above mentioned conditions for the obtained function. For such a purpose the double many-body expansion method was used.

1.5.1 The double many-body expansion method

Starting from the work of London, Eyring, Polanyi and Sato (LEPS) [41] and the "diatomics in molecules" (DIM) method [42] a many-body expansion (MBE) was developed by Murrell and co-workers [1]. The essential idea of the MBE method is to describe the total interaction of the polyatomic system by adding all the many-body interactions of each fragment.

The many-body expansion for a single-valued potential energy surface of an n-atomic system is written as follows [43]:

$$\begin{aligned} V_{\mathrm{ABC\cdots N}}(\mathbf{R}) &= \sum V^{(1)}_{\mathrm{A}} + \sum V^{(2)}_{\mathrm{AB}}(R_{\mathrm{AB}}) + \sum V^{(3)}_{\mathrm{ABC}}(R_{\mathrm{AB}}, R_{\mathrm{AC}}, R_{\mathrm{BC}}) + \cdots \\ &\quad + V^{(n)}_{\mathrm{ABC\cdots N}}(\mathbf{R}) \end{aligned}$$

Summation indicates addition of all terms of the corresponding m-body fragments ($1 \leq m \leq n$). $V^{(1)}_{\mathrm{A}}$ is the energy of the atom A in the state which is produced by adiabatically removing this atom from the cluster. $\sum V^{(1)}_{\mathrm{A}}$ is the sum of all the one-body terms. If the reference energy is taken as the energy of all the atoms in their ground states, then $V^{(1)}_{\mathrm{A}}$ will be different from zero if, on dissociation, atom A is in an excited state. $V^{(2)}_{\mathrm{AB}}(R_{\mathrm{AB}})$ is a two-body energy term, depending on the distance separating the two atoms, and which goes to zero as R_{AB} tends to infinity. $V^{(3)}_{\mathrm{ABC}}(R_{\mathrm{AB}}, R_{\mathrm{AC}}, R_{\mathrm{BC}})$ is a three-body energy which depends on the three distances of the triangle ABC. All of these three-body terms, should be zero

if one of the atoms is removed away from the other two. The last term in the expansion $V^{(n)}_{\mathrm{ABC\cdots N}}(\mathbf{R})$ is the n-body energy. Such a term will become zero if any of the atoms is moved to infinity. It depends, as the total potential function, on the $3N-6$ internal coordinates (inter-atomic distances).

Thus far, there seems to be no simplification of the problem, once to get the full potential, a function depending on the whole set of variables is required. However, when there is a rapid convergence of the series or exist simple functional forms for high-order terms of the expansion such a representation becomes attractive. As a matter of fact, in all tetratomic system studied by this means (see Ref. 1 and references therein) the main features of the surface appear to be contained in the two- and three-body energy terms, and the four-body term can be regarded as fine tuning to give a desired chemical accuracy.

Even though there is no rapid convergence in the many-body expansion, the potential is designed to satisfy all dissociation limits, and it also provides a strategy for building up larger polyatomic systems.

MBE method is proposed to provide an analytical representation of potential energy surfaces for all possible configurations of the system. Then, its functional form must properly reproduce all the regions, from short range interactions to long range ones. However, the method fails in keeping only one function to reproduce both ranges. Thus, the idea of splitting each many-body terms into two parts arise. In such spirit Varandas [4, 39, 44, 45] extended the many-body expansion to the double many-body expansion (DMBE) in which each many-body term is split into two parts: one accounting for the long range or dynamical correlation energy and the other describing the short range or extended-Hartree-Fock energies.

In DMBE method, the extended-Hartree-Fock energy is essentially built up by the first-order exchange and electrostatic energy contributions, together with the second-order induction energy [39]. In turn, dynamical correlation energy includes all cases of double and multiple excitations in one of the atoms (intraatomic correlation) as well as single and multiple excitations in more than one atom (interatomic correlation and intra-inter coupling terms) [39].

The advantage of the DMBE model over other representations lies on the possibility to describe the region in the short range, of large interest when comparing with spectroscopic results, with accurate polynomial representation while long

range interactions, of interest for dynamics calculations, are phenomenologically described by multipolar expansions [46, 47]. Furthermore, and also significant, is the fact that once DMBE is a many-body expansion, each n-body energy terms, once deduced, can be used in all the polyatomics in which such n-body systems are contained.

In a series of papers Varandas and co-workers [39, 44, 46–49] presented general expressions for n-body dynamics correlation energy term, to reproduce the proper asymptotic behavior of the potential energy surface. Extended Hartree-Fock approximate correlation energy for two- and three-body interactions (EHFACE2 and EHFACE3) have also been proposed [46] while EHFACE2U was introduced to properly represent the united atom limit for diatoms [47].

The DMBE method has been successfully applied to numerous triatomic systems, particularly to those of interest in this thesis [50–52], tetratomic [53, 54] and larger polyatomic systems [55, 56]. With such a preceding experience, and the extensive use of these DMBE PESs for dynamical calculations (Ref. 2 and references therein), we believe DMBE offers a reliable method to construct a global potential energy surfaces for the HSO_2 molecular system.

1.6 Properties of potential energy functions

Once a potential energy function (PES) has been properly represented, it must be analyzed to determine information about the chemical system. The PES is the most complete description of all the conformers, isomers, and energetically accessible motions of a system [1, 16]. Minima on this surface correspond to optimized geometries, any movement away from a minimum gives a configuration with higher energy. The lowest-energy minimum is called the global minimum. There can be many local minima, such as higher-energy conformers or isomers. The transition structure between the reactants and products of a reaction, or the highest energy configuration between them, is a saddle point on this surface. A PES can be used to find both saddle points and reaction coordinates, and, as done in this work, to subsequently study reaction dynamics. The vibrational properties of the molecular system can also be obtained from the PES [16].

Let us represent the potential energy function as $f(\mathbf{x})$ depending on a set of

variables $\mathbf{x} = (x_1, x_2, ..., x_N)$. Optimization is a general term for finding stationary points of a function *i.e.* points where all the first derivatives are zero. Stationary points condition can be written in terms of the gradient $\mathbf{g}$, a vector formed by the first order derivatives of f, and the Hessian $\mathbf{H}$, a symmetric matrix with the second derivatives as elements. By means of orthogonal transformations [57] the matrix $\mathbf{H}$ can be diagonalized, becoming in $\mathbf{H}'$. When all the diagonal elements of $\mathbf{H}'$ are positive, the stationary point correspond to a minimum configuration, *i.e.* if:

$$\mathbf{g}(\mathbf{x}_0) = 0, \ \mathbf{H'}_{ii}(\mathbf{x}_0) > 0, \tag{1.43}$$

at given $\mathbf{x}_0$ the function will reach a local minimum. If the function value at this point is the smallest one of all the minima, then $\mathbf{x}_0$ stands for the global minimum configuration. When one of diagonal elements of $\mathbf{H}'$ is negative, then the configuration $\mathbf{x}_0$ correspond to a saddle point.

Hessian, once diagonalized gives not only a condition to define whether a configuration is a minimum or a saddle point, but also the normal modes frequencies, whose values are proportional to the square root of the diagonal elements. Therefore, a saddle point will be an stationary point with an imaginary frequency. Such an imaginary frequency will characterize the coordinate connecting the two minima. Stationary points also exist which have more than one imaginary frequency. However, in general these do not have any special meaning.

To find those configurations corresponding to minima and saddle points, optimization techniques are required [58]. In the optimization of the PES presented in this thesis a package [59] available at the Coimbra Theoretical & Computational Chemistry group was used. This code uses a mixture of optimization methods, and it has been specifically designed for potential energy functions of molecular systems, once the function has been given.

The dissociation products of a polyatomic system correspond to regions at infinity where the potential energy surface is flat in one or more dimensions. Thus, gradient of the PES is zero. The asymptotic regions can be referred as valleys. The slope of the valley gradually changes when the atoms approach each other. If they moves towards a saddle point the slope will be positive while a negative value indicate the approximation towards a minimum.

The term path is used to name the curve (hyper-curve, to denote its multidimensional character) defined by the energy function where the coordinates change from one configuration to another. Thus a reaction path is a path leading from the reactants valley the to products configuration. A minimum-energy reaction path follows the optimum way, it means, of all the possible paths, that corresponding to the steepest descent from saddle point to both products and reactants limits [60]. The saddle point is the maximum energy configuration in the minimum-energy reaction path.

Due to the current level of constantly increasing computing power, construction of potential energy surfaces might produce a feeling of an obsolete idea. An strong temptation comes from the desire to carry direct or on the fly dynamics *i.e.* obtain *ab initio* energies, gradients and force constants once required for a given configuration of the trajectory [61, 62], therefore, with no need of a function representation. Besides, by using large computational facilities to think in a very dense grid of *ab initio* points instead of a continuous function could be the trend [63]. However, it should be kept in mind that *ab initio* calculations are not the exact solution of the Schrödinger equation neither within the Born-Oppenheimer approximation. Actually, as was mentioned in previous sections, a large number of approximations was used for such a goal. Thus, even at the *state of the art* level of theory one might eventually get inappropriate solutions for the real problem. On the other hand, representations of PESs through functions provides a global view [2]; besides, once the selected method to represent the interaction comes with real physical meaning, it is possible to guarantee appropriate behavior in the range or regions were *ab intio* calculations could fail [39]. Furthermore, and as final words on this topic, a function representing a PES can be further corrected with experimental evidences [56] and, as in DMBE method, such a function may be used in the representation of larger systems. While, for example, in one on-the-fly-trajectory, once it is finished the calculated electronic energies can hardly be used for other studies.

Bibliography

[1] J. N. Murrell, S. Carter, S. C. Farantos, P. Huxley, and A. J. C. Varandas, *Molecular Potential Energy Functions* (Jonh Wiley & Sons, 1984).

[2] A. J. C. Varandas, Int. Rev. Phys. Chem. **19**, 199 (2000).

[3] A. J. C. Varandas, *Conical Intersections Electronic Structure, Dynamics and Spectroscopy* (World Scientific, 2004), chap. Modeling and interpolation of global multi-sheeted potential energy surfaces, p. 205.

[4] A. J. C. Varandas, in *Reaction and Molecular Dynamics*, edited by A. Laganá and A. Riganelli (Springer, Berlin, 2000), vol. 75 of *Lecture Notes in Chemistry*, p. 33.

[5] M. Born and R. Oppenheimer, Ann. d. Phys. **84**, 457 (1927).

[6] J. Z. H. Zhang, *Theory and Application of Quantum Molecular Dynamics* (World Scientific, 1999).

[7] A. S. Davydov, *Quantum Mechanics* (Edicion Revolucionaria, La Habana, 1965).

[8] A. F. Sax, editor, *Potential energy surfaces*. Springer (1999).

[9] M. Piris, *Física Cuántica* (Editorial ISCTN, La Habana, 1999).

[10] M. Born and K. Huang, *Dynamical theory of Crystal lattices* (Oxford Univ. Press, 1955).

[11] D. R. Hartree, Proc. Cambr. Phil. Soc. **24**, 89 (1928).

[12] V. Fock, Z. Phys. **61**, 126 (1930).

[13] D. C. Young, *Computational Chemistry* (John Wiley & Sons, 2001).

[14] I. N. Levine, *Quantum Chemistry* (Prentice Hall, 1999), 5th edn.

[15] T. Helgaker, P. Jørgensen, and J. Olsen, *Molecular electronic structure theory* (John Wiley & Sons, 2000).

[16] F. Jensen, *Introduction to computational chemistry* (John Wiley & Sons, 2001).

[17] B. Roos and P. R. Taylor, Chem. Phys. **48**, 157 (1980).

[18] H.-J. Werner and P. J. Knowles, MOLPRO is a package of *ab initio* programs written by H.-J. Werner, P. J. Knowles, with contributions from J. Almlöf, R. D. Amos, M. J. O. Deegan, S. T. Elbert, C. Hampel, W. Meyer, K. A. Peterson, R. Pitzer, A. J. Stone, P. R. Taylor, R. Lindh (1998).

[19] C. Møller and M. S. Plesset, Phys. Rev. p. 0618 (1934).

[20] T. H. Dunning, Jr. and K. A. Peterson, J. Chem. Phys. **108**, 4761 (1998).

[21] B. O. Roos, P. Linse, P. E. M. Siegbahn, and M. R. A. Blomberg, Chem. Phys. **66**, 197 (1982).

[22] K. Andersson, P. Malmqvist, B. O. Roos, A. J. Sadlej, and K. Wolinski, J. Phys. Chem. **94**, 5483 (1990).

[23] H.-J. Werner, Mol. Phys. **89**, 645 (1996).

[24] J. A. Pople, M. Head-Gordon, D. J. Fox, K. Raghavachari, and L. A. Curtis, J. Chem. Phys. **90**, 5622 (1989).

[25] B. J. Smith, K. Branson, and G. Schüürmann, Chem. Phys. Lett. **342**, 402 (2001).

[26] P. Hohenberg and W. Kohn, Phys. Rev. B (1964).

[27] J. P. Perdew and Y. Wang, Phys. Rev. B **33**, 8800 (1986).

[28] A. D. Becke, Phys. Rev. A **38**, 3098 (1988).

[29] C. T. Lee, W. T. Yang, and R. G. Parr, Phys. Rev. B **37**, 785 (1988).

[30] A. D. Becke, J. Chem. Phys. **98**, 5648 (1993).

[31] K. Hirao, Chem. Phys. Lett. **190**, 374 (1992).

[32] K. Hirao, Chem. Phys. Lett. (1992).

[33] O. Sinanoglu, Adv. Chem. Phys. **6**, 315 (1964).

[34] J. C. Slater, Phys. Rev. **36**, 0057 (1930).

[35] S. F. Boys, Proc. R. Soc., London **200**, 542 (1950).

[36] T. H. Dunning, Jr., J. Chem. Phys. **90**, 1007 (1989).

[37] R. A. Kendall, T. H.Dunning Jr., and R. J. Harrison, J. Chem. Phys. **96**, 6796 (1992).

[38] D. L. Bunker, Methods Comput. Phys. **10** (1971).

[39] A. J. C. Varandas, Adv. Chem. Phys. **74**, 255 (1988).

[40] J. S. Wright and S. K. Gray, J. Chem. Phys. **69**, 67 (1978).

[41] S. Sato, J. Chem. Phys. p. 2465 (1955).

[42] F. O. Ellison, J. Am. Chem. Soc. p. 3540 (1963).

[43] A. J. C. Varandas and J. N. Murrell, Faraday Discuss. Chem. Soc. **62**, 92 (1977).

[44] A. J. C. Varandas, Mol. Phys. **53**, 1303 (1984).

[45] A. J. C. Varandas, Chem. Phys. Lett. **194**, 333 (1992).

[46] A. J. C. Varandas, J. Mol. Struc (THEOCHEM) **120**, 401 (1985).

[47] A. J. C. Varandas and J. D. da Silva, J. Chem Soc. Farad. Trans. II **82**, 593 (1986).

[48] A. J. C. Varandas and J. Brandão, Mol. Phys. **45**, 857 (1982).

[49] A. J. C. Varandas and J. Brandão, Mol. Phys. **57**, 387 (1986).

[50] M. R. Pastrana, L. A. M. Quintales, J. Brandão, and A. J. C. Varandas, J. Phys. Chem. **94**, 8073 (1990).

[51] A. J. C. Varandas and S. P. J. Rodrigues, Spectrochim. Acta **58**, 629 (2002).

[52] E. Martínez-Núñez and A. J. C. Varandas, J. Phys. Chem. A **105**, 5923 (2001).

[53] A. J. C. Varandas and A. A. C. C. Pais, in *Theoretical and Computational models for organic chemistry*, edited by S. Formosinho, I. Czismadia, and L. Arnaut (Kluwer Academic Publishers, 1991), p. 55.

[54] H. G. Yu and A. J. C. Varandas, Chem. Phys. Lett. **334**, 173 (2001).

[55] A. J. C. Varandas and L. Zhang, Chem. Phys. Lett. **331**, 474 (2000).

[56] A. J. C. Varandas and L. Zhang, Chem. Phys. Lett. **385**, 409 (2004).

[57] H. Golstein, *Classical Mechanics* (Addison-Wesley, London, 1950).

[58] R. Fletcher, *Practical methods of optimization* (Wiley, 2000), 2nd edn.

[59] S. P. J. Rodrigues, A Monte Carlo based program for optimization of potential energy surfaces, Developed at the T&CC group, Coimbra.

[60] *IUPAC Compendium of chemical terminology* (IUPAC, 1997), 2nd edn.

[61] M. A. Collins, Adv. Chem. Phys. **93**, 389 (1996).

[62] M. A. Collins, Theor. Chem. Acc. **108**, 313 (2002).

[63] T. Hollebeek, T. Ho, and H. Rabitzn, Ann. Rev. Chem. Phys. **50**, 537 (1999).

Chapter 2

A global potential energy function for HSO_2

Phys. Chem. Chem. Phys **7**, 2305 (2005).

Double many-body expansion potential energy surface for ground state HSO_2

M. Y. Ballester and A.J.C. Varandas

Departamento de Química, Universidade de Coimbra
P-3049 Coimbra Codex, Portugal.

(Received: 20th January 2005, Accepted 18th April 2005)

Abstract

A global potential energy surface is reported for the ground electronic state of HSO_2 by using the double many-body expansion (DMBE) method. It employs realistic DMBE functions previously reported from accurate *ab initio* calculations (in some cases, fine tuned to spectroscopic data) for the triatomic fragments, and four-body energy terms that were modelled by fitting novel *ab initio* FVCAS/AVTZ calculations for the tetratomic system. In some cases, FVCAS/AVDZ energies have been employed after being scaled to FVCAS/AVTZ ones. To assess the role of the dynamical correlation, exploratory single-point Rayleigh-Schrdinger perturbations calculations have also been conducted at one stationary point. All reported calculations are compared with previous *ab initio* results for the title system. The potential energy surface predicts HOSO to be the most stable configuration, in good agreement with other theoretical data available in the literature. In turn, the HSO_2 isomer with H bonded to S is described as a local minimum, which is stable with respect to the $H + SO_2$ dissociation asymptote.

1 Introduction

Sulfur has long been recognized as a major contaminant in the atmosphere. It comes both from natural and anthropogenic sources, having significant implications in environmental issues such as acid rain, air pollution, and global climate changes. Although a significant part of sulfur containing molecules reacts with water in the troposphere and eventually precipitates as sulfur aerosols, some (such as COS) may reach the stratosphere and have implications in the ozone budget.[1] Among the sulfur compounds, the HSO_2 isomers are supposed to play an important role in atmospheric and combustion chemistry.[2–13] In particular, the HSO_2 adduct is thought to be responsible for the catalytic removal of atomic hydrogen in flames[14–16] through the following reactions:

$$H + SO_2 + M \rightarrow HSO_2 + M \quad (1)$$

$$HSO_2 + H \rightarrow SO_2 + H_2 \quad (2)$$

In turn, the thylperoxyl radical (HSOO) has been pointed out to play a role in the atmosphere via oxidation of sulfur species,[17] including the action as a sink of SH through the addition reaction:[18]

$$SH + O_2 + M \rightarrow HSOO + M \quad (3)$$

Table 1 compiles the energetics of all exothermic processes that may occur on the title potential energy surface, as extracted from experimental sources quoted in cited references.

Despite some theoretical studies of the HSO_2 isomers using *ab initio* MO calculations[3–12] and DFT[13] theory, no global potential energy surface has thus far been reported for the electronic ground state of HSO_2. Such a scarcity of electronic structure calculations on the full six-dimensional configuration space of HSO_2 has prompted us to model a global potential energy surface for the title species by using double many-body expansion (DMBE) theory.[19–21] This approach has been successfully applied to a wealth of triatomic systems (including all ground-state triatomic fragments of HSO_2, namely, HO_2,[22] SO_2,[23] and HSO[24]) as well as tetratomic (O_4[25, 26] and HO_3[27]) and even larger polyatomic (HO_4[28] and HO_5[29]) systems. Of course, an alternative to the use of a global potential energy surface,

Table 1. Energetics of the exothermic processes occurring on the ground-state HSO_2 potential energy surface[a].

Process	classical exothermicity[b] ($kcal\,mol^{-1}$)	Refs.
$HS + O_2 \rightarrow H + SO_2$	51.7	24,42,43
$HS + O_2 \rightarrow OH + SO$	24.1	24,42,23
$OH + SO \rightarrow H + SO_2$	27.6	24,43,24,23
$H + SOO \rightarrow S + HO_2$	30.6	22,23
$H + SOO \rightarrow HS + O_2$	63.3	23,24,42
$H + SOO \rightarrow OH + SO$	87.5	23,24,43
$H + SOO \rightarrow H + SO_2$	115.0	23
$O + HSO \rightarrow HS + O_2$	21.7	24,42
$O + HSO \rightarrow OH + SO$	45.8	24,43
$O + HSO \rightarrow H + SO_2$	73.4	24,23
$S + HO_2 \rightarrow O + HSO$	11.0	22,24
$S + HO_2 \rightarrow HS + O_2$	32.8	22,24
$S + HO_2 \rightarrow OH + SO$	56.9	22,43,24
$S + HO_2 \rightarrow H + SO_2$	84.4	22,23

[a]Except where indicated in the original papers, the reported energies are mostly experimental, and are reproduced by the DMBE potential energy surface of the present work.

[b]The quantum mechanical zero-point energy of the reactants and products is not taken into account.

would be to carry out dynamics studies where the latter is calculated on the fly (for a review see, *e.g.*, Ref. 30). Although the potential energy surface generated from such calculations could eventually be employed for further dynamics studies, it is hard to anticipate whether a sufficiently accurate function can be generated via such a scheme. There are two major reasons for our worry. First, if the electronic structure calculations were done purely *ab initio* (for a semi-empirical, yet expensive, scheme based on the scaling of the dynamical correlation energy, see Ref. 31), this would in principle require an awful amount of computational time to achieve sufficient accuracy for the dynamics studies, as it involves many electrons with a second-row sulfur atom. Second, as discussed later, the reaction path may evolve through the HOSO deep chemical well (with a well depth of about $70\,\mathrm{kcal\,mol^{-1}}$) and hence exploratory dynamics calculations have shown that the trajectories generating the potential energy surface might involve typically 10^5 solutions of the electronic Schrdinger equation (to calculate the energy, gradients, and eventually force constants) per trajectory for proper conservation of the total energy and angular momentum. Thus, the DMBE approach definitely stands as a viable one, particularly having in mind its fair predictive character when the cluster expansion is truncated at the three-body energy terms for which realistic DMBE functions have already been reported (see section 3.1).

The paper is organized as follows. Section 2 describes the results of new *ab initio* calculations carried out for HSO_2, while the DMBE methodology is discussed and applied in section 3 by focusing on the title system. The characterization of the most relevant stationary points of the novel HSO_2 DMBE potential energy surface is then presented in section 4. Section 5 gathers the major conclusions.

2 *Ab initio* calculations

The results of *ab initio* calculations[3–12] for ground state HSO_2 differ across the various studies reported in literature. In order to get further information, we have performed our own *ab initio* calculations at the FVCAS (full valence complete active space) level aiming at characterizing the most relevant stationary points of the electronic ground state of HSO_2. The aug-cc-pVDZ (AVDZ) and aug-cc-pVTZ (AVTZ) basis sets of Dunning[32, 33] have been employed on the framework

of the MOLPRO[34] code. We are aware that the choice of such basis sets may be problematic when second-row atoms are involved. In fact, it has been argued[35, 36] that the original Dunning's[32, 33] correlation consistent basis sets for the third row elements lack proper core polarization functions to be reliable. Although schemes[35, 36] have been suggested to overcome such a limitation, the calculations would still be rather expensive and hence such basis sets have not been employed here. In fact, calculations on the tetratomic have been mostly used to calibrate the saddle point for the reaction $H + SO_2 \rightleftharpoons HOSO$, for which our AVDZ calculations scaled to AVTZ ones have shown a satisfactory agreement with the best attributes reported in the literature.[8, 10] In fact, such an agreement will be shown later to be extensive to all characterized stationary points when compared with a wealth of theoretical data from other sources. As starting guesses for the geometry optimizations, we have employed the results reported by Goumri *et al.*[10] from MP2 calculations. Following a recommendation in the MOLPRO manual, the rational functional approach has been used as the search algorithm for the minima, while the quadratic steepest descent method has been employed for transition state optimizations. To obtain the dissociation energy, we have calculated the energy of $H + SO_2$ by keeping SO_2 frozen at its optimum FVCAS/AVTZ geometry while moving away the hydrogen atom until convergence was reached (see Table 2). Due to computational limitations, and because the final results will hopefully not differ drastically, we have characterized the transition states only at the FVCAS/AVDZ level. The Z-matrix format for geometries has been used throughout the calculations.

Table 2 collects the *ab initio* results from the present work. Considering that there has not been a review of the results appeared recently in the literature, we compile the available theoretical properties in two tables, including (for completeness) our results: Unfortunately, only the geometries and absolute energies are compiled in most cases, which may prevent a realistic judgment of the relevant energetics. Table 3 gathers the reported minima, and Table 4 the transition states. In turn, Figure 1 defines the various coordinates: from left to right, γ is the dihedral angle formed by the planes defined by OSO and HOS, OSO and HSO, and SOO and HSO. As seen from Table 2, the global minimum is predicted to have a *cis*-HOSO structure. Note that the calculated $S-O$ and $O-H$ bond

Table 2. Properties of the stationary points in the *ab initio* HSO_2 potential energy surface.

Feature	R_1/a_0	R_2/a_0	R_3/a_0	α/deg	β/deg	γ/deg	E/E_h	ΔE	frequencies/cm^{-1}		
HOSO (FVCAS/AVDZ), min.	2.861	3.137	1.795	108.4	109.7	0.0	−547.91646579		3897	1744	1307
									1013	487	396
HOSO (FVCAS/AVTZ), min.	2.802	3.055	1.790	108.6	111.2	12.8	−547.98517652	−43.1[a]	4074	1215	1131
									853	421	63
HSO_2(FVCAS/AVDZ), min.	2.846	2.846	2.612	123.3	106.0	122.1	−547.85381505	39.3[a]	2329	1149	955
									949	777	429
HSO_2(FVCAS/AVTZ), min.	2.763	2.763	2.589	123.1	106.7	123.7	−547.93165522	33.6[b]	2370	1149	1042
								−6.0[c]	1024	842	471
HSOO(FVCAS/AVTZ), min.	2.517	3.280	2.551	91.1	112.3	87.1	−547.87753994	67.5[b]	2833	1025	956
									650	402	221
HOSO ⇌ H + SO_2(FVCAS/AVDZ), TS_1	2.834	2.910	2.959	115.5	117.7	79.0	−547.82524579	57.2[a]	1130	937	583
								−3.3[d]	463	259	2178i
HOSO ⇌ H + SO_2(FVCAS/AVTZ), TS_1							−547.89447282[e]	56.9[b]			
								17.4[c]			
HOSO ⇌ H + SO_2(CASPT2/AVDZ), TS_1							−548.25528270[e]	7.9[f]			
HOSO ⇌ H + SO_2(CASPT2/AVTZ), TS_1							−548.44894745[e]	9.2[g]			
HOSO ⇌ HSO_2(FVCAS/AVTZ), TS_2	2.840	3.165	2.809	116.0	53.2	60.1	−547.88598339	62.2[b]	2058	1120	750
									666	381	1854i

[a]Energy in kcal mol^{-1} referred to the AVDZ global minimum. [b]Energy in kcal mol^{-1} referred to AVTZ global minimum. [c]Energy in kcal mol^{-1} referred to the H + SO_2 AVTZ asymptote (E = −547.92217966 E_h). [d]Energy in kcal mol^{-1} referred to AVDZ H + SO_2 asymptote (E = −547.8199366 E_h). [e]Energy calculated with at the geometry optimzed using FVCAS/AVDZ. [f]Energy in kcal mol^{-1} referred to the CASPT2/AVDZ H + SO_2 asymptote (E = −548.2679272 E_h). [g]Energy in kcal mol^{-1} referred to the CASPT2/AVTZ H + SO_2 asymptote (E = −548.46365757 E_h).

distances are found to be in good agreement (within 3% or so) with those reported by Qi *et al.*[8] from MP2/6-311G** calculations. In addition, the well depth of the FVCAS/AVTZ global minimum (referred to the $H + SO_2$ dissociation asymptote) is predicted to be 37.8 kcal mol^{-1}, a value that lies close to the DFT estimate[13] of $\Delta_f H^o = (-42.6 \pm 2)$ kcal mol^{-1} for the reaction

$$HOSO \rightarrow H + SO_2 \qquad (4)$$

Two local minimum with H bound to S are also predicted (see the third and fourth entries of Table 2). Of these, the HSO_2 isomer has been previously reported[4–6, 8, 10, 12] as being a stable species with respect to the dissociation asymptote in reaction (4), although there are important differences in the reported relative energies. The optimum geometry of this isomer is found to lie only 4.2 kcal mol^{-1} below the $H + SO_2$ dissociation limit. It corresponds to an almost undisturbed SO_2 molecule with a hydrogen bound to sulfur such as to form a structure with C_{2v} symmetry. The other isomer reported in the fifth entry of Table 2 corresponds to a HSOO structure. This has also been previously reported in the literature,[5, 37] and judged to be a possible sink of SH in the atmosphere via reaction (3). Note that the $H + SO_2$ recombination process to form HOSO has to overcome an energy barrier (transition state TS_1) of 7.9−17.4 kcal mol^{-1}. Such a result agrees with the commonly accepted fact[12] that the reverse of reaction (4) is a highly energetic process. Similarly, the transition state (TS_2) for the isomerization reaction HOSO $\rightleftharpoons$ HSO_2 (see tenth entry of Table 2) shows a barrier height of 62.2 kcal mol^{-1}, also in agreement with experiment.[12]

Except for the global minimum calculated at the FVCAS/AVDZ level, the harmonic frequencies of all reported stationary points have been computed using the program FREQUENCIES implemented in MOLPRO. For the former, they have been determined by fitting a grid of 972 *ab initio* points to a complete cubic polynomial. We emphasize that geometry optimizations of saddle points are carried out only at the FVCAS/AVDZ level. To show that such saddle points are actual transition states, we depict in Figure 2 the vibrational normal modes associated with the corresponding imaginary frequencies. Despite the good agreement with previously reported values in the literature, a higher level of *ab initio* calculations including dynamical correlation will naturally be required for additional accu-

Table 3. Properties of *ab initio* minima reported in the literature for HSO_2.

Feature	R_1/a_0	R_2/a_0	R_3/a_0	α/deg	β/deg	γ/deg	E/E$_h$	
HOSO	2.765	3.054	1.788	108.2	112.4	61.1	−547.8133	HF/6-311G**[8]
	2.782	3.127	1.831	106.7	109.7	0.0	−548.3392	MP2/6-311G**[8]
	2.774	3.067	1.801	108.2	111.5	59.5		HF/6-31G*[3]
	2.801	3.139	1.858	109.8	106.9	0.0		MP2/6-31G*[5]
	2.853	3.069	1.833	107.5	115.2	74.7	−545.0903	HF/3-21G*[3]
	2.797	3.141	1.892	111.4	111.0	0.0	−545.4553	MP2/3-21G*[3]
	2.772	3.069	1.799	107.1	111.5			UHF/DZP[4]
	2.814	3.156	1.861	109.6	109.7			MP2/DZP[4]
	2.806	3.154	1.833	108.8	105.9	0.4	−548.4601	MP4/6-311++G(2d,2p)[11]
	2.861	3.137	1.795	108.4	109.7	0.0	−547.916466	FVCAS/AVDZ[a]
	2.802	3.055	1.790	108.6	111.2	12.8	−547.985177	FVCAS/AVTZ[a]
HSO_2	2.706	2.706	2.557	123.3	126.8		−547.7546	HF/6-311G**[8]
	2.770	2.770	2.602	125.3	105.6		−548.2933	MP2/6-311G**[8]
	2.719	2.719	2.532	123.6	106.6			HF/6-31G*[3]
	2.734	2.734	2.532	122.5	106.8		−545.0213	HF/3-21G*[3]
	2.797	2.797	2.606	125.1	106.4		−545.4125	MP2/3-21G*[3]
	2.734	2.734	2.549		106.6			UHF/DZP[4]
	2.812	2.812	2.615		106.0			MP2/DZP[4]
	2.784	2.784	2.593	124.4	105.6	122.0	−548.418867	MP4/6-311++G(2d,2p)[11]
	2.846	2.846	2.612	123.3	106.0	122.1	−547.853815	FVCAS/AVDZ[a]
	2.763	2.763	2.589	123.1	106.7	123.7	−547.931655	FVCAS/AVTZ[a]
HSOO	2.506	3.177	2.476	96.5	113.3	86.2		HF/6-31G*[5]
	2.534	3.281	2.659	97.3	110.7	86.2		MP2/3-21G*[5]
	2.538	3.313	2.481	94.6	112.7	83.7		MP2/6-31G*[5]
	2.517	3.280	2.551	91.1	112.3	87.1	−547.877540	FVCAS/AVTZ[a]
gauche	2.530	3.275	2.457	94.7	113.0	84.0	−548.36285	MP2/cc-pVTZ[37]
anti	2.428	3.315	2.425	91.1	110.4	178.0	−548.36134	MP2/cc-pVTZ[37]

[a]This work.

Table 4. Properties of *ab initio* transition states reported in literature for HSO_2.

Feature	R_1/a_0	R_2/a_0	R_3/a_0	α/deg	β/deg	γ/deg	E/E$_h$	Calculation level
$H + SO_2 \rightleftharpoons HOSO$	2.700	2.729	2.819	120.2	127.8	77.7	−548.2440	MP2/6-311G**[8]
	2.723	2.772	2.929	120.5	124.9	81.8	−545.3616	MP2/3-21G*[3]
	2.723	2.797	2.848	120.2	125.2	78.2		MP2/6-31G(d)[10]
	2.748	2.806	3.042	117.0	121.7	78.8		QCISD/6-311G(d,p)[10]
	2.834	2.910	2.959	115.5	117.7	79.0	−547.894447	FVCAS/AVTZ[a]
$HOSO \rightleftharpoons HSO_2$	2.702	3.002	2.538	113.6	60.3	104.8	−547.7100	HF/6-311G**[8]
	2.755	2.969	2.695	117.1	57.9	107.5	−548.2409	MP2/6-311G**[8]
	2.717	3.020	2.553	114.0	60.6	104.9		HF/6-31G*[5]
	2.736	3.069	2.583	113.8	60.7	105.3	−544.9725	HF/3-21G*[3]
	2.799	3.078	2.630	118.1	57.4	106.5	−545.3579	MP2/3-21G*[3]
	2.780	2.993	2.670	118.1	58.5			MP2/6-31G(d)[10]
	2.840	3.165	2.809	116.0	53.2	60.1	−547.885984	FVCAS/AVTZ[a]
$HS + O_2 \rightleftharpoons HSOO$	2.239	4.382	2.513	115.3	87.3	101.0	−548.39245	MRMP2(9,10)/cc-pVTZ[37]

[a]This work.

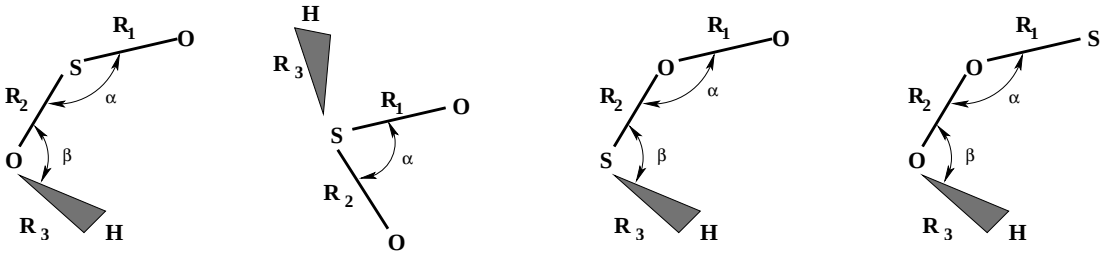

Figure 1. Coordinates used to describe the stationary points of HSO_2 potential energy surface: HOSO, HSO_2, HSOO, and HOOS geometries.

racy. For example, perturbation calculations using the CAS wave function (*i.e.*, CASPT2 with AVXZ, X = 2, 3) have been found[38] to give good results for SO_2, and hence such an approach may be recommendable for the title system. Since such data is here used only to characterize the stationary points, we believe that the current level of theory may have no serious implications on the quality of the global DMBE potential energy surface reported in the present work.

3 The double many body expansion formalism

The DMBE method has been reviewed in detail elsewhere,[19–21] and hence we review only the basic details. It has also been used to construct the potential energy surfaces of all triatomic fragments of relevance in the present work,[22–24] with the reader being referred to the original papers for details. In DMBE theory, the energy is partitioned into its dynamical correlation (*dc*) and extended Hartree-Fock (EHF) components, with each term being developed as a cluster (many-body) expansion. For a N-atom system, a single-sheeted potential energy surface assumes the form:

$$V(\mathbf{R^N}) = \sum_{n=2}^{N} \sum_{\mathbf{R^n} \subset \mathbf{R^N}} [V_{\rm EHF}^{(n)}(\mathbf{R^n}) + V_{\rm dc}^{(n)}(\mathbf{R^n})] \tag{5}$$

where

$$V_x(\mathbf{R^N}) = \sum_{\alpha\beta} V_x^{(2)}(\mathbf{R^2}) + \sum_{\alpha\beta\gamma} V_x^{(3)}(\mathbf{R^3}) + \sum_{\alpha\beta\gamma\rho} V_x^{(4)}(\mathbf{R^4})... \qquad x = EHF, dc \tag{6}$$

In Eq. (5), $\mathbf{R^n}$ specifies any set of $n(n-1)/2$ interatomic distances referring to n-atoms while, in Eq. (6), $V_x^{(2)}$, $V_x^{(3)}$ and $V_x^{(4)}$ are two-, three-, and four-body terms

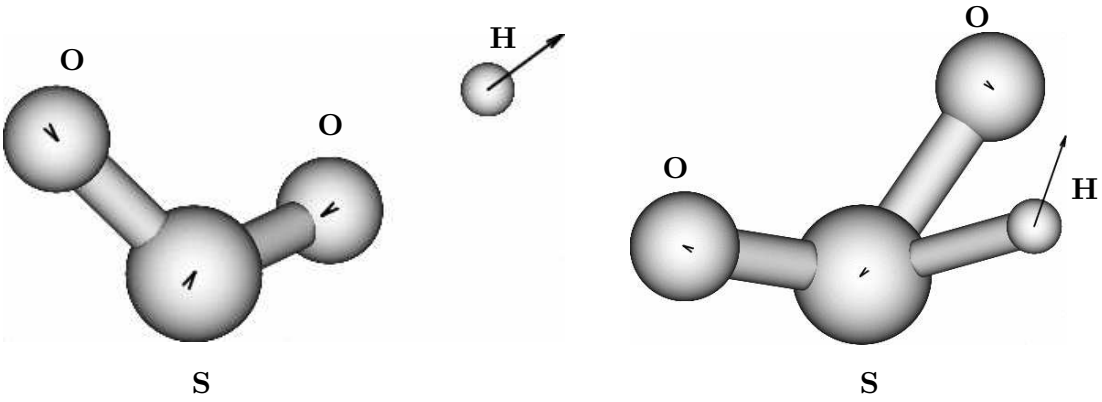

Figure 2. Geometry of *ab initio* saddle points TS_1 and TS_2. The arrows indicate the force constants associated with the imaginary frequencies.

of the x-energy component, respectively; $\mathbf{R^N}$ denotes the full set of interatomic coordinates $\mathbf{R^N} \equiv R_1, R_2, ..., R_{N(N-1)/2}$. Note that the summations over $\alpha\beta$ and $\alpha\beta\gamma$ imply all diatomic and triatomic fragments, and so on. In the following, we focus on the two and three-body energy terms used to construct the HSO_2 DMBE potential energy surface.

The two-body EHF energy assumes the form:

$$V^{(2)}_{\rm EHF}(R) = DR^{-1}\left(1 + \sum_{i=1}^{3} a_i r^i\right)\exp(-\gamma(r)r) + \chi_{\rm exc}(R)V^{asym}_{\rm exc}(R) \qquad (7)$$

where

$$V^{asym}_{\rm exc}(R) = -\tilde{A}R^{\tilde{\alpha}}(1 + \tilde{a}_1 R + \tilde{a}_2 R^2)\exp(-\tilde{\gamma}R), \qquad (8)$$

is the asymptotic exchange energy, and $\chi_{\rm exc}(R)$ a convenient damping function to account for charge overlap effects (this is usually expressed as the dispersion damping function χ_n for the lowest n-th power in the dynamical correlation expansion; see later): $\tilde{A}$, $\tilde{a}_i$ $(i = 0 - 2)$, $\tilde{\alpha}$, and $\tilde{\gamma}$ are usually taken[39] as *a priori* theoretical parameters. In turn, the range determining exponent in the short-range contribution is expressed as[39]

$$\gamma = \gamma_0[1 + \gamma_1 \tanh(\gamma_2 r)] \qquad (9)$$

where $r = R - R_e$ is the displacement coordinate from the equilibrium diatomic geometry, and γ_i $(i = 0 - 2)$ are coefficients to be determined to fulfill specific

requirements.[39]

The two-body dynamical correlation is in turn written as:

$$V_{\rm dc}^{(2)}(R) = -\sum_n C_n \chi_n(R) R^{-n} \tag{10}$$

with the associated damping functions χ_n assuming the form

$$\chi_n(R) = \left[1 - \exp\left(-A_n \frac{R}{\rho} - B_n \frac{R^2}{\rho^2}\right)\right]^n \tag{11}$$

where $A_n = \alpha_0 n^{-\alpha_1}$ and $B_n = \beta_0 \exp(-\beta_1 n)$ are auxiliary functions defined by the following dimensionless universal parameters: $\alpha_0 = 16.36606$, $\alpha_1 = 0.70172$, $b_0 = 17.19338$, $\beta_1 = 0.09574$. Moreover, for a given pair of atoms XY, one has $\rho = 5.5 + 1.25\left(\langle r_X^2\rangle^{1/2} + \langle r_Y^2\rangle^{1/2}\right)$. The remaining coefficients appearing in Eqs. (7)-(11), including the expectation values of the squared radii $\langle r_X^2\rangle$ of the outermost electrons in atom X used to define[40] R_0 [and, eventually, the order of the exchange damping function in Eq. (7)], are chosen to reproduce available theoretical and experimental data in the diatomic. When available, the long-range (electrostatic and induction) components of the extended Hartree-Fock energy, are also modelled[19–21] using a formalism similar to that employed for the dynamical correlation.

To represent the three-body dynamical correlation and electrostatic energies, we use the general form:[41]

$$V_{\rm ele}^{(3)}(\mathbf{R^3}) = \sum_i \sum_n f_i(\mathbf{R^3}) C_n^{(i)}(R_i, \theta_i) \chi_n(r_i) r_i^{-n} \tag{12}$$

where i labels the I − JK channel, and (r_i,R_i,θ_i) are the corresponding Jacobi coordinates. In turn, $C_n^{(i)}(R_i, \theta_i)$ are long range coefficients, which assume the values $n = 4, 5$, respectively for the dipole-quadrupole and quadrupole-quadrupole interactions. For $n = 6, 8$, and 10, $C_n^{(i)}(R_i, \theta_i)$ represent atom-diatom dispersion coefficients. As already noted, χ_n are damping functions defined in Eq. (11) for each specific value of n, while the switching functions f_i assume the form:

$$f_i(\mathbf{R^3}) = \frac{1}{2}\{1 - \tanh[\xi(\eta s_i - s_j - s_k)]\} \tag{13}$$

where $s_i = R_i - R_i^{ref}$ (i=1 − 3) is the displacement from a reference geometry. Finally, the three-body extended Hartree-Fock energy assumes the form:

$$V_{\rm EHF}^{(3)}(\mathbf{R^3}) = \sum_i^n P_i^{(3)}(\mathbf{R^3}) T_i^{(3)}(\mathbf{R^3}) \tag{14}$$

where $P_i^{(3)}$ is a three-body polynomial, $T_i^{(3)}$ a range-determining function, and n the number of distributed[24] three-body polynomials used for the fit (the number and degree of such polynomials depend on the fitting requirements that were actually imposed on modelling the various triatomic systems).

3.1 Two-body and three-body energy terms in HSO_2

Using for the coefficients in Eq. (7) to Eq. (14) the numerical data reported in the literature,[22–24, 42, 43] one may write a two plus three-body DMBE potential energy surface for the ground state of HSO_2 as:

$$V(\mathbf{R^4}) = \sum_{\rm i=1}^{6} {\rm V}^{(2)}(\mathbf{R_i^2}) + \sum_{\rm j=1}^{4} {\rm V}^{(3)}(\mathbf{R_j^3}) \tag{15}$$

where $\mathbf{R_i^2} \equiv R_i$ is the interatomic distance of the i-th diatomic pair, and $\mathbf{R_j^3}$ denotes a collective variable of the three bond distances which specify the geometry of the j-th triatomic fragment.

As pointed out elsewhere,[41] due to an overcounting of the two-body dynamical correlation energy, each $V_{\rm dc}^{(2)}(\mathbf{R_i^2})$ term in the DMBE potential energy surfaces of HSO[24] and SO_2[23] has been multiplied by a switching function like Eq. (13), which transforms such contributions into three-body like ones. Thus, an extra three-body energy term should be added to Eq. (15). Taking into account the properties of $f_i(\mathbf{R})$, such an additional term may be written as follows:

$$V_{\rm add}^{(3)} = \sum_{i=1}^{9} V_{\rm dc}^{(2)}(\mathbf{R_i^2}) \left[f_i(\mathbf{R_i^3}) - 1 \right] \tag{16}$$

which, when taken into account, reproduces all the asymptotic limits of the tetratomic potential energy surface (*i.e.*, if one of the atoms is placed far away from the remaining triatomic, the resulting potential energy surface matches exactly that of the triatomic fragment). We should note that such considerations

do not apply to the HO_2 DMBE potential energy surface, which has been constructed using an earlier formalism. A final remark to point out that the diatomic potentials (OH and O_2) originally employed in HO_2 are somewhat simpler (and hence somewhat less accurate) than those used for HSO and SO_2 (see Tables 1 and 2 of Ref. 24, and Table 1 of Ref. 38). For consistency, we have replaced them by corresponding updated diatomic curves.[44] As shown in Table 5, such an update does not affect significantly the attributes of the HO_2 potential energy surface in comparison with those of the original form.

3.2 Four-body electrostatic energy term

To represent the four-body electrostatic energy, we have generalized the form[41] employed for the three-body energy in Eq. (12) by using the expression:

$$V_{\rm ele}^{(4)}(\mathbf{R^4}) = \sum_i \sum_{n=3,4,5} f_i(\mathbf{R^4}) C_n^{(i)}(R_i, R_{i+3}, \theta_i, \theta_{i+3}, \phi_i) \chi_n(r_i) r_i^{-n} \qquad (17)$$

where $\mathbf{R^4}$ is now a collective variable for the six distances defining the tetratomic. Thus, (r_i, θ, ϕ) are the intermolecular coordinates illustrated in Figure 3, while $f_i(\mathbf{R^4})$ are switching functions similar to those in Eq. (13) but expressed in terms of the generalized coordinates $S_i = s_i + s_{i+3}$,

$$f_i(\mathbf{R^4}) = \frac{1}{2}\{1 - \tanh[\beta(\eta S_i - S_j - S_k)]\} \qquad (18)$$

with $s_i = R_i - R_i^{ref}$ being the displacement coordinate from the equilibrium distance in the i-th diatomic fragment, R_i^{ref}; corresponding definitions apply to the indexes j and k. The values of the β and η parameters are chosen from the requirement that $f_i(\mathbf{R^4})$ must vanish when one of the atoms is placed infinitely far apart from the remaining triatomic. Moreover, it must be equal to unit at the diatom-diatom dissociation limit; for the equilibrium distances of all diatomics, see Table 7. In turn, $\chi_n(r_i)$ are the damping functions defined in Eq. (11), while R_0 is here calculated from $R_0 = 2\left(\langle r_{\rm AB}^2\rangle^{\frac{1}{2}} + \langle r_{\rm CD}^2\rangle^{\frac{1}{2}}\right)$, where $\langle r_{\rm X_1X_2}^2\rangle$ is the expectation value of the squared radius for the outermost electrons in the united atom that originates from the coalescing diatomic X_1X_2 when the internuclear separation approaches zero.

To represent the electrostatic long range coefficients as a function of the inter-

Table 5. Attributes of HO_2 DMBE potential energy surface[22] before and after replacing the diatomic potentials with their updated versions

Classification	Property	DMBE-IV	DMBE-IV-modified
Global Minimum	R_1	2.5143	2.5206
	R_2	1.8345	1.8315
	R_3	3.4590	3.4516
	E	−0.2790	−0.2786
	ω_1	1100.38	1071.51
	ω_2	1352.94	1320.97
	ω_3	3484.28	3479.76
Saddle point for	R_1	2.8062	2.8069
HO_2 isomerization	R_2	2.2715	2.2758
	R_3	2.2715	2.2758
	E	−0.2141	−0.2157
	ω_1	2235.8i	2217.9i
	ω_2	925.62	962.97
	ω_3	2719.46	2726.48
van der Waals	R_1	2.2819	2.2820
$H\cdots O_2$ structure	R_2	9.8289	9.4606
	R_3	7.5470	7.1786
	E	−0.1916	−0.1917
	ω_1	4.74i	8.78i
	ω_2	40.42	59.50
	ω_3	1576.21	1542.12
Hydrogen-bond	R_1	5.6632	5.7511
$OH\cdots O$ structure	R_2	3.8211	3.9084
	R_3	1.8421	1.8427
	E	−0.1738	−0.1728
	ω_1	237.83	247.92
	ω_2	156.59	117.76
	ω_3	3694.92	3671.13

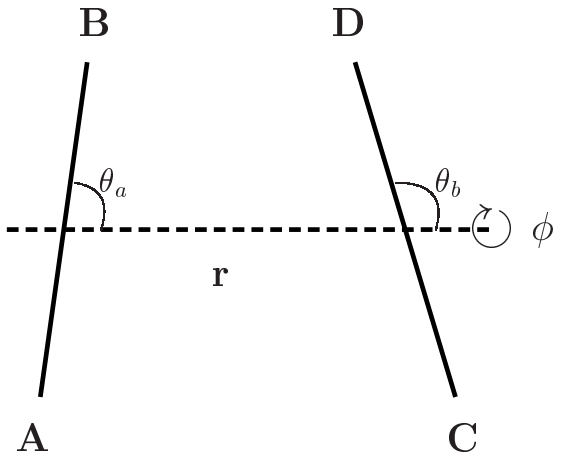

Figure 3. Intermolecular coordinates used to define four-body electrostatic energy term.

molecular coordinates (Figure 3), we use the well established forms:[45]

$$C_3 = -\mu_{\mathrm{AB}}(R_{\mathrm{AB}})\mu_{\mathrm{CD}}(R_{\mathrm{CD}})(2\cos\theta_a\cos\theta_b - \sin\theta_a\sin\theta_b\cos\phi) \tag{19}$$

$$C_4 = \frac{3}{4}\{\mu_{\mathrm{AB}}(R_{\mathrm{AB}})\Theta_{\mathrm{CD}}(R_{\mathrm{CD}})[\cos\theta_a(3\cos^2\theta_b - 1) - 2\sin\theta_a\sin\theta_b\cos\theta_b\cos\phi]\} - \\ - \mu_{\mathrm{CD}}(R_{\mathrm{CD}})\Theta_{\mathrm{AB}}(R_{\mathrm{AB}})[\cos\theta_b(3\cos^2\theta_a - 1) - 2\sin\theta_a\sin\theta_b\cos\theta_a\cos\phi]\} \tag{20}$$

$$C_5 = \frac{3}{16}\Theta_{\mathrm{AB}}(R_{\mathrm{AB}})\Theta_{\mathrm{CD}}(R_{\mathrm{CD}})[1 - 5\cos^2\theta_a - 5\cos^2\theta_b - 15\cos^2\theta_a\cos^2\theta_b + \\ + 2(\cos\theta_a\cos\theta_b - \sin\theta_a\sin\theta_b\cos\phi)^2] \tag{21}$$

where $\mu(R_{\mathrm{X_1X_2}})$ and $\Theta(R_{\mathrm{X_1X_2}})$ are the permanent dipolar and quadrupolar electric moments of the $\mathrm{X_1X_2}$ pair as a function of diatomic distance $R_{\mathrm{X_1X_2}}$. To express the angles in terms of the more convenient set of bond distances, we have used approximate expressions reported elsewhere:[27]

$$\cos\theta_a \approx \frac{R_{\mathrm{BD}} + R_{\mathrm{BC}} - R_{\mathrm{AC}} - R_{\mathrm{AD}}}{2R_{\mathrm{AB}}} \tag{22}$$

$$\cos\theta_b \approx \frac{R_{\mathrm{BD}} + R_{\mathrm{AD}} - R_{\mathrm{AC}} - R_{\mathrm{BC}}}{2R_{\mathrm{CD}}} \tag{23}$$

$$\sin\theta_a\sin\theta_b\cos\phi \approx \frac{(R_{\mathrm{BD}} - R_{\mathrm{BC}} + R_{\mathrm{AC}} - R_{\mathrm{AD}})(R_{\mathrm{AD}} + R_{\mathrm{AC}})}{2R_{\mathrm{AB}}R_{\mathrm{CD}}} \tag{24}$$

Note that this should not have significant implications in the least-squares fit used in the calibration procedure (see later), as this is done subsequently to the

replacement of the trigonometric functions. A final remark to point out that the quadrupole moments are specified using the convention of Hirschfelder *et al.*:[46]

$$\Theta = \Theta_{zz} = \sum_i e_i(3z_i^2 - r_i^2\delta_\alpha^\beta) \tag{25}$$

This is a relevant issue, since the potential energy surfaces of SO_2[23] and HSO[24] have followed the Buckingham[45] convention which includes a multiplicative factor of 1/2. The four-body electrostatic energy calculated from Eq. (17) is illustrated in panels (a) of Figures 4-7, which show an atom moving around the remaining triatomic. The most salient feature from such plots is possibly the fact that the electrostatic energy may change sign with the geometrical arrangement of the four atoms, and hence can play a significant role especially at low energies. Also shown is the fact that $V_{\rm ele}^{(4)}(\mathbf{R^4})$ vanishes when one atom is removed to infinitely far away from the remaining triatomic fragment.

3.3 Four-body extended Hartree-Fock energy term

As a first step in the construction of the four-body extended Hartree-Fock energy term $V_{\rm EHF}^{(4)}$, we have first analyzed the features of the potential energy surface that is obtained by using only the two-body, three-body and four-body electrostatic terms (hereafter referred to as $2+3+4_{\rm ele}$ DMBE potential energy surface). By comparing the $2+3+4_{\rm ele}$ DMBE potential energy surface so obtained with the theoretical results reported in the literature and our own *ab initio* calculations, we have established the major differences that require being corrected. They are a too deep well predicted by the $2+3+4_{\rm ele}$ DMBE potential energy surface for the HSO_2 isomer [see Figure 4(b) and properties of HSO_2 in Table 3 at different levels of calculation], the absence of a barrier for formation of HOSO from $H + SO_2$ [see Figure 8(a)], and a too deep minimum obtained when SH approaches O_2 to form a HSOO structure [see Figure 9(a)]. Thus, we have found satisfactory to employ simple local four-body EHF forms that could bring the final DMBE surface into agreement with such *ab initio* data (namely, at the regions close to the TS_1 transition state and local minima of HSOO and HSO_2). These functions are further required to die-off quickly as one moves away from the regions surrounding such stationary points. One should note that the geometry of the HSO_2 isomer

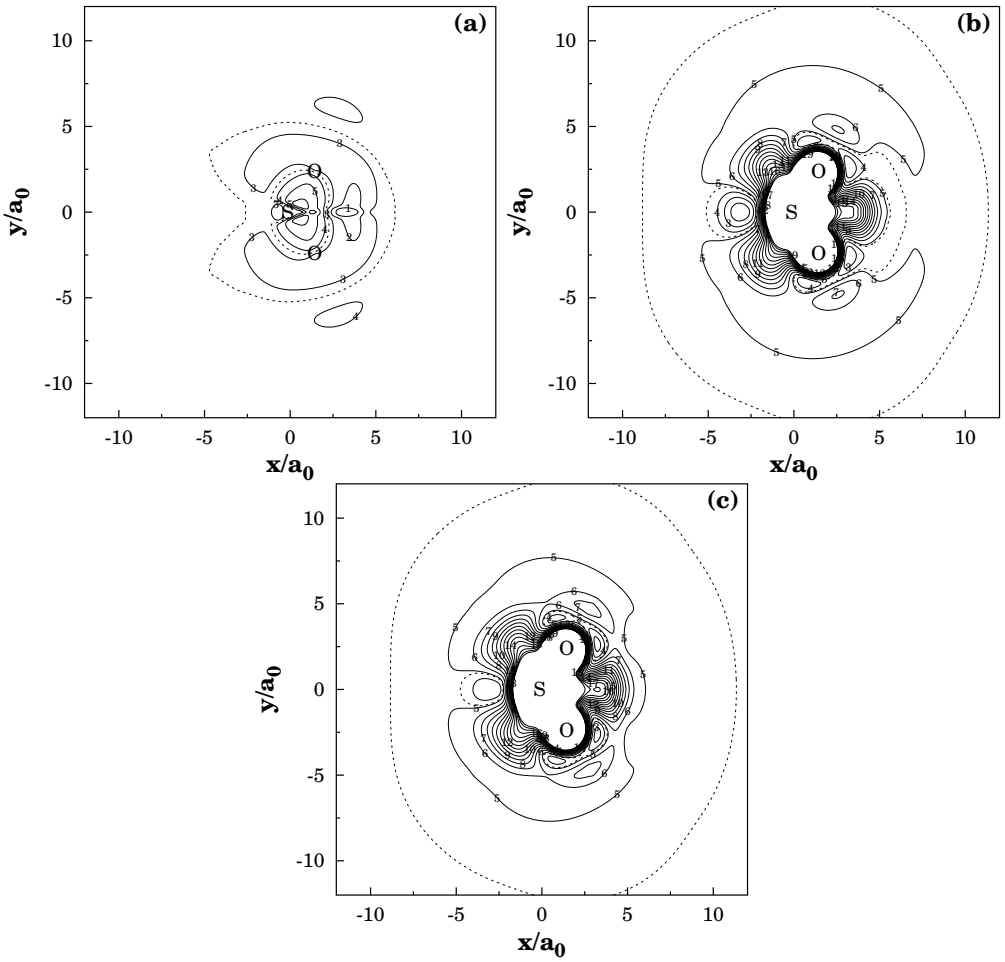

Figure 4. Contour plot for H moving coplanarly around a partially relaxed SO_2. Panel (a) shows the four-body electrostatic energy term, with contours starting at $-0.01\,E_h$, equally spaced by $0.003\,E_h$. The dashed contour indicates the zero of energy. Shown in panel (b) is the potential energy surface including only the four-body electrostatic energy terms, while panel (c) shows the full DMBE surface. Contours in panels (b) and (c) start at $-0.4770\,E_h$, and are equally spaced by $0.017\,E_h$. The dashed contours shown in panels (b) and (c) indicate the $H + SO_2$ dissociation limit ($-0.4132\,E_h$). Note that, except in the case of the electrostatic energy where such contours correspond to the change of sign of this energy contribution, they refer in these and subsequent plots to the indicated energies which are quoted to four significant figures. Thus, they may differ by as much as $0.1\,mE_h$ from the true asymptote; apparent barriers should therefore be checked against Figure 11, and the text.

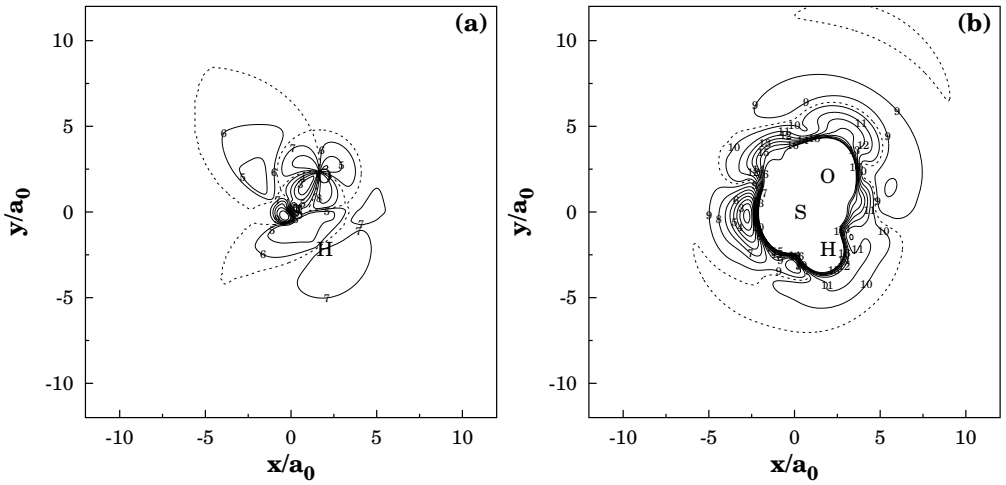

Figure 5. Contour plot for O moving coplanarly around a partially relaxed HSO molecule. Panel (a) shows the four-body electrostatic energy term, with contours starting at $-0.031\,\mathrm{E_h}$, equally spaced by $0.005\,\mathrm{E_h}$. The dashed contour indicates the zero of energy. Panel (b) shows the full DMBE potential energy surface; contours start at $-0.4420\,\mathrm{E_h}$, and are equally spaced by $0.017\,\mathrm{E_h}$. The dashed contour in panel (b) indicates the HSO dissociation limit ($-0.2962\,\mathrm{E_h}$).

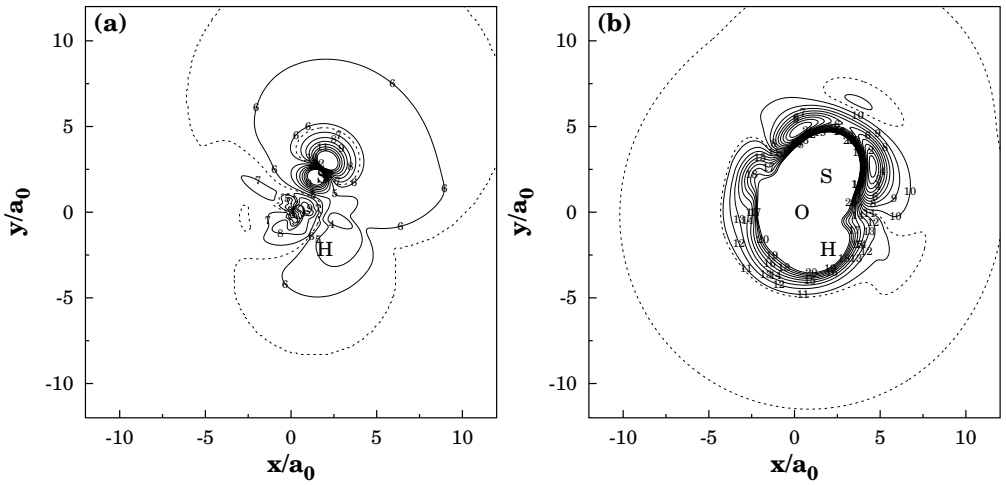

Figure 6. Contour plot for O moving coplanarly around a partially relaxed HOS molecule. Panel (a) shows the four-body electrostatic energy term, with contours starting at $-0.037\,\mathrm{E_h}$, equally spaced by $0.005\,\mathrm{E_h}$. The dashed contour indicates the zero of energy. Panel (b) shows the full DMBE potential energy surface; contours start at $-0.4600\,\mathrm{E_h}$, and are equally spaced by $0.017\,\mathrm{E_h}$. The dashed contour in panel (b) indicates the HOS dissociation limit ($-0.2947\,\mathrm{E_h}$).

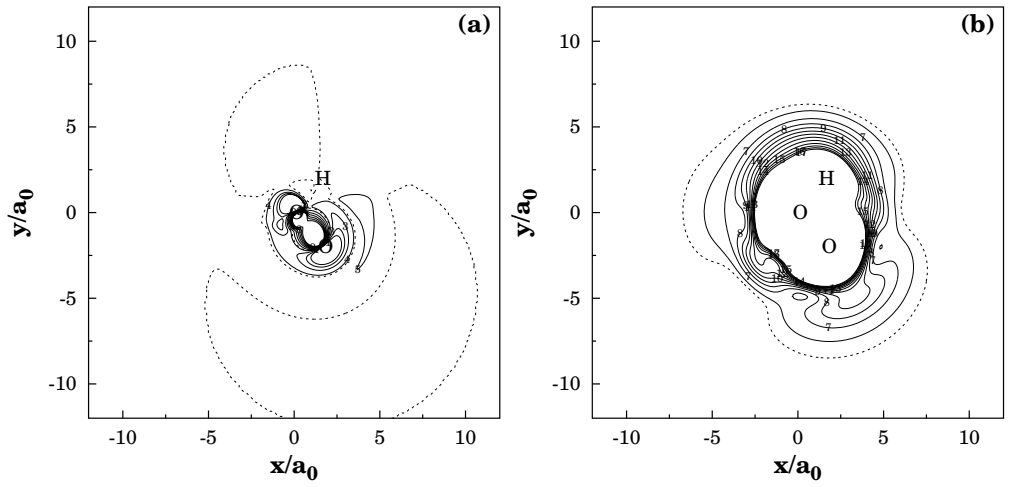

Figure 7. Contour plot for S moving coplanarly around a partially relaxed HO_2 molecule. Panel (a) shows the four-body electrostatic energy term, with contours starting at $-0.026\,E_h$, equally spaced by $0.008\,E_h$. The dashed contour indicates the zero of energy. Panel (b) shows the full DMBE potential energy surface; contours start at $-0.3560\,E_h$, and are equally spaced by $0.017\,E_h$. The dashed contour in panel (b) indicates the HO_2 dissociation limit ($-0.2986\,E_h$).

lies, in the $2+3+4_{ele}$ DMBE potential energy surface, very close to that of the TS_2 transition state for the isomerization process HOSO $\rightleftharpoons$ HSO_2. Thus, the local function to be added at the HSO_2 geometry should not significantly affect the energy of this transition state. Moreover, the *ab initio* calculations (see Table 2) and the $2+3+4_{ele}$ DMBE potential energy surface predict the energy of the above mentioned transition state to lie below the energy of OH + SO, allowing the isomerization process HOSO $\rightleftharpoons$ HSO_2 to take place without any translational energy requirements in OH + SO collisions. Thus, an additional constraint in choosing the necessary correction term is that such a TS should be kept below the energy of OH + SO isolated reactants. A convenient four-body EHF energy term that satisfy the above requirements is

$$V_{\rm EHF}^{(4)} = V_S^{(4)} + V_T^{(4)} + P^{(4)}T^{(4)} \tag{26}$$

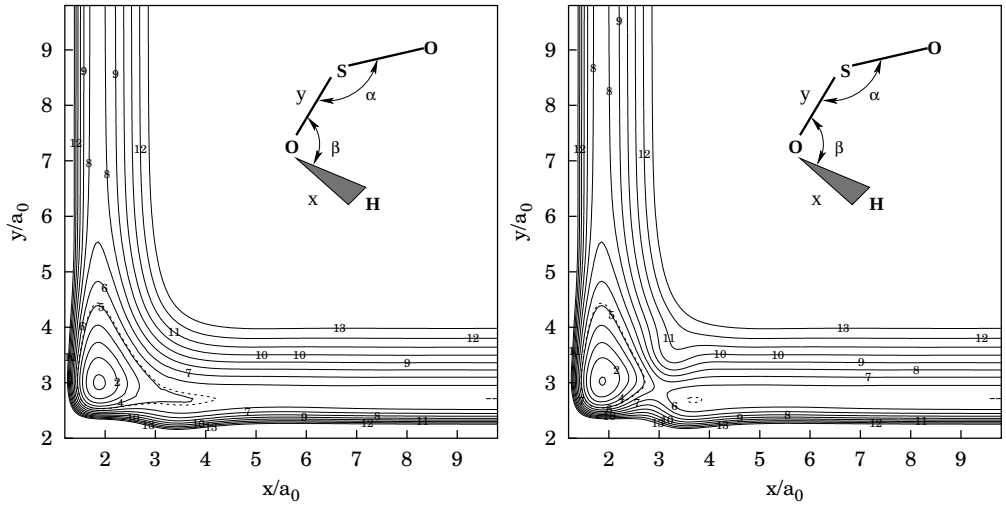

Figure 8. Contour plot for the channel OH+SO $\rightleftharpoons$ HOSO $\rightleftharpoons$ H+SO_2. Contours start at $-0.4831\,E_h$, and are equally spaced by $0.017\,E_h$. The SO distance, α, β, and dihedral angles are partially relaxed. Indicated by the dashed line is the H + SO_2 dissociation energy ($-0.4132\,E_h$). Panel (a) shows the $2 + 3 + 4_{ele}$ DMBE surface, while panel (b) shows the full DMBE potential energy surface.

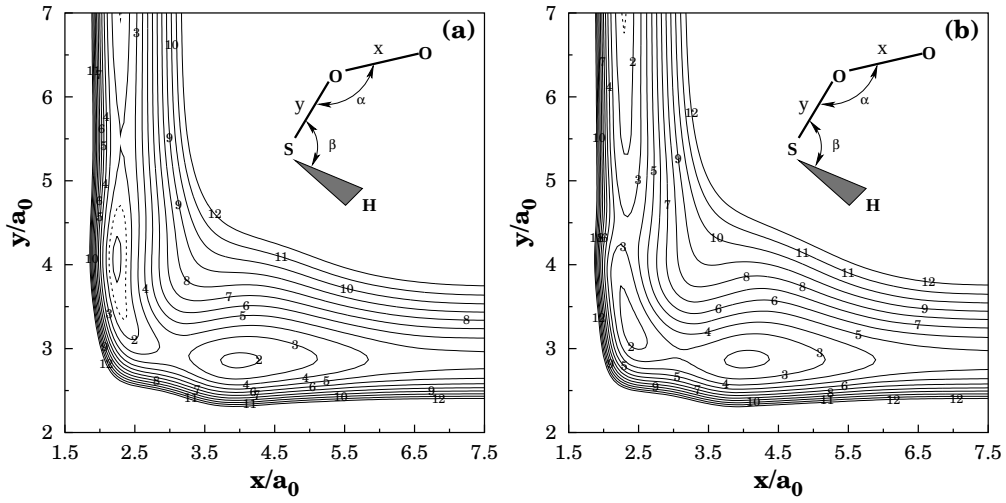

Figure 9. Contour plot for the channel HS+O_2 $\rightleftharpoons$ HSOO $\rightleftharpoons$ HSO+O. Contours start at $-0.3350\,E_h$, being equally spaced by $0.01\,E_h$. The HS distance, α, β and dihedral angles are partially relaxed. Indicated by the dashed line is the HS + O_2 dissociation energy ($-0.3307\,E_h$). Panel (a) shows the $2+3+4_{ele}$ DMBE surface, while panel (b) refers to the full DMBE potential energy surface.

where $V_S^{(4)}$ and $V_T^{(4)}$ are four-body Gaussian-type functions defined by

$$V_S^{(4)} = C_0^{\mathcal{S}} \exp[-\sum_{i=1}^{6} C_i^{\mathcal{S}} (R_i - R_i^{\mathcal{S},ref})^2] \tag{27}$$

$$V_T^{(4)} = C_0^{\mathcal{T}} \exp[-\sum_{i=1}^{6} C_i^{\mathcal{T}} (R_i - R_i^{\mathcal{T},ref})^2] \tag{28}$$

In turn, $P^{(4)}$ is a 2nd-order polynomial,

$$P^{(4)} = a_0 + \sum_{i=1}^{6} a_i (X_i - X_i^{ref}) + \sum_{i,j=1}^{6} b_i b_j (X_i - X_i^{ref})(X_j - X_j^{ref}) \tag{29}$$

and $T^{(4)}$ is a range-determining factor also chosen to be of the Gaussian-type:

$$T^{(4)} = \exp\left[-\sum_{i=1}^{6} g_i (X_i - X_i^{ref})^2\right] \tag{30}$$

where $R_i^{\mathcal{S},ref}$ and $R_i^{\mathcal{T},ref}$ are respectively the geometries of the HSO_2 and HSOO minima in the $2 + 3 + 4_{ele}$ DMBE potential energy surface; see Table 7. The coefficients $C_i^{\mathcal{S}}$, $C_i^{\mathcal{T}}$ $(i = 0-6)$ in Eqs. (27) and (28) have been calculated using a trial and error procedure by imposing the conditions discussed in the previous paragraph. Their numerical values are reported in Table 6. Note that $\{X_i\}$ is a set of valence-bond type coordinates: three distances, two planar angles, and one dihedral angle (expressed in radians), all calculated for each set of the six interatomic distances; see Figure 1. Note further that $\{X_i^{ref}\}$ is a reference geometry (Table 7), namely the *ab initio* geometry of TS_1. Finally, the linear coefficients appearing in Eq. (29) have been calibrated from a least-squares fitting procedure to our own *ab initio* points. Specifically, a grid of 945 *ab initio* energies referring to geometries in the vicinity of the transition state TS_1 has been employed. Note that such points (calculated at FVCAS/AVDZ level, and subsequently scaled to simulate AVTZ results) have been referred to the *ab initio* $H + SO_2$ dissociation energy. It was the difference between such values and those calculated using the $2 + 3 + 4_{ele}$ DMBE potential energy surface (also referred to its own $H + SO_2$ dissociation energy) that were actually fitted to the above mentioned four-body EHF-type functions. The g_i parameters in Eq. (30) have themselves been chosen via a trial and error procedure. Table 6 summarizes the linear coefficients so

obtained, while the nonlinear g_i appear in Table 7. Finally, we recall that the *ab initio* calculations used for the calibration procedure may suffer from several deficiencies, namely due to employing a relatively modest basis set and missing the dynamical correlation (see later). Despite such limitations, they are believed to be accurate enough to reliably define the shape of the potential energy surface in the vicinity of the transition state. Thus, we have obtained two variants of the complete DMBE potential energy surface. One, shows a barrier height of 17.4 kcal mol^{-1} for the transition state of the reaction HOSO $\rightleftharpoons$ H $\cdots$ OSO, as predicted from our own FVCAS/AVTZ calculations. In the other, we have downscaled the barrier height to about a half of that value (9.1 kcal mol^{-1}) such as to reproduce the estimate of Goumri *et al.*[10] from G2 calculations. Unless specified otherwise, it is to this surface that we refer in the remaining of this work.

4 Characterization of DMBE potential energy surface

Figure 11 shows a schematic diagram of the energetics of the title system according to the DMBE potential energy surface reported in the present work, while Table 8 summarizes the properties of its major stationary points; for the coordinates, see Figure 1. Several views of the potential energy surface for an atom moving coplanarly around a partially relaxed triatomic are displayed in Figures 4-7. Also shown are two-dimensional contour plots for the most relevant reactions that may occur on the title potential energy surface; Figures 8-10. Note that minima and saddle points in these views may not necessarily correspond to such attributes in the full configuration space of the tetratomic. Ball and stick drawings of the most relevant stationary points are shown in Figures 12 and 13. These structures will be discussed in the following.

Global minimum

This corresponds to a staggered HOSO configuration, with the hydrogen atom connected to one of the oxygen atoms of SO_2; its attributes are summarized in the first entry of Table 8. Although *ab initio* calculations at the Hartree-Fock (HF) level using 6-311G**,[8] 6-31G**[5] and 3-21G**[3] basis sets report a global minimum

Table 6. Coefficients in four-body extended Hartree-Fock energy defined in Eqs. (27)-(30).

$C_0^{\mathcal{S}}$=0.033	$C_0^{\mathcal{T}}$=0.06	a_0=0.03217616	b_{11}=0.44635187	b_{23}=0.26529542	b_{36}=−0.00364268
$C_1^{\mathcal{S}}$=0.70	$C_1^{\mathcal{T}}$=1.00	a_1=0.00051323	b_{12}=−0.05997085	b_{24}=0.11395901	b_{44}=0.34579546
$C_2^{\mathcal{S}}$=0.700	$C_2^{\mathcal{T}}$=1.00	a_2=−0.00021041	b_{13}=0.08443367	b_{25}=0.07185930	b_{45}=−0.01833119
$C_3^{\mathcal{S}}$=0.250	$C_3^{\mathcal{T}}$=1.00	a_3=−0.00034408	b_{14}=0.08828140	b_{26}=0.00002378	b_{46}=−0.00142153
$C_4^{\mathcal{S}}$=0.700	$C_4^{\mathcal{T}}$=1.00	a_4=0.00015197	b_{15}=0.02477545	b_{33}=−0.00938667	b_{55}=0.18064411
$C_5^{\mathcal{S}}$=0.250	$C_5^{\mathcal{T}}$=0.20	a_5=0.00120912	b_{16}=0.00228627	b_{34}=−0.07207120	b_{56}=−0.01020253
$C_6^{\mathcal{S}}$=0.250	$C_6^{\mathcal{T}}$=0.20	a_6=0.00027423	b_{22} = 0.25454764	b_{35} =−0.03282833	b_{66}=0.04777738

Table 7. Parameters and reference geometries used in four-body switching functions of Eq. (18) (first column), and four-body EHF term of Eqs. (27)-(30).

$R_{\rm SO}^{ref}$=2.7988	$g_1 = 3.0$	$R_1^{\mathcal{S},ref}$=2.7053	$R_1^{\mathcal{T},ref}$=4.6928	X_1^{ref}=2.83405
$R_{\rm SH}^{ref}$=2.5334	$g_2 = 3.0$	$R_2^{\mathcal{S},ref}$=2.7053	$R_2^{\mathcal{T},ref}$=4.6928	X_2^{ref}=2.91075
$R_{\rm OO}^{ref}$=2.2818	$g_3 = 3.0$	$R_3^{\mathcal{S},ref}$=3.0630	$R_3^{\mathcal{T},ref}$=2.5996	X_3^{ref}=2.95889
$R_{\rm OH}^{ref}$=1.8344	$g_4 = 3.0$	$R_4^{\mathcal{S},ref}$=4.5812	$R_4^{\mathcal{T},ref}$=2.1891	X_4^{ref}=115.52$^{\rm o}$
η=3.5	$g_5 = 3.0$	$R_5^{\mathcal{S},ref}$=4.8379	$\rm R_5^{\mathcal{T},ref}$=5.8152	X_5^{ref}=117.71$^{\rm o}$
β=2.5	$g_6 = 1.0$	$R_6^{\mathcal{S},ref}$=4.8379	$R_6^{\mathcal{T},ref}$=5.8152	X_6^{ref}=78.952$^{\rm o}$

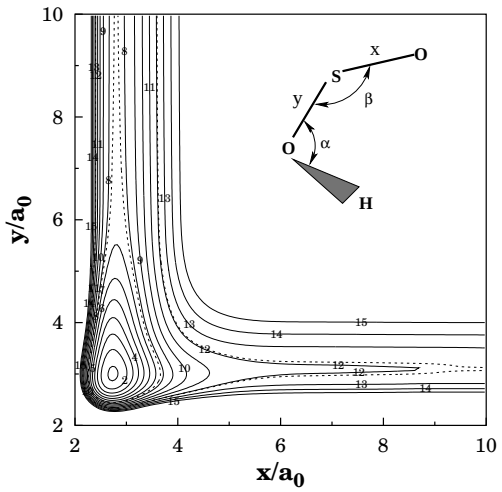

Figure 10. Contour plot of the full HSO_2 DMBE potential energy surface for the channel $O + SOH \rightleftharpoons HOSO \rightleftharpoons OH + SO$. Contours start at $-0.4830\,E_h$, being equally spaced by $0.017\,E_h$. The OH distance, α, β, and dihedral angles have been partially relaxed. Indicated by the dashed line is the $O + HOS$ dissociation energy ($-0.2947\,E_h$). The corresponding plot for the $2+3+4_{ele}$ DMBE potential energy surface is nearly indistinguishable, and hence is not shown.

with a similar configuration, correlated Moller-Plesset (MP2) calculations using 6-311G**,[8] 6-31G**[5] and 3-21G**[3] basis sets predicted a planar structure. Similarly to these, our own *ab initio* calculations predict a planar HOSO geometry as indicated in Table 2. Unfortunately, to our knowledge, there is no experimental evidence concerning the structure of such a species. However, all such studies agree on the fact that this HOSO structure should be the global minimum of the title potential energy surface. We emphasize that the well depth of such a minimum is predicted to be $44.2\,\mathrm{kcal\,mol^{-1}}$ (relative to the $H + SO_2$ dissociation limit) in excellent agreement with the DFT calculations of Denis and Ventura.[13] In turn, we predict the OH stretching frequency in the DMBE HOSO minimum to be $3710\,\mathrm{cm^{-1}}$ while Isoniemi *et al.*[12] report a value of $3554\mathrm{cm^{-1}}$ from spectroscopic measurements in an argon matrix. Indeed, the same work reports two other stretching frequencies for this isomer, which differ by less than 15% from the DMBE values here reported. Such differences are acceptable in view of the anharmonicity of the potential energy surface and sensitivity of the force constants to numerical determination from a set of discrete points.

HSO_2 isomer

The attributes of the corresponding local minimum, referred to as HSO_2 (with C_{2v} symmetry), are given in the second entry of Table 8. As panels (b) and (c) of Figure 4 clearly show, both the DMBE $2 + 3 + 4_{\mathrm{ele}}$ and DMBE potential energy surfaces predict this structure to be stable with respect to the $H + SO_2$ dissociation asymptote. However, by inclusion of the four-body EHF energy term in the full DMBE potential energy surface, its well depth has been decreased such as to lie $21.9\,\mathrm{kcal\,mol^{-1}}$ below the $H + SO_2$ dissociation limit at a geometry close to our *ab initio* prediction.

HSOO isomer

Shown in the third entry of Table 8 are the geometric and energetic properties of the HSOO minimum, which are very similar to those recently reported by Resende *et al.*[37] As noted above, such an isomer is possibly related to the sink of SH via the three-body recombination reaction (3). The contour plot in panel

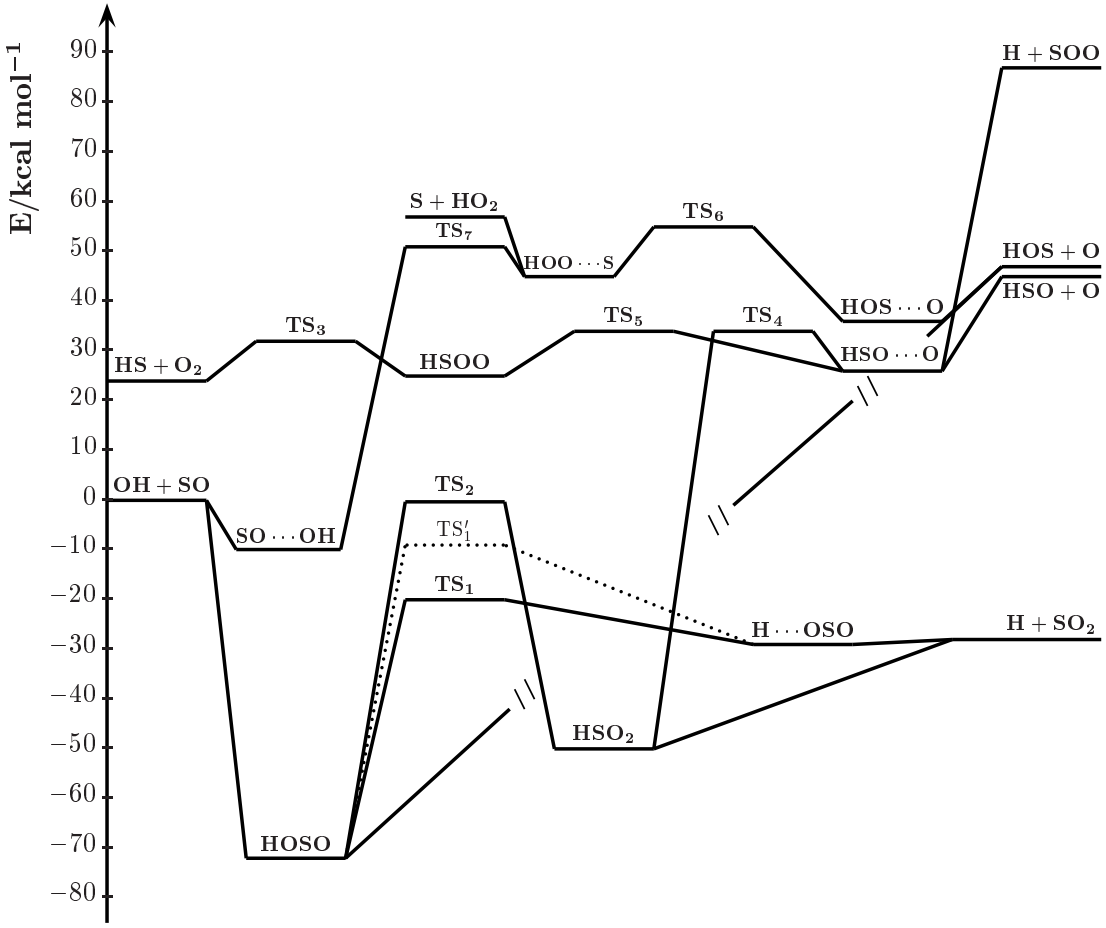

Figure 11. Energetics of full HSO_2 DMBE potential energy surface. For ball and stick three-dimensional views of the various structures, see Figures 12 and 13. Shown by the dotted line is the path based on the FVCAS/AVDZ scaled to FVCAS/AVTZ calculations from the present work, while the interrupted solid line shows the barrier-free path connecting O+SOH to the deep HOSO minimum.

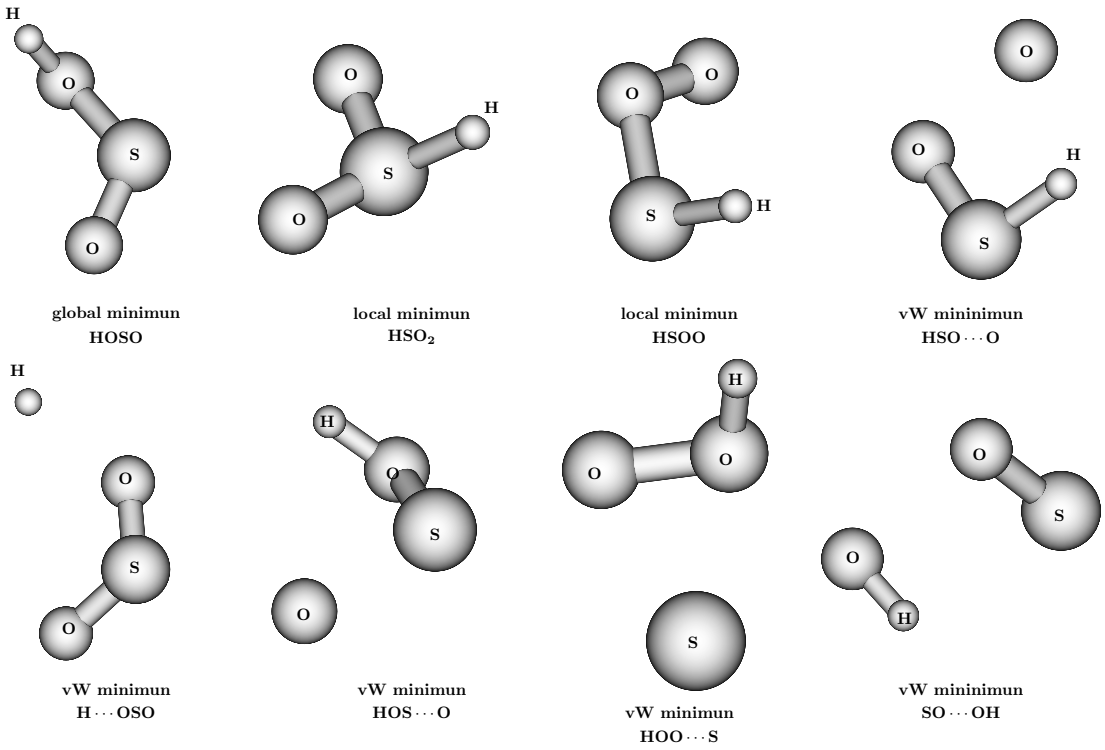

Figure 12. Ball and stick drawings of the structures associated to minima in the HSO_2 DMBE potential energy surface.

(b) of Figure 9 shows that such a structure is the intermediate for the reactions $HS + O_2 \rightleftharpoons HSO + O$.

HSO···O van der Waals minimum

When the terminal oxygen in HSO is attacked by another oxygen atom, an intermediate HSO···O van der Waals species may be formed (such weakly bound species are heretofore indicated by the usual triple dot notation). Its properties are collected in the fourth entry of Table 8, while the contour plot of Figure 9 shows such a process to be barrier free.

H···OSO van der Waals minimum

The fifth entry of Table 8 summarizes the properties of this van der Waals species, also shown in panel (a) of Figure 8. Note that it has an energy below the dissociation limit $H + SO_2$, which arises already at the $2 + 3 + 4_{ele}$ body level of the DMBE potential energy surface. Panel (c) of Figure 4 shows the position of such a minimum.

O···SOH, S···OOH, and SO···OH van der Waals minima

Three van der Waals type minima correlate with the O + SOH asymptote, being their attributes summarized on the sixth to eighth entries of Table 8. The former two minima correspond to T-shaped structures with the O (S) atom attacking the middle atom of HOS (HOO), as one might anticipate from the interaction between their permanent electric moments: atomic quadrupoles and triatomic dipoles. The third of those minima involves two interacting diatomic species having permanent electric dipole moments, namely SO and OH. In all cases, the well depths have several $kcal\,mol^{-1}$ with respect to the appropriate asymptote. To our knowledge, no accurate *ab initio* data or empirical information is available that might allow an assessment on the reliability of such predictions.

Transition state for the reactions HOSO ⇌ H···OSO, TS_1

As observed from panel (a) of Figure 8, there is only a small energy barrier of about $2\,kcal\,mol^{-1}$ for the $H + SO_2$ reaction to occur in the $2 + 3 + 4_{ele}$ DMBE

Table 8. Properties of stationary points of the full DMBE potential energy surface of HSO_2.

Feature	R_1/a_0	R_2/a_0	R_3/a_0	α/deg	β/deg	γ/deg	E/E_h	ΔE	frequencies/cm^{-1}		
HOSO, min.	2.742	3.027	1.865	119.9	112.7	83.1	−0.4837	−44.2[a]	445	686	852
									1264	1329	3710
HSO_2, min.	2.716	2.716	2.857	115.1	112.7	131.1	−0.4482	22.3[b]	381	668	1013
								−21.9[a]	1103	1316	1381
HSOO, min.	2.405	3.222	2.662	114.6	110.9	76.7	−0.3293	96.9[b]	347	484	652
								0.9[c]	1136	1231	2541
$HSO\cdots O$, min.	3.988	2.881	2.521	112.6	99.5	42.6	−0.3274	2.1[c]	129	302	437
									801	1064	2643
$H\cdots OSO$, min.	2.727	2.680	3.598	118.0	122.1	73.6	−0.4181	−3.1[a]	368	616	871
									1205	1520	1897
$HOS\cdots O$, min.	6.221	3.253	1.925	44.8	110.4	102.2	−0.3124	−10.2[d]	192	268	612
									710	1124	3255
$HOO\cdots S$, min.	5.300	2.504	1.853	72.2	102.9	95.6	−0.2980	−12.2[e]	217	250	854
									993	1298	3440
$SO\cdots OH$, min.	2.865	4.691	1.914	114.1	96.0	38.1	−0.3847	−9.7[f]	82	166	272
									847	1006	3384
$H\cdots OSO \rightleftharpoons HOSO$, TS_1	2.776	2.852	2.987	116.6	119.2	77.5	−0.3987	9.1[a,g]	588	768	1372
								53.4[b]	1522	1887	2595i
$HOSO \rightleftharpoons HSO_2$, TS_2	2.762	2.962	2.887	110.1	57.0	62.5	−0.3697	71.5[b]	209	731	1043
								49.2[h]	1402	1989	1919i
$HS + O_2 \rightleftharpoons HSOO$, TS_3	2.269	4.246	2.638	104.9	104.4	150.5	−0.3179	8.0[c]	144	439	841
									1456	2497	262i
$HSO\cdots O \rightleftharpoons HSO_2$, TS_4	4.236	2.819	2.581	81.1	104.1	92.8	−0.3159	83.0[h]	433	574	947
								7.2[i]	1018	2555	322i
$HSO\cdots O \rightleftharpoons HSOO$, TS_5	3.095	2.934	2.615	112.1	107.5	77.5	−0.3159	7.2[i]	377	503	1015
								8.4[j]	1072	2426	548i
$HOS\cdots O \rightleftharpoons HOO\cdots S$, TS_6	5.948	3.196	1.946	41.4	97.7	105.4.5	−0.2810	19.7[j]	309	332	1041
								10.7[l]	1477	3290	418i
$HOO\cdots S \rightleftharpoons SO\cdots OH$, TS_7	4.092	2.479	1.853	101.5	103.0	90.8	−0.2875	6.6[l]	370	761	993
									1284	3387	377i

[a]Energy in kcal mol^{-1} referred to $H+SO_2$ ($-0.4132\,E_h$). [b]Energy in kcal mol^{-1} referred to global minimum HOSO. [c]Energy in kcal mol^{-1} referred to $HS+O_2$ ($-0.3307\,E_h$). [d]Energy in kcal mol^{-1} referred to $HOS+O$ ($-0.2947\,E_h$). [e]Energy in kcal mol^{-1} referred to HO_2+S ($-0.2786\,E_h$). [f]Energy in kcal mol^{-1} referred to $OH+SO$ ($-0.3692\,E_h$). [g]If the energy calculated in this work is used (see dotted line in Figure 11), one gets from left to right in the above units: 2.772, 2.849, 2.972, 116.7, 119.5, 76.4, −0.3837, 18.5, 455, 712, 1251, 1368, 1816, and 3049i. [h]Energy in kcal mol^{-1} referred to local minimum HSO_2. [i]Energy in kcal mol^{-1} referred to local minimum $HSO\cdots O$. [j]Energy in kcal mol^{-1} referred to local minimum HSOO. [k]Energy in kcal mol^{-1} referred to local minimum $HOS\cdots O$. [l]Energy in kcal mol^{-1} referred to local minimum $HOO\cdots S$.

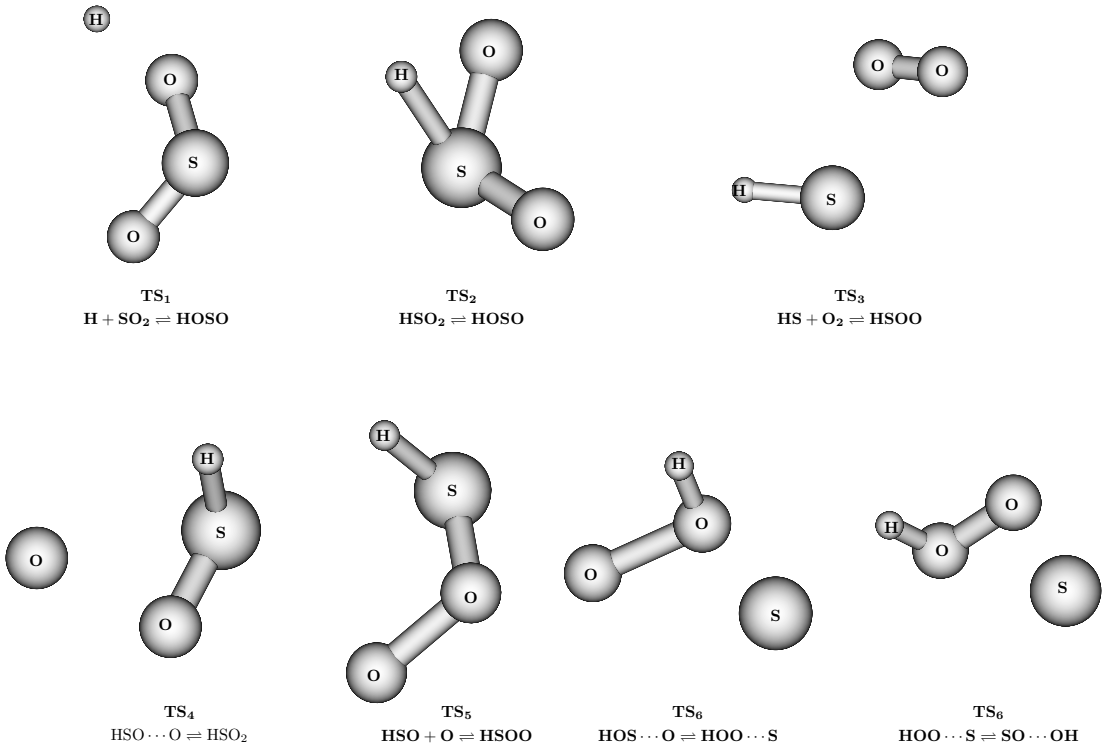

Figure 13. Ball and stick drawings of the structures associated to saddle points (of index 1, *i.e.*, a single imaginary frequency) in the HSO_2 DMBE potential energy surface.

potential energy surface, being such a barrier located at large $H-O$ distances. The addition of the four-body EHF energy term has transformed this low-barrier process for formation of HOSO into a high-barrier one. In fact, the full DMBE potential energy surface is shown in panel (b) of Figure 8 to have a barrier of $9.1\,\mathrm{kcal\,mol^{-1}}$ lying at somewhat shorter $H-O$ separations; see also the ninth entry of Table 8 where the properties of the TS_1 transition state are collected. Recall that the barrier height predicted from our FVCAS/AVTZ calculations is $17.4\,\mathrm{kcal\,mol^{-1}}$. Note also that no particularly good experimental data relating to TS_1 is available in the literature. Indeed, a comparison of the temperature and pressure dependences with master equation calculations seem to suggest[47] an increase of the energy of this transition state from $2.1-3.2\,\mathrm{kcal\,mol^{-1}}$ relative to the above estimate based on the G2 calculations of Goumri *et al.*,[10] thus narrowing slightly the gap relative to our own *ab initio* FVCAS/AVTZ prediction for this attribute. Of course, the FVCAS calculations lack an account for the dynamical correlation, and hence one wonders about the effect of the latter on such a value. With a view to explore this issue we have conducted exploratory single-point Rayleigh-Schrdinger perturbation-theory calculations from the FVCAS reference wave function (CASPT2) at this stationary point. We have obtained barrier heights of 7.9 and $9.2\,\mathrm{kcal\,mol^{-1}}$ with the AVDZ and AVTZ basis sets (respectively), which compare well with the G2 estimate[10] of $9.1\,\mathrm{kcal\,mol^{-1}}$. Since our CASPT2 estimates may still be considered to be preliminary, we have found no reason to alter the two values here considered for the modelling procedure, although this may trivially be done by fine tuning a_0 in Eq. (29) such as to reproduce any accurate information that becomes available. An additional remark to note that panel (b) of Figure 8 also shows that the HOSO formation from OH + SO is an essentially barrier free process, and hence is likely to be controlled by the leading long range forces associated to the permanent electric moments of the reactants.

Transition state connecting HSO_2 to HOSO, TS_2

The properties of the transition state for the isomerization process $HSO_2 \rightleftharpoons$ HOSO are reported in the tenth entry of Table 8. Clearly, such an isomerization implies important structural transformations, as manifested by the high energy

barrier that must be overcome for such a reaction to occur. All *ab initio* calculations available in the literature agree with such an expectation, and so does the DMBE potential energy surface here reported. Specifically, it predicts a barrier height for the forward process of 49.2 kcal mol^{-1}, while for the reverse process is 71.5 kcal mol^{-1}. Note that HSO_2 lies 22.3 kcal mol^{-1} above HOSO.

Transition state for the reaction $HS + O_2 \rightleftharpoons HSOO$, TS_3

The addition of SH and O_2 to form HSOO is seen to involve a 8.0 kcal mol^{-1} energy barrier (TS_3), whose properties are collected in the eleventh entry of Table 8. Although Resende *et al.*[37] predict a barrier of 12.3 kcal mol^{-1} for this process from their multireference (MRMP2) calculations, the geometries of the corresponding transition state (referred to as[37] TS_1) are (except for the low-frequency torsional modes) similar to the one here reported. Note that, for the reaction $OH + O_2 \rightleftharpoons HO_3$, the equivalent barrier height has been predicted to lie between 1.4 and 3.9 kcal mol^{-1} (see Ref. 48, and references therein).

Transition state connecting $HSO \cdots O$ to HSO_2, TS_4

According to the diagram in Figure 11, we may distinguish two regions in the HSO_2 potential energy surface: an upper-energy region including the $HS + O_2$ channel, the HSOO structures, and the HSO + O dissociation channel; a lower-energy region including the two more stables isomers HOSO and HSO_2, as well as the dissociation channels $OH + SO$ and $H + SO_2$. Such regions are connected via the transition state TS_4 for the isomerization process $HSO \cdots O \rightleftharpoons HSO_2$. The corresponding attributes are summarized in entry twelve of Table 8. As shown, the barrier for the direct isomerization process is of 7.2 kcal mol^{-1} and for the reverse one 83.0 kcal mol^{-1}. To our knowledge, no *ab initio* data concerning this process has been reported thus far. Yet, in Figure 1 of their paper, Goumri *et al.*[10] suggest from their schematic drawing a simple connection between $HSO + O$ and HSO_2. Clearly, our DMBE potential energy surface shows such a transition state to naturally link $HSO \cdots O$ to HSO_2.

Transition state connecting HSO···O to HSOO, TS_5

The thirteenth entry of Table 8 gathers the properties of the transition state connecting the HSO··· O and HSOO isomers, which is graphically illustrated in Figure 9. The energy of this TS_5 is nearly the same as for TS_4. Thus, in the absence of further information, one may conjecture that both competing processes are likely to occur with an equal frequency.

Transition states connecting O···HOS, S···HOO, and SO···OH: TS_6 and TS_7

The attributes of these transition states are given on the last two entries of Table 8. The transition state TS_6 connects the O···HOS and S···HOO van der Waals minima, and lies 10.7 kcal mol^{-1} (19.7 kcal mol^{-1}) above the latter (former). In turn, TS_7 connects the S···HOO and SO···OH van der Waals minima, being 6.6 kcal mol^{-1} above the former. Of them, TS_6 is expected to be the determinant transition state for the reaction O + SOH → OH + SO, with a classical barrier height of about 8.6 kcal mol^{-1}. Note that the reaction O + SOH → S + HO_2 is slightly endothermic, with a classical endothermicity of about 10.14 kcal mol^{-1}, *i.e.*, the products channel lies 1.51 kcal mol^{-1} above TS_6. We further note that the reaction O + SOH → OH + SO may evolve through the deep HOSO minimum, a rather exothermic process that involves no reaction barrier. The relevant DMBE contour plot for this reaction is shown in Figure 10; the corresponding plot for the $2+3+4_{ele}$ DMBE potential energy surface is omitted, since this is essentially indistinguishable from the former. Note that, similarly to the associated van der Waals minima, no *ab initio* or empirical information exists that may allow an assessment of the accuracy of the above saddle points. A final remark to observe that HOS + O asymptote lies less than 1 kcal mol^{-1} above the HSO + O one. Thus, although one might intuitively think that both could be connected to the HS + O_2 and OH + SO asymptotes, this turns out to be possible only in the case of HSO + O. For HOS + O to evolve to HS + O_2, one requires in principle that the isomerization HOS ⇌ HSO will firstly occur, which involves an energy of 45.7 kcal mol^{-1}.[24]

5 Conclusions

A singled-sheeted DMBE potential energy surface has been reported for the ground electronic state of HSO_2, partly based on FVCAS/AVDZ(AVTZ) calculations for the tetratomic also reported in the present work. These have been shown to be in fair agreement with previously reported *ab initio* results. The attributes of the most relevant stationary points have also been presented. As in previous studies, the most stable isomer is predicted to have a HOSO structure, while the HSO_2 isomer (having the hydrogen and middle sulfur atoms connected) corresponds to a local minimum. It has further been shown that the global minimum can be reached from the $H + SO_2$ reactants by overcoming an energy barrier that is likely to be of the order of $9\,\mathrm{kcal\,mol^{-1}}$ (the value actually used for the DMBE calibration procedure). An HSOO isomer has additionally been found and characterized, as well as the paths connecting this minimum to other structures. Furthermore, a barrier of $8\,\mathrm{kcal\,mol^{-1}}$ has been predicted to separate such a minimum from the SH + O_2 asymptote. Finally, our results suggest that a high energy is required for the isomerization reaction $HSO_2 \rightleftharpoons$ HOSO to occur. Of course, the accuracy limitations encountered in the theoretical work and the topological intricacies of the potential energy surface leave it clear that the HSO_2 DMBE potential energy surface from the present work may not be definite. This can only be answered through dynamics studies of the various chemical reactions occurring in it.

Acknowledgments

This work has the support of Fundação para a Ciência e Tecnologia, Portugal, under programmes POCTI/QUI/40154/2001 and FEDER. M.Y.B. thanks the Instituto Superior de Ciencias y Tecnología Nucleares, Havana, Cuba, for leave of absence during his PhD studies.

References

[1] R. P. Wayne, *Chemistry of atmosphere* (Oxford Univ Press, 2000), 3rd edn.

[2] C. A. M. Dowell, F. G. Herring, and J. C. Tait, J. Chem. Phys. **63**, 3278 (1975).

[3] P. Binns and P. Marshall, J. Phys. Chem. A **95**, 4940 (1991).

[4] V. R. Morris and W. M. Jackson, Chem. Phys. Lett. **223**, 445 (1994).

[5] D. Laakso, C. E. Smith, A. Goumri, J. D. R. Rocha, and P. Marshall, Chem. Phys. Lett. **227**, 377 (1994).

[6] A. Goumri, J. D. R. Rocha, and P. Marshall, J. Phys. Chem. A **99**, 10834 (1995).

[7] A. J. Frank, M. Sadìlek, J. G. Ferrier, and J. Tureček, J. Am. Chem. Soc. **118**, 11321 (1996).

[8] J. X. Qi, W. Q. Deng, K. L. Han, and G. Z. He, J. Chem. Soc. Faraday Trans. **93**, 25 (1997).

[9] A. J. Frank, M. Sadìlek, J. G. Ferrier, and J. Tureček, J. Am. Chem. Soc. **119**, 12343 (1997).

[10] A. Goumri, J. D. R. Rocha, D. Laakso, C. E. Smith, and P. Marshall, J. Phys. Chem. A **103**, 11328 (1999).

[11] E. Isoniemi, L. Kriadchtchev, J. Lundell, and M. Räsänen, J. Mol. Struct. Theochem **563**, 261 (2001).

[12] E. Isoniemi, L. Kriadchtchev, J. Lundell, and M. Räsänen, Phys. Chem. Chem. Phys. **4**, 1549 (2002).

[13] R. A. Denis and O. N. Ventura, Chem. Phys. Lett. **344**, 221 (2001).

[14] M. R. Zacharia and O. I. Smith, Combust. Flame **69**, 125 (1987).

[15] R. A. Drurie, G. M. Jonhson, and M. Y. Smith, Combust. Flame **17**, 197 (1971).

[16] A. S. Kallend, Combust. Flame **19**, 227 (1972).

[17] G. S. Tyndall and A. R. Ravishankara, Int. J. Chem. Kinet. **23**, 483 (1991).

[18] A. A. Turnipseed, S. B. Barone, and A. R. Ravishankara, J. Phys. Chem. **96**, 7502 (1992).

[19] A. J. C. Varandas, Adv. Chem. Phys. **74**, 255 (1988).

[20] A. J. C. Varandas, in *Lecture Notes in Chemistry*, edited by A. Laganá and A. Riganelli (Springer, Berlin, 2000), vol. 75, pp. 33.

[21] A. J. C. Varandas, in *Conical Intersections: Electronic Structure, Dynamics and Spectroscopy*, edited by D. Yarkony, H. Köppel, and W. Domcke (World Scientific Publishing, Singapore, 2004).

[22] M. R. Pastrana, L. A. M. Quintales, J. Brandão, and A. J. C. Varandas, J. Phys. Chem. **94**, 8073 (1990).

[23] A. J. C. Varandas and S. P. J. Rodrigues, Spectrochimica Acta A **58**, 629 (2002).

[24] E. Martínez-Núñez and A. J. C. Varandas, J. Phys. Chem. A **105**, 5923 (2001).

[25] A. J. C. Varandas and A. A. C. C. Pais, in *Theoretical and Computational Models for Organic Chemistry*, edited by S. Formosinho, I. Czismadia, and L. Arnaut (Kluwer, Dordrecht, 1991), pp. 55.

[26] A. J. C. Varandas and J. L. Llanio-Trujillo, Chem. Phys. Lett. **356**, 585 (2002).

[27] A. J. C. Varandas and H. G. Yu, Mol. Phys. **91**, 301 (1997).

[28] A. J. C. Varandas and L. Zhang, Chem. Phys. Lett. **331**, 474 (2000).

[29] A. J. C. Varandas and L. Zhang, Chem. Phys. Lett. **385**, 409 (2004).

[30] M. A. Collins, Adv. Chem. Phys. **93**, 389 (1996).

[31] A. J. C. Varandas and P. E. Abreu, Chem. Phys. Lett. **293**, 261 (1998).

[32] T. H. Dunning, J. Chem. Phys. **90**, 1007 (1989).

[33] R. Kendall, T. Dunning Jr., and R. Harrison, J. Chem. Phys. **96**, 6769 (1992).

[34] H.-J. Werner and P. J. Knowles, MOLPRO is a package of *ab initio* programs written by H.-J. Werner, P. J. Knowles, with contributions from J. Almlf, R. D. Amos, M. J. O. Deegan, S. T. Elbert, C. Hampel, W. Meyer, K. A. Peterson, R. Pitzer, A. J. Stone, P. R. Taylor, R. Lindh, (1998).

[35] J. Martin and O. Uzan, Chem. Phys. Lett. **282**, 16 (1998).

[36] J. Martin, Chem. Phys. Lett. **310**, 271 (1999).

[37] S. M. Resende and F. Ornellas, Phys. Chem. Chem. Phys. **5**, 4617 (2003).

[38] S. P. J. Rodrigues, J. A. Sabn, and A. J. C. Varandas, J. Phys. Chem. A **106**, 556 (2002).

[39] A. J. C. Varandas and J. D. Silva, J. Chem. Soc. Faraday Trans. **88**, 941 (1992).

[40] R. J. Le Roy, Spec. Period. Rep. Chem. Soc. Mol. Spectrosc. **1**, 113 (1973).

[41] A. J. C. Varandas, J. Chem. Phys. **105**, 3524 (1996).

[42] A. J. C. Varandas and A. I. Voronin, Mol. Phys. **85**, 497 (1995).

[43] A. J. C. Varandas and A. I. Voronin, Chem. Phys. **194**, 91 (1995).

[44] P. J. S. B. Caridade and A. J. C. Varandas, (unpublished work).

[45] A. D. Buckingham, Adv. Chem. Phys. **12**, 107 (1967).

[46] J. O. Hirschfelder, C. F. Curtis, and R. B. Bird, *Molecular Theory of Gases and Liquids* (Wiley, New York, 1954).

[47] M. J. Pilling, (private communication, January 2005).

[48] A. J. C. Varandas, ChemPhysChem **3**, 433 (2002).

Part II

Molecular Dynamics

Chapter 3

Theoretical Framework

Once the electronic problem is solved, resulting in an appropriate representation of the potential energy function as referred in the previous part, a chemical reaction may be understood as the motion of atomic nuclei trough such a potential. Thus, classical or quantum mechanical methods can be used to characterize the chemical reaction. For the study of reactions presented in this thesis a quasiclassical trajectory (QCT) method [1–4] was used. The basis of QCT as well as some features of molecular reaction dynamics are briefly reviewed in this chapter.

3.1 Classical Trajectories

Classical trajectories are the limits of high particle masses and high energies of quantum-mechanical scattering process [1, 5]. They are used when dealing with a molecular process in all the complexity and reality. They provide a feasible connection between experimental observations and the interaction potential of the atoms. When using classical trajectories one question arises: are chemical reactions close to classical simplicity or do they require the detailed attention of quantum considerations? The answer is that we usually think of these processes as classical ones, with quantum corrections required under certain conditions [6]. A qualitative argument is that de Broglie wavelength are short enough and that so far has not been shown that tunneling corrections are very important to classical interpretations [1]. Besides, as remarked in a series of works by Karplus *et al.* [3, 7, 8], in a classical and quantum treatment of the same molecular system, no significant differences have been obtained. Of course, some discrepancies might

appear for low translational energy processes when quantum effects are expected to be significant [1].

In a classical trajectory study the motions of the individual atoms are simulated by solving classical equations of motion, usually in the form of Hamilton's equations [9]:

$$\frac{\partial H}{\partial q_i} = -\frac{dp_i}{dt}, \ \frac{\partial H}{\partial p_i} = \frac{dq_i}{dt} \tag{3.1}$$

where the Hamiltonian function of the system, H, is the sum of the kinetic $T(\mathbf{p}, \mathbf{q})$ and potential $V(\mathbf{q})$ energies:

$$H = T(\mathbf{p}, \mathbf{q}) + V(\mathbf{q}) \tag{3.2}$$

The potential energy function $V(\mathbf{q})$ is the already mentioned potential energy surface. Hamilton's equations (3.1) are solved numerically and numerous algorithms have been developed for this task [1]. When a set of trajectories is completed, the final values of momenta and coordinates are transformed into quantities, like reaction rate constant, which may be compared with experiment.

A significant aspect of a trajectory simulation is the choice of the initial coordinates and momenta. These initial conditions are chosen such that results from an ensemble of trajectories may be compared with experiment and theory and be used for predictions about the system's molecular dynamics. Monte Carlo methods are commonly used [2–4] for sampling appropriate distributions of initial values of coordinates and momenta.

In the molecular collisions studied in this thesis, the VENUS [10] code was utilized. Such a package uses Monte Carlo method for selecting initial conditions of the reactants. Integration of the classical equations of motions is carried out in a combination of fourth-order Runge-Kutta and sixth-order Adams Multon algorithms [1]. Some details are presented in the following.

3.1.1 Quasiclassical model for bi-molecular reactions

As was mentioned in preceding paragraphs, a dynamical study of a molecular collision can be carried out by means of classical equations. However, once configurations of the separated reagents are described by their vibrational and rotational (ro-vibrational) quantum states, initial conditions of the collision should be

generated accounting for them. This is the idea of quasiclassical trajectories [7]: to solve classical equations of motion considering the initial conditions of the reactants according to their quantum states. Similarly, the states of the product molecules can be assigned by determining the quantum numbers describing the best their ro-vibrational motion.

In order to introduce some basic concepts of collisions, let us consider two reactant molecules A and B. The reactants approach with a relative velocity $\mathbf{v}_{rel}$ (with module v_{rel}), which may be oriented such that the reactants approach head-on (along a line connecting the center of masses) or with a glancing blow collision. The difference between these two encounters is quantified by the impact parameter of the collision b, which is defined as the distance of closest approach of the reactants in the absence of any interactions between them. Thus, head-on collision occurs when $b = 0$, and $b > 0$ stands for oblique direction or glancing blow collision. The maximum value of b which leads to reaction is called maximum impact parameter, b_{max}. Beyond b_{max} the collisions are so glancing that probability of reaction is vanishingly small.

A measure of the effective collision area is given by the cross section. The cross section for the reaction between A and B to form products:

$$\mathrm{A} + \mathrm{B} \rightarrow \text{products} \tag{3.3}$$

may be given as a function of the A + B relative translational energy E_{tr} and the ro-vibrational energy levels of both species [11]. A reactive cross section may be expressed as: $\sigma_R = \sigma_R(E_{\mathrm{tr}}, v, J)$ where v and J denotes the vibrational and rotational quantum numbers of the reactants respectively. It is usually referred to as specific reactive cross section to remark that it comes from an specific or fixed ro-vibrational configuration of the reactants [12, 13]. If specific values are not selected but a distribution of values is used according to some temperature-dependent function, the reactive cross section becomes:

$$\sigma_r(E_{\mathrm{tr}}, T) = \sum_v \sum_J \sigma_R(E_{\mathrm{tr}}, v, J)\mathcal{P}_v(T)\mathcal{P}_J(T) \tag{3.4}$$

where $\mathcal{P}_v(T)$ and $\mathcal{P}_J(T)$ are population distributions of the vibrational and rotational quantum numbers of the reactants respectively. T is the temperature and both summations run over all the quantum numbers.

Multiplying $\sigma(E_{\rm tr};T)$ by the relative velocity $v_{\rm rel}$ and integrating over the Boltzmann distribution one gets the bi-molecular thermal rates constant:

$$k(T) = \int_0^\infty v_{\rm rel}\sigma(E_{\rm tr};T)\mathcal{P}_B(v_{\rm rel};T)\mathrm{d}v_{\rm rel} \tag{3.5}$$

or if it is written in terms of relative translational energy:

$$k(T) = \left(\frac{8k_BT}{\pi\mu}\right)^{1/2}\int_0^\infty \sigma(E_{\rm tr};T)\frac{E_{\rm tr}}{(k_BT)^2}e^{-E_{\rm tr}/k_BT}\mathrm{d}E_{\rm tr} \tag{3.6}$$

where μ is the reduced mass of the system, and k_B the Boltzmann constant.

When a batch of N_T trajectories are calculated and N_r of them were reactive, the reaction cross section (whether for specific ro-vibrational levels or not) may be calculated as [3]:

$$\sigma_r = \frac{N_r}{N_T}\pi b_{max}^2 \tag{3.7}$$

being b_{max} the largest impact parameter that leads to reaction.

3.1.2 Initial conditions

For the molecular collisions studied in this thesis, the VENUS [10] code was used. A brief survey of the procedure to select initial conditions for bi-molecular reaction (3.3) trajectories [4], using Monte Carlo sampling as implemented in VENUS package, will be given in the following.

Choosing initial Cartesian coordinates and momenta for a symmetric top polyatomic reactant follows in part a procedure for normal modes sampling [14], the components of the angular momentum are found from:

$$\begin{aligned} j &= \sqrt{J(J+1)}\hbar \\ j_z &= K\hbar \\ j_x &= (j^2 - j_z^2)^{1/2}\sin 2\pi R \\ j_y &= (j^2 - j_z^2)^{1/2}\cos 2\pi R \end{aligned} \tag{3.8}$$

where R is a random number, J and K are the rotational quantum numbers, $\hbar$ is the Planck constant. When calculating thermally averaged cross-sections

$\sigma_r(E_{\rm tr};T)$ it is sufficiently accurate to sample j and j_z from their classical Boltzmann distributions [15]:

$$\mathcal{P}(j_z) = e^{(-j_z^2/2I_z k_{\rm B}T)} \quad 0 \le j_z \le \infty \tag{3.9}$$

$$\mathcal{P}(j) = j e^{(-j^2/2I_x k_{\rm B}T)} \quad j_z \le j \le \infty \tag{3.10}$$

The von Neumann rejection method [16] is used to sample j_z from $P(j_z)$, while j is sampled by the cumulative distribution formula [15]:

$$j = [j_z^2 - 2I_x k_{\rm B} T \ln(1-R)]^{1/2} \tag{3.11}$$

The components j_x and j are found from equation (3.8). The vibrational quantum number $v_{\rm A}$ of the reactant is fixed when calculating the state specific cross-section. However, to calculate $\sigma_r(E_{\rm tr};T)$ each vibrational quantum number is selected from its quantum probability distribution:

$$\mathcal{P}(v_i) = \frac{1}{Q_i} e^{[-(v_i+1/2)\hbar\omega_i/k_{\rm B}T]} \tag{3.12}$$

This distribution may be sampled by the rejection method [16] or by cumulative distribution function:

$$\sum_{v_i=0}^{v_i} \frac{e^{[-(v_i+1/2)\hbar\omega_i/k_{\rm B}T]}}{Q_i} = R \tag{3.13}$$

where R is a random number and Q_i the partition function.

The next step is to transform the rotational angular momentum and its components and the vibrational quantum numbers for the polyatomic reactant A to Cartesian coordinates and momenta. The energies for the individual normal modes are given by:

$$E_i = \frac{P_i^2 + \omega_i^2 Q_i^2}{2} \tag{3.14}$$

which are then transformed to normal mode coordinates and momenta by means of:

$$Q_i = [(2E_i)^{1/2}/\omega_i]\cos(2\pi R_i) \text{ and } P_i = -(2E_i)^{1/2}\sin(2\pi R_i) \tag{3.15}$$

The normal mode coordinates and momenta ($\mathbf{Q}$ and $\mathbf{P}$) and the rotational angular momentum are then transformed to Cartesian coordinates and momenta in the center-of-mass frame of reactant A, by the following procedure:

- The $\mathbf{Q}$ and $\mathbf{P}$ are transformed to Cartesian coordinates $\mathbf{q}$ and momenta for N atoms using the normal mode eigenvector $\mathbf{L}$ [17]:

$$\begin{aligned} \mathbf{q} &= \mathbf{q_0} + \mathbf{M^{-1/2}LQ} \\ \mathbf{p} &= \mathbf{M^{1/2}LP} \end{aligned} \tag{3.16}$$

  where $\mathbf{q_0}$ is a vector of the equilibrium coordinates and $\mathbf{M}$ is a diagonal matrix whose elements are the atomic masses. Since normal modes are approximate for finite displacements [17], a spurious angular momentum j_s arises following this transformation [18, 19].

- The spurious angular momentum is found from:

$$\mathbf{j_s} = \sum_{\mathbf{i=1}}^{\mathbf{N}} \mathbf{r_i} \times \mathbf{m_i}\dot{\mathbf{r}}_\mathbf{i} \tag{3.17}$$

  where m_i is the mass of the ith atom and $\mathbf{r_i}$ its position vector. The desired angular momentum $\mathbf{j_0}$ is added to the molecule by forming the vector

$$\mathbf{j} = \mathbf{j_0} - \mathbf{j_s} \tag{3.18}$$

  and adding the rotational velocity $\boldsymbol{\omega} \times \boldsymbol{r_i}$ to each atom, where:

$$\boldsymbol{\omega} = \mathbf{I^{-1}j} \tag{3.19}$$

  and $\mathbf{I^{-1}}$ is the inverse of inertia tensor [9].

- The actual internal energy E for the Cartesian coordinates and momenta, chosen from two previous steps, is calculated using the correct Hamiltonian and compared with the intended (provided) energy E^0. If they do not agree within some acceptance criterion, the Cartesian coordinates and momenta are scaled according to:

$$\begin{aligned} \mathbf{q}_i' &= \mathbf{q}_i^0 + (\mathbf{q_i} - \mathbf{q}_i^0)(E^0/E)^{1/2} \\ \mathbf{p}_i' &= \mathbf{p}_i(E^0/E)^{1/2} \end{aligned} \tag{3.20}$$

  any spurious center-of-mass translational energy is subtracted from the molecule and the procedure loops back to the second step.

The above Cartesian coordinates selected for the polyatomic are then randomly rotated through Euler's angles [20] to give a random orientation:

$$\mathbf{q} = \mathbf{R}(\theta, \phi, \chi)\mathbf{q}^0 \quad \dot{\mathbf{q}} = \mathbf{R}(\theta, \phi, \chi)\dot{\mathbf{q}}^0 \tag{3.21}$$

a dot above a quantity represent its time derivative, $\mathbf{q}^0$ and $\dot{\mathbf{q}}^0$ are vectors of the Cartesian coordinates and velocities selected above and $\mathbf{R}(\theta, \phi, \chi)$ is the Euler rotation matrix. The angles θ, ϕ, χ are randomly chosen according to:

$$\cos\theta = 2R_1 - 1, \ \phi = 2\pi R_2, \ \chi = 2\pi R_3 \tag{3.22}$$

where R_1, R_2 and R_3 are three different random numbers.

Since the polyatomic reactant A has a random orientation in the space-fixed coordinates frame, the atom B may be placed in the yz plane without loss of generality. The x, y, z coordinates of B are then:

$$x = 0, \ \ y = b, \ \ z = (s^2 - b^2)^{1/2} \tag{3.23}$$

where s is the initial separation between both reactants centers of mass, and b the impact parameter.

The A + B relative velocity v_{rel} is now added along the z-axis with restraint that the A+B center of mass remains at rest. The space fixed Cartesian momenta are then:

$$\mathbf{P} = \mathbf{M}(\dot{\mathbf{q}} - \dot{\mathbf{q}}_{\text{rel}}) \tag{3.24}$$

the elements of the relative velocity $\dot{\mathbf{q}}_{\text{rel}}$ are zero for x and y components and equal $[m_{\text{A}}/(m_{\text{A}} + m_{\text{B}})]v_{\text{rel}}$ for the z component of each atom of B and equal to $-[m_{\text{B}}/(m_{\text{A}} + m_{\text{B}})]v_{\text{rel}}$ for the z component of each atom of A. Thus, the initial configuration is already determined.

3.1.3 Product properties

In classical calculations, a trajectory is ended once provided conditions of product formation are accomplished (see table 1 of Chapter 4, as example). Then, the resulting information is collected in terms of the whole set of coordinates and linear momenta of all the atoms. These variables must be transformed into those of physical interest [4].

In the chemical reaction:

$$\mathrm{A} + \mathrm{B} \rightarrow \mathrm{C} + \mathrm{D} \tag{3.25}$$

the properties with interest are commonly: the C + D relative translational energy, the C and D vibrational and rotational energies and the scattering angle between the initial A + B and the final C + D relative velocity vectors. These properties are calculated from space-fixed Cartesian coordinates and momenta at the termination of a classical trajectory. The procedures here described are incorporated in the general chemical dynamics program VENUS [10] used to calculate the trajectories for the reactions studied in this thesis.

3.1.3.1 Relative velocity and translational energy

The product relative velocity is the difference between the velocities of the centers of mass of C and D. For example for the x component of the center of mass position and velocity of product D is given by:

$$X_{\mathrm{D}} = \sum_{i=1}^{n_{\mathrm{D}}} m_i x_i / M_{\mathrm{D}} \,, \;\; \dot{X}_{\mathrm{D}} = \sum_{i=1}^{n_{\mathrm{D}}} m_i \dot{x}_i / M_{\mathrm{D}} \tag{3.26}$$

where the sum is over n_{D}, the number of atoms in D, m_i are the masses and x_i are the x coordinates of the atoms. M_{D} is the mas of D, upper case variables identify the center of mass position and velocity. The product relative velocity is the time derivative of the relative coordinate:

$$\begin{aligned} \mathbf{R} &= \mathbf{R}_{\mathrm{D}} - \mathbf{R}_{\mathrm{C}} \\ &= (X_{\mathrm{D}} - X_{\mathrm{C}})\mathbf{i} + (Y_{\mathrm{D}} - Y_{\mathrm{C}})\mathbf{j} + (Z_{\mathrm{D}} - Z_{\mathrm{C}})\mathbf{k} \\ &= R_x\mathbf{i} + R_y\mathbf{j} + R_z\mathbf{k} \\ \dot{\mathbf{R}} &= \dot{R}_x\mathbf{i} + \dot{R}_y\mathbf{j} + \dot{R}_z\mathbf{k} \end{aligned} \tag{3.27}$$

where $\mathbf{i}, \mathbf{j}, \mathbf{k}$ are the unitary vectors in the x,y,z directions respectively. The product translational energy is:

$$E_{rel} = \frac{\mu_{\mathrm{CD}} \dot{\mathbf{R}} \cdot \dot{\mathbf{R}}}{2} \tag{3.28}$$

where $\mu_{\mathrm{CD}} = M_{\mathrm{C}}M_{\mathrm{D}}/(M_{\mathrm{C}} + M_{\mathrm{D}})$ is the CD reduced mass. E_{rel} may also be written as the sum of the relative translational energy along the line of centers C − D and the energy of the orbital (angular) motion:

$$E_{rel} = \frac{\mu_{\mathrm{CD}}\dot{R}^2}{2} + \frac{l^2}{2\mu_{\mathrm{CD}}R^2} \tag{3.29}$$

being $\dot{R}$ the module of the velocity along line of centers (radial velocity), and R the distance between them:

$$R = (\mathbf{R}\cdot\mathbf{R})^{1/2}\,,\ \dot{R} = \frac{R_x\dot{R}_x + R_y\dot{R}_y + R_z\dot{R}_z}{R} \tag{3.30}$$

$\mathbf{l}$ is the orbital angular momentum (and l its module):

$$\mathbf{l} = \mu_{\mathrm{CD}}\mathbf{R}\times\dot{\mathbf{R}} = l_x\mathbf{i} + l_y\mathbf{j} + l_z\mathbf{k} \tag{3.31}$$

3.1.3.2 Velocity scattering angle

The velocity scattering angle θ_v is the angle between the relative velocity vector for the reactants $\dot{\mathbf{R}}^0$ and the product's relative velocity vector $\dot{\mathbf{R}}$, given by:

$$\theta_v = \cos^{-1}\left(\frac{\dot{\mathbf{R}}\cdot\dot{\mathbf{R}}^0}{\dot{R}\dot{R}^0}\right) \tag{3.32}$$

3.1.3.3 Internal energy

To calculate the internal rotational and vibrational energy of the products requires the coordinates and velocities of each atom of the molecule in the center of mass frame of the molecule:

$$x'_i = x_i - X_{\mathrm{D}}\,,\ \dot{x}'_i = \dot{x}_i - \dot{X}_{\mathrm{D}}\,,\ i = \overline{1, n_{\mathrm{D}}} \tag{3.33}$$

the internal energy of D is:

$$E_{\mathrm{D}} = T_{\mathrm{D}} + V_{\mathrm{D}} \tag{3.34}$$

where T_{D} and V_{D} are the kinetic and vibrational energies of D respectively. V_{D} is determined from the potential energy function and T_{D} is given by:

$$T_{\mathrm{D}} = \sum_{i=1}^{n_{\mathrm{D}}} \frac{m_i(\dot{x}_i^2 + \dot{y}_i^2 + \dot{z}_i^2)}{2} \tag{3.35}$$

3.1.3.4 Rotational angular momentum

The rotational angular momentum $\mathbf{j}$ of the product molecule D is the sum of the angular momentum $\mathbf{j}_i$ of the individual atoms of D relative to its center of mass:

$$\mathbf{j}_{\mathrm{D}} = \sum_{i=1}^{n_{\mathrm{D}}} \mathbf{j}_i = j_x\mathbf{i} + j_y\mathbf{j} + j_z\mathbf{k} \tag{3.36}$$

the atomic angular momentum is given by:

$$\mathbf{j}_i = m_i\mathbf{r}'_i \times \dot{\mathbf{r}}'_i \tag{3.37}$$

The total angular momentum of the C + D products is the vector sum:

$$\boldsymbol{\mathcal{L}} = \mathbf{l} + \mathbf{j}_{\mathrm{C}} + \mathbf{j}_{\mathrm{D}} \tag{3.38}$$

3.1.3.5 Rotational and vibrational energies

If the product correspond to a diatomic species, same procedure as previously described in equations (3.28-3.31) can be used. The internal energy T_{D} of a diatomic molecule 1-2, can be written:

$$T_{\mathrm{D}} = \frac{\mu_{12}\dot{r}^2}{2} + \frac{j^2}{2\mu_{12}r^2} \tag{3.39}$$

where μ_{12} is the reduced mass of D, r is the 1-2 bond length. Similar expressions than (3.28-3.31) are used for r and $\dot{r}$. The rotational quantum number J for D is found from the expression:

$$j = \sqrt{J(J+1)}\hbar \tag{3.40}$$

Since calculation is classical, non-integer values are obtained for J; then, rounding is often used.

The vibrational quantum number is obtained with help of semi-classical quantization condition [21, p71]:

$$\oint p_r \mathrm{d}r = (n + \frac{1}{2})2\pi\hbar \tag{3.41}$$

where the momentum $p_r = \mu\dot{r}$ and the cyclic integral denotes integration over one orbit. From the equations (3.34) and (3.39) p_r is given by:

$$p_r = \left[2\mu_{12}\left(E_{\mathrm{D}} - \frac{j^2}{2\mu_{12}r^2} - V_{\mathrm{D}}(r)\right)\right]^{1/2} \tag{3.42}$$

as for J, non-integer values of n are often obtained.

If D is a polyatomic species it is not a simple to calculate rotational and vibrational quantum numbers [4]. Semi-classical quantization can be used as in case of diatomic molecules, presented above. However, mostly because of the multidimensional character, such a task is tedious. As a result most of the semi-classical quantization has been limited to triatomics. So far, there is not a general form to calculate both rotational and vibrational quantum numbers from its Cartesian coordinates [4].

It is always possible to calculate the average vibrational and rotational energies of a polyatomic product:

$$E_{\mathrm{D}} = \langle E_{\mathrm{D}}^{vib} \rangle + \langle E_{\mathrm{D}}^{rot} \rangle \tag{3.43}$$

Because of the ro-vibrational coupling the vibrational and rotational energies of D, E_{D}^{vib} and E_{D}^{rot}, will fluctuate as the molecule vibrates. An instantaneous rotational energy for D may be calculated from:

$$E_{\mathrm{D}}^{rot} = \frac{1}{2}\boldsymbol{\omega}_{\mathrm{D}} \cdot \mathbf{j}_{\mathrm{D}} \tag{3.44}$$

$\mathbf{j}_{\mathrm{D}}$ has been defined in Eqn. 3.36 and $\boldsymbol{\omega}_{\mathrm{D}}$, the angular velocity of D, can be determined from equation (3.19).

The average rotational energy is computed by averaging over the longest vibrational period of the product. Then, by means of equation (3.44), the average vibrational energy can also be obtained.

3.2 Excitation functions and rate constant

Molecular beam experiments provide high initial collision energy resolution [22]. That is why they are often employed to measure the translational energy dependence of the reaction cross section (excitation function). Much of the interesting information about an elementary chemical reaction can be summarized in such a function [23]. Besides, it is also needed to calculate the rate constant for specific ro-vibrational states of the reactants. Once its value is obtained for a given translational energy, some models are used to represent it.

3.2.1 Reaction with barrier

Based on the fitting of available data, LeRoy [23] proposed some particular models:

Class I reactions

$$\sigma(E_{\rm tr}) = \begin{cases} C(E_{\rm tr} - E_{\rm tr}^{\rm th})^n e^{-m(E_{\rm tr}-E_{\rm tr}^{\rm th})} & E_{\rm tr} \geq E_{\rm tr}^{\rm th} \\ 0 & E_{\rm tr} < 0 \end{cases} \tag{3.45}$$

where $m, n \geq 0$. Those functions increase from 0 at $E_{\rm tr} = E_{\rm tr}^{\rm th}$, the exponential term causes the excitation function to pass through a maximum as the energy increase. Such a dependence describe properly the excitation functions for neutral-neutral reactions. The reaction presented in chapter 5 of this thesis properly fit to this model.

By substituting (3.45) into (3.6), an analytical expression for the rate constant is obtained:

$$\begin{aligned} k(T) &= C\left(\frac{8k_BT}{\pi\mu}\right)^{1/2} \frac{(k_BT)^n e^{-E_{\rm tr}^{\rm th}/k_BT}}{(1+mk_BT)^{n+2}} \times \\ &\quad \times \left[\Gamma(n+2) + \Gamma(n+1)\frac{(1+mk_BT)E_{\rm tr}^{\rm th}}{k_BT}\right] \end{aligned} \tag{3.46}$$

where Γ is the Gamma function, see appendix.

Class II reactions

$$\sigma(E_{\rm tr}) = \begin{cases} \frac{C(E_{\rm tr}-E_{\rm tr}^{\rm th})^n}{E_{\rm tr}} e^{-m(E_{\rm tr}-E_{\rm tr}^{\rm th})} & E_{\rm tr} \geq E_{\rm tr}^{\rm th} \\ 0 & E_{\rm tr} < 0 \end{cases} \tag{3.47}$$

these functions are very similar to the previous one, however they include the excitation function for the collision of hard spheres which requires a critical energy $E_{\rm tr}^{\rm th}$ [22]. This excitation function yields to a rate constant:

$$k(T) = C\left(\frac{8k_BT}{\pi\mu}\right)^{1/2} \frac{(k_BT)^{n-1}\Gamma(n+1)e^{-E^{\rm th}/k_BT}}{(1+mk_BT)^{n+1}} \tag{3.48}$$

Class III reactions

$$\sigma(E_{\rm tr}) = \begin{cases} CE_{\rm tr}^n & E_{\rm tr} \geq E_{\rm tr}^{\rm th} \\ 0 & E_{\rm tr} < 0 \end{cases} \tag{3.49}$$

This type of functions applies for collisions between low energy ions and polarizable molecules [23]. For these functions, the rate constant becomes:

$$k(T) = C\left(\frac{8k_BT}{\pi\mu}\right)^{1/2}(k_BT)^n[\Gamma(n+2) - P(n+2, E_{\rm tr}^{\rm th}/k_BT)] \tag{3.50}$$

being P the incomplete Gamma function, see appendix.

3.2.2 Barrier-free reactions

In the collision of two particles (with masses m_1 and m_2) interacting along the centers of mass line, the two-body problem can be simplified into a one-body problem. There, a particle of mass μ ($\mu = m_1m_2/(m_1+m_2)$) moves under the influence of an effective potential ($V_{\rm eff}$) given by the sum of the interaction between both particles and a centrifugal potential [9].

For reactions which proceed through an attractive potential energy surface, without a barrier (capture-like), the centrifugal barrier on the effective potential $V_{\rm eff}$ may still prevent reaction. To obtain a simple model of such a kind of collision, structureless reactants will be assumed. Considering also a long-range attractive potential in the form:

$$V(R) = -\frac{C_n}{R^n} \tag{3.51}$$

where C_n and n are parameters depending on the interaction type, with n=3 when there are dipole-dipole like, n=4 for quadrupole-dipole and so on [24, 25]. The distance between reactants is represented by R. Of course the above assumption is a large simplification of the problem as in real collisions we deal with reactants having different electric multipoles and also their values can change as the reaction proceeds. However, these effects are supposed to be included in the values on n and C_n with some intermediate values, not corresponding exactly to any specific multipole interaction, but to a mixture of them.

The effective potential becomes:

$$V_{\rm eff}(R) = E_{\rm tr}\frac{b^2}{R^2} - \frac{C_n}{R^n} \tag{3.52}$$

where b is the impact parameter. $V_{\rm eff}(R)$ has a maximum value at $R = R_0$:

$$R_0 = \left(\frac{nC_n}{2E_{\rm tr}b^2}\right)^{1/(n-2)} \tag{3.53}$$

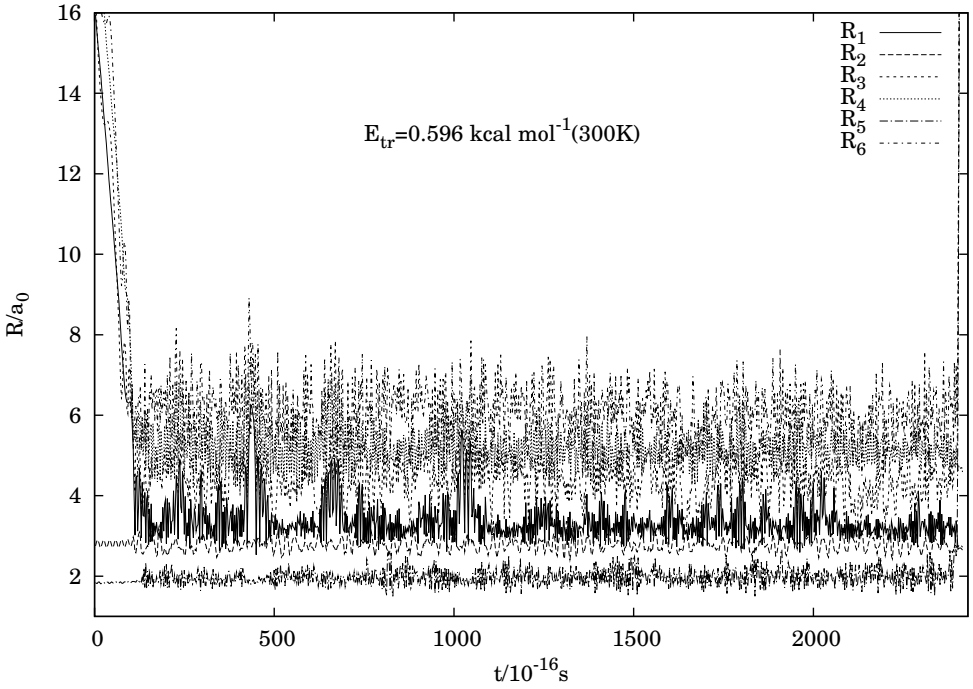

Figure 1. Distance *vs.* time plot for a typical trajectory of the reaction OH + SO → H + SO_2, for low translational energies of the reactants.

With the condition that the translational energy must equal the maximum value of the effective potential for $b{=}b_{max}$, the excitation function then becomes:

$$\sigma(E_{\rm tr}) = \pi b_{max}^2 = n\pi(n-2)^{(2-n)/n}\left(\frac{C_n}{2E_{\rm tr}}\right)^{2/n} \tag{3.54}$$

By substituting the previous expression into Eq. (3.6), the rate constant is obtained as:

$$k(T) = 2n\pi(n-2)^{(2-n)/n}\left(\frac{2}{\pi\mu}\right)^{1/2}\left(\frac{C_n}{2}\right)^{2/n}\Gamma\left(\frac{2n-2}{n}\right)(k_BT)^{(n-4)/2n} \tag{3.55}$$

Even when this result was obtained for a simplified model of interaction, it fits particularly well the radical-radical reactions [26]. Molecular collisions OH + SO and S + HO_2 presented respectively in chapters 4 and 6 of this thesis are properly described by such a model; though further corrections are needed in the former to account for recrossing effects.

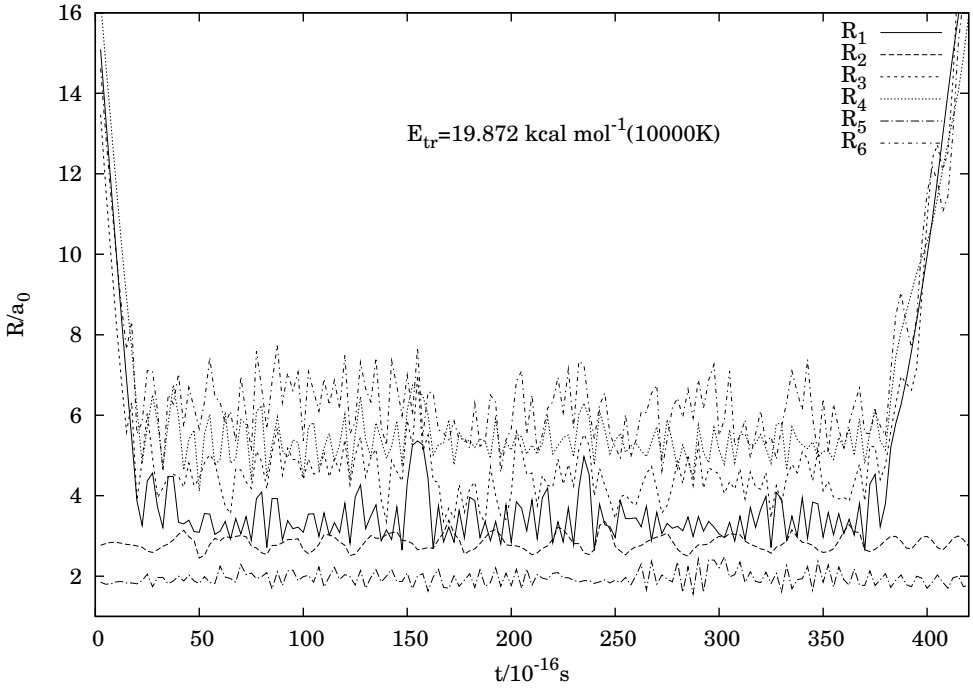

Figure 2. Distance *vs.* time plot for a typical recrossing trajectory in the OH + SO collision, for high translational energies of the reactants.

3.3 Complex formation

An important information one gets from quasi-classical trajectories is the reaction mechanism. Very useful are the distances *vs* time plots such as shows in Figures 1 and 2. By means of such a kind of plot, and with the knowledge of the topology of the PES, it is possible to describe the intermediate species or structures formed in the path from reactants to products (in the general sense products may also be recoiled reactants, as in inelastic scattering). However, a detailed check of all the plots produced by each of the computed trajectory is a cumbersome task. What it is actually done is to choose a certain number of trajectories and define a criterion to identify whether such structure is formed or not, and implement it in the code used for computing trajectories. Such a criteria should be carefully tested in a significant number of trajectories.

For example, by checking 100 trajectories at $E_{\rm tr} = 0.6$ and $E_{\rm tr} = 20.0$kcal mol^{-1} of the reaction OH + SO (see chapter 4) in detail, we verify that OH bond length remains shorter than the HS bond length. This observation led to the conclusion

that there is no formation of an HSO_2 conformer in the C_{2v} structure with the H atom bonded to the S atom. HOSO with hydrogen bonded to one of the oxygen atoms is formed instead. The selected criterion can also provide life-times of the formed complex. Usually geometry conditions are used to define it (distances between atoms, comparison between them, etc.) but energetic conditions may be used as well.

When a trajectory enters into a configuration corresponding to a complex and returns back to the reactants it is said a recrossing has occurred [26]. This effect is common in reactions with a deep well in the interaction potential, corresponding to the complex, followed by a barrier which must be overcame for continuing the way to the products. For these cases, it is particularly important to detect whether or not the complex was formed during the trajectory. We may need to account for recrossing effects as a correction in the rate constant or in the excitation function [26]. Thus, the probability of a recrossing needs to be known. In the study of the reaction OH + SO presented in chapter 4 of this thesis, a correction to the capture excitation function is done to account for such effect.

3.4 Electronic degeneracy factor

Degeneracy of the electronic states in a molecular systems were not included in the picture presented so far, of the nuclei moving on a potential energy surface. The results of having different electronic states have a quantitative effect when studying molecular collisions. As early as 1936, it was pointed out by Ravinowich [27], that theoretically calculated rate constants differ in a factor from experimental results. This factor depends upon the electronic degeneracy of the involved species. Bunker and Davidson [28, 29] remarked the role of such a factor. In the work of Truhlar [30] the proper inclusion of the electronic degeneracy was presented while Muckerman and Newton [31] pointed out its dependence on temperature. Main ideas of the degeneracy factor are briefly presented in the following.

In some collision processes (*e.g.* He+Ne) both collision partners have the same degeneracy g ($g = 2$). It is a good approximation to consider that internuclear motion is governed by one potential energy surface, corresponding to the lowest

energy (degenerate or not) electronic state of the system. For most collision problems one must consider more than one electronic state: *e.g.* $I^2P_{3/2}$ has $g = 4$ so the collision partners in I + I have $g = 16$. However, the ground state of I_2 is non-degenerate. Coupling between the 16 states of I_2 is expected at large internuclear distances where the states are nearly degenerate. In the absence of a detailed treatment of this non-adiabatic coupling it is reasonable to use BOA at all internuclear distances. In this approximation each collision occurs on one potential energy surface, but only 1/16 of the collisions occurs in the ground state surface [30].

Thus, when comparing rate constants with experimental values a factor:

$$g_e = \frac{g_{\text{comp}}}{g_{\text{react1}} g_{\text{react2}}} \tag{3.56}$$

should be included. The numerator denotes the degeneracy of the whole molecular system and the denominator accounts for the degeneracies of the reactants. Note that these factors must include the dependence on temperature of spin orbit splitting.

Molecular system studied in this thesis is $HSO_2(^2A)$, a doublet. When studying molecular collision *e.g.* $OH(^2\Pi) + SO(^3\Sigma)$, g_e assumes the form:

$$g_e(T) = \frac{2}{3(2[1 + \exp(-205/T)])} \tag{3.57}$$

the two pi (Π) levels of OH split into two double-fold levels when spin-orbit interaction (first order) is considered, there is an energy gap of 205 K between them [32]. As the three degenerate states of SO are sigma (Σ) states they remain the same as spin-orbit coupling is accounted. In the same way, in all dynamics studies carried out in this work, such a factor was included.

3.5 Quantum corrections to classical calculations

Even when classical calculations may provide an appropriate description of molecular collisions, quantum nature of the molecular world should be preserved. Thus, some behaviors in the classical calculations must be corrected.

The so-called tunnel effect is a direct consequence from quantum mechanics [21], when a particle is passing through a potential energy barrier. Of course,

classical calculations do not account for such effect. Some attempts have been made to include tunneling in classical calculations (see Ref. [33] and references therein). In molecular collisions studied in this work, tunneling effects will not be considered.

An important error uprising from classical calculations are the "sub-threshold" reactive trajectories appearing in some reactions for translational energies below the quantum threshold [34]. This fact could be significant, especially for barrier-type reactions, where the threshold energy dictates the magnitude and the slope of the rate constant. In the reactions presented here it was followed the idea of Varandas and collaborators [35] to circumvent this problem. There, the authors calculated trajectories for translational energies above the energy threshold, whose value is fixed to the conventional transition state enthalpy.

Classical calculations does not forbid molecular systems to have vibrational energy bellow the lowest value given by quantum calculations. This is usually referred as zero-point energy (ZPE) leakage. To account for ZPE leakage of classical calculations several strategies have been proposed [36–41]. In the quasiclassical study of the reactions presented in this thesis the following methods were used:

- **IEQMT** [39]. Internal Energy Quantum Mechanics Threshold. Each product is demanded to have an internal energy larger than its corresponding ZPE.

- **VEQMT** [40]. Vibrational Energy Quantum Mechanical Threshold. The vibrational energy of each product must be larger than its corresponding ZPE.

- **VEQMT$_{\mathbf{C}}$** [41] Vibrational Energy Quantum Mechanical Threshold of the Complex. The vibrational energy of the complex, just before dissociation, must be larger than the sum of the ZPE energies of the formed products.

It must be noted, as a final remark on this chapter, that although quantum mechanics should be used for the exact treatment of the dynamics of molecular systems, classical methods are affordable means to obtain cross sections for the majority of systems of chemical interest. This is valid for large polyatomics as much as small systems containing heavy atoms.

Bibliography

[1] D. L. Bunker, Methods Comput. Phys. **10** (1971).

[2] G. H. Peslherbe, H. Wang, and W. L. Hase, Adv. Chem. Phys. **105**, 171 (1999).

[3] M. Karplus, R. Porter, and R. D. Sharma, J. Chem. Phys. **43**, 3259 (1965).

[4] W. L. Hase, *Encyclopedia of Computational Chemistry* (Wiley, New York, 1998), chap. Classical Trajectory Simulations: Final Conditions, p. 399.

[5] R. D. Levine and R. B. Bernstein, *Molecular dynamics reaction* (Oxford University Press: New York, 1974).

[6] A. J. C. Varandas, Chem. Phys. Lett. **225**, 18 (1994).

[7] M. Karplus, R. Porter, and R. D. Sharma, J. Chem. Phys. **40**, 2033 (1964).

[8] M. Karplus and K. T. Tang, Discussions Faraday Society **44**, 56 (1967).

[9] H. Golstein, *Classical Mechanics* (Addison-Wesley, London, 1950).

[10] W. L. Hase, MERCURY: a general Monte-Carlo classical trajectory computer program, QCPE#453. An updated version of this code is VENUS96: W. L. Hase, R. J. Duchovic, X. Hu, A. Komornik, K. F. Lim, D.-H. Lu, G. H. Peslherbe, K. N. Swamy, S. R. van de Linde, A. J. C. Varandas, H. Wang, R. J. Wolf, QCPE Bull 1996, *16*, 43.

[11] R. D. Levine and R. B. Bernstein, *Molecular dynamics reaction and Chemical Reactivity* (Oxford University Press: New York, 1987).

[12] P. J. S. B. Caridade, M. Betancourt, J. D. Garrido, and A. J. C. Varandas, J. Phys. Chem. A **105**, 7435 (2001).

[13] P. J. S. B. Caridade, L. Zhang, J. D. Garrido, and A. J. C. Varandas, J. Phys. Chem. A **105**, 4395 (2001).

[14] W. L. Hase and D. G. Buckowski, Chem. Phys. Lett. **74**, 284 (1980).

[15] D. L. Bunker and E. A. G. Simpson, Faraday Discuss. Chem. Soc. **55**, 93 (1973).

[16] J. M. Hammersley and D. C. Handscomb, *Monte Carlo Methods* (Metthuen, London, 1964).

[17] S. Califano, *Vibrational States* (Wiley, New York, 1976).

[18] S. Chapman and D. L. Bunker, J. Chem. Phys. **62**, 2980 (1975).

[19] C. S. Sloane and W. L. Hase, J. Chem. Phys. **66**, 1523 (1977).

[20] E. B. Wilson Jr, J. C. Decius, and P. C. Cross, *Molecular Vibrations* (McGraw-Hill, New York, 1995).

[21] A. S. Davydov, *Quantum Mechanics* (Edicion Revolucionaria, La Habana, 1965).

[22] M. Brouard, *Reaction Dynamics*, Oxford University Primers (Oxford Unversity Press, 1998).

[23] R. L. LeRoy, J. Phys. Chem. **73**, 4338 (1969).

[24] J. D. Jackson, *Classical Electrodynamics* (Academic Press, New York, 1999), 3rd edn.

[25] J. O. Hirschfelder, C. F. Curtis, and R. B. Bird, *Molecular Theory of Gases and Liquids* (Wiley, New York, 1954).

[26] A. J. C. Varandas, in *Conferencias Plenarias de la XXIII Reunión bienal de Qímica*, edited by A. S. Feliciano, M. Grande, and J. Casado, Universidad de Salamanca (1991), p. 321.

[27] E. Ravinowich, Trans. Faraday Soc. **33**, 283 (1936).

[28] D. Bunker and N. Davidson, J. Am. Chem. Soc. **80**, 5090 (1958).

[29] D. Bunker, J. Chem. Phys. **32**, 1001 (1960).

[30] D. G. Truhlar, J. Chem. Phys. **56**, 3189 (1972).

[31] J. T. Muckerman and M. D. Newton, J. Chem. Phys. **56**, 3191 (1972).

[32] K. P. Huber and G. Herzberg, *Constants of diatomics molecules* (Van Nostrand, Princeton, 1979).

[33] A. J. C. Varandas and G. V. Mil'nikov, Chem. Phys. Lett. **259**, 605 (1996).

[34] G. C. Schatz, J. Chem. Phys. **79**, 5386 (1983).

[35] A. J. C. Varandas, P. J. S. B. Caridade, J. Z. H. Zhang, Q. Cui, and K. L. Han, J. Chem. Phys. **125**, 064312 (2006).

[36] W. H. Miller, W. L. Hase, and C. L. Darling, J. Chem. Phys. **91**, 2863 (1989).

[37] J. M. Bowman, B. Gazdy, and Q. Sun, J. Chem. Phys. **91**, 2859 (1989).

[38] A. J. C. Varandas and J. M. C. Marques, J. Chem. Phys. **100**, 1908 (1194).

[39] A. J. C. Varandas, J. Brandão, and M. R. Pastrana **96**, 5137 (1992).

[40] A. J. C. Varandas, J. Chem. Phys. **99**, 1076 (1993).

[41] A. J. C. Varandas and L. Zhang, Chem. Phys. Lett. **340**, 62 (2001).

Chapter 4

The reaction $\mathbf{OH + SO \rightarrow H + SO_2}$

Chem. Phys. Lett. **433**, 279-285 (2007).

Dynamics of the reaction $OH + SO \rightarrow H + SO_2$

M. Y. Ballester and A.J.C. Varandas

Departamento de Química, Universidade de Coimbra
P-3049 Coimbra Codex, Portugal.

(Received: 27 October 2006; in final form: 14 November 2006)

Abstract

We report a quasiclassical trajectory study of the title reaction using a recently reported double many-body expansion potential energy surface for ground state HSO_2. Two methods that aim to account for zero point energy leakage are used. A capture-type behavior is predicted, with recrossing effects manifesting mainly at high translational energies. Reaction cross sections and a comparison of the calculated rate constant with available literature data are also reported.

1 Introduction

The SO radical plays a significant role in combustion chemistry [1], while tropospheric oxidation of sulfur is driven by hydroperoxyl radicals [2]. In particular, the reaction

$$OH + SO \rightarrow H + SO_2 \tag{1}$$

has been much studied, both theoretically and experimentally [3–10]. Although some of these works have suggested mechanisms [7, 8], they have all been based on studies using partial information about the HSO_2 system. Our aim here is to report a dynamics and kinetics study of reaction (1) using a single-sheeted (global) double many-body expansion (DMBE) potential energy surface recently reported [11] for HSO_2, hoping to clarify how the reaction proceeds. The paper is organized as follows. Section 2 surveys briefly the potential energy surface, while the technicalities of the computational method are addressed in section 3. The results and discussion are in section 4, and the conclusions in section 5.

2 Potential Energy Surface

All calculations employed the six-dimensional double many-body expansion potential energy surface for the electronic ground state of HSO_2. Since this has already been described in detail elsewhere [11], we focus on its major topographical features which are of relevance for the title reaction. Figure 1 depicts schematically its energetics, as predicted from the HSO_2 DMBE potential energy surface. As it is shown in this diagram, the title reaction can proceed via one or two intermediate structures: HOSO and/or HSO_2. Figure 2 shows a perspective view of the HSO_2 potential energy surface for regions of configuration space with relevance for the title reaction: the x-axis stands for the $O-H$ distance relating to the hydrogen and oxygen atoms in the hydroxyl radical, while the y-axis indicates the distance between sulfur in SO and oxygen in OH. Note that $\angle$OSO, $\angle$SOH, and the dihedral angle, as well as the SO distance, are partially relaxed in this plot.

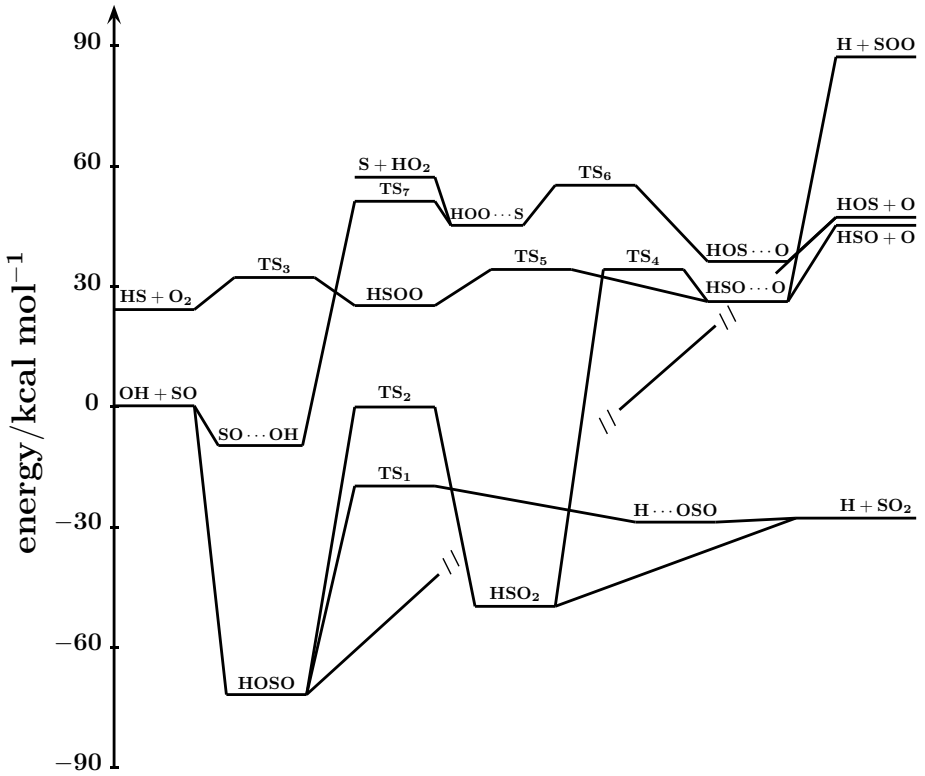

Figure 1. Energetics of the single-sheeted DMBE potential energy surface [11] for HSO_2.

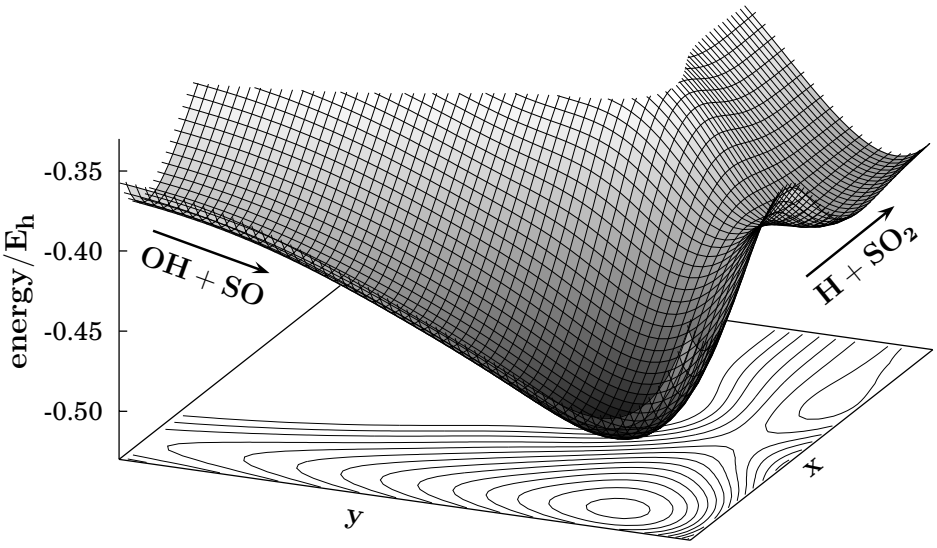

Figure 2. 3D perspective view of the $OH + SO \rightarrow H + SO_2$ channel of the HSO_2 DMBE potential energy surface [11]. Energy is in E_h, with contours starting at $-0.4800\,E_h$, equally spaced by $0.01\,E_h$.

3 Computational procedure

To run the quasi-classical trajectories, we have utilized an adapted version of the VENUS96 [12] code which accommodates the HSO_2 DMBE potential energy surface. Calculations have done for diatom-diatom translational energies in the range $0.2 \leq E_{\rm tr}/\text{kcal mol}^{-1} \leq 19.9$. In all cases the vibrational and rotational quantum numbers of the reactants have been fixed at the ground level. This implies $v_{\rm OH} = v_{\rm SO} = 0$ for the vibrational quantum numbers, while the rotational quantum numbers are $j_{\rm OH} = 1$ and $j_{\rm SO} = 0$ assuming [13] that OH fits Hund's rule case b) (according, the smallest N' value should be $N' = 1, 2, \ldots$; for consistency, we use j instead of N' in this work). Of course, a thermalized rotational-vibrational distribution would be necessary if one seeks a comparison with thermal rate coefficients. We focus here more on dynamical issues for specific initial states and translational energies, leaving a direct thermalized calculation of the rate constant for future consideration.

The step size used for numerical integration is 2.5×10^{-16} s, which warrants conservation of the total energy to better than 1 part in 10^3. The reactant diatomic molecules were initially separated by 9 Å, a value considered sufficiently large to make the interaction energy essentially negligible. The procedure employed to assign reactive channels has been described elsewhere [14]. There are 14 possible arrangement channels if we do not distinguish those leading to isomers of a given species. Table 1 collects their assignments according to the geometries of the four-atom species (channel 1 identifies the reactants). In turn, the maximum impact parameter (b_{max}) has been found by running batches of 100 trajectories at fixed values, with b_{max} being diminished until reaction (this implies an exit channel distinct from # 1) takes place. Such a procedure allows to determine b_{max} within ±0.1 Å. For a given translational energy, batches of trajectories have then been run, and the reactive cross section calculated as $\sigma_r(E_{\rm tr}) = \pi b_{max}^2 P_r$, with the associated 68 % uncertainties being $\Delta\sigma_r(E_{\rm tr}) = \sigma_r \left[(N_T - N_r) / N_T N_r \right]^{1/2}$; N_r is the number of reactive trajectories in a total of N_T, and $P_r = N_r/N_T$ the reaction probability. From this, and assuming a Maxwell-Boltzmann distribution over the translational energy ($E_{\rm tr}$), the specific thermal rate coefficient is obtained as

$$k(T) = g_e(T) \left(\frac{2}{k_B T} \right)^{3/2} \left(\frac{1}{\pi \mu} \right)^{1/2} \int_0^\infty E_{\rm tr} \sigma_r(E_{\rm tr}) \exp\left(-\frac{E_{\rm tr}}{k_B T} \right) dE_{\rm tr} \qquad (2)$$

Table 1. Assignment of reaction channels.

Channel	Products	R_1/Å	R_2/Å	R_3/Å	R_4/Å	R_5/Å	R_6/Å
1	$O_aH + SO_b$	∞	1.481	∞	∞	0.971	∞
2	$O_bH + SO_a$	1.481	∞	∞	∞	∞	0.971
3	$HS + O_2$	∞	∞	1.340	1.208	∞	∞
4	$H + SO_2$	1.431	1.431	∞	2.470	∞	∞
5	$O_a + HSO_b$	∞	1.512	1.386	∞	∞	2.374
6	$O_b + HSO_a$	1.512	∞	1.386	∞	2.374	∞
7	$S + HO_2$	∞	∞	∞	1.331	0.971	1.831
8	$O_a + H + SO_b$	∞	1.481	∞	∞	∞	∞
9	$S + O_b + HO_a$	∞	∞	∞	∞	0.971	∞
10	$O_b + H + SO_a$	1.481	∞	∞	∞	∞	∞
11	$S + O_a + HO_b$	∞	∞	∞	∞	∞	0.971
12	$S + H + O_2$	∞	∞	∞	1.208	∞	∞
13	$O_a + O_b + HS$	∞	∞	1.340	∞	∞	∞
14	$S + O_a + O_b + H$	∞	∞	∞	∞	∞	∞

where T is the temperature, and $g_e(T)$ the electronic degeneracy factor which assumes [15, 16] the form:

$$g_e(T) = \frac{1}{3[1 + \exp(-205/T)]} \tag{3}$$

Note that $OH(^2\Pi)$ splits into two double-fold degenerate states [$OH(^2\Pi_{1/2})$ and $OH(^2\Pi_{3/2})$] when first-order spin-orbit interaction is considered, with 205 K being the energy difference between them [17]. In turn, $SO(^3\Sigma)$ is a triplet, while the complex is a doublet.

To monitor complex formation, we have first studied in detail 100 trajectories at translational energies of 0.596 and 19.87 kcal mol^{-1} (respectively, 300 and 10000 K). From the analysis of time vs bond-distance plots (not shown for brevity), a geometric criterion has been set to define whether complex formation has occurred. According to such a criterion, complex formation is defined by means of only two bond-lengths: one ensuring that the incoming hydroxyl is bonded to sulfur, the other checking whether the H atom is part of the four-body moiety or, instead, far away forming $H + SO_2$ products. A complex is then any

arrangement of the four atoms where the HS and SO_a distances become shorter than 1.3 times their values at the global minimum. Such a definition leads to complex lifetimes that agree well with those obtained from inspection of the above referred bond distance vs time plots. Indeed, we find such a procedure to be sufficiently rigorous to avoid the cumbersome observation of the bond distance vs time plots for all trajectories that have been run, although checks have been performed here and there to warrant the accuracy of the method during mass production of the trajectory results. We note at this stage that in no single case has HSO_2 been formed. The same applies to the oxygen interchange process $HO_a + SO_b \rightarrow HO_b + SO_a$, as in no case it has been observed.

A well know problem of classical trajectories is the so-called zero-point energy leakage. Both 'active' and 'non-active' methods have been suggested (Ref. 18, and references therein) to overcome it in an approximate manner. In the active methods, a constraint is introduced to prevent the trajectories from entering the region of phase space which allows vibrational modes to have less than its ZPE. Instead, in the non-active ones, trajectories leading to aphysical products (with vibrational/internal energies below a given threshold) are thrown out and replaced [13] by running novel trajectories. The perturbed statistics may eventually be corrected *a posteriori* [19]. Thus, no trajectory calculations, besides those run in the traditional QCT method are eventually required when using a non-active method. Clearly, the above mentioned schemes are not free from ambiguity, and we use only two simple non-active methods in this work, namely $VEQMT_C$ [20] and IEQMT [21]. The former demands that the total vibrational energy of the products is larger than the sum of their ZPEs [20] while the latter, less restrictive, requires that the total internal energy of each molecular product is larger than the corresponding ZPE [21].

4 Results and discussion

According to Figures 1 and 2, the title reaction takes place without a potential barrier. Computational difficulties arise as a significant number of trajectories (around 10 %) falls into the deep well of the potential energy surface and remains there up to 4×10^5 steps, thus leading to convergence problems. This is especially

critical at low collisional energies as this leads to a drastic increase in computational cost.

Table 2 summarizes the trajectory calculations, with non-converged trajectories removed from the total number run, N_T. N_c is the number of complex-forming trajectories, and N_r the number of trajectories leading to SO_2 + H formation. This is a subset of N_c, while N_{rec} is the number of recrossing trajectories (those that form a complex but subsequently re-dissociate back to reactants). Once the complex is formed (note that most are long lived), vibrational energy of OH is transfered to other modes. Thus, when the trajectory dissociates back to reactants, it often does so by loosing vibrational energy with respect to its original value, in this case the ground-state vibrational energy. In fact, only for high translational energies, does OH keep its vibrational energy above ZPE. As a result, nearly all recrossing trajectories in the low-translational energy regime suffer from ZPE-leakage. Disregarding such trajectories from the final statistics may imply that reactivity will likely be overestimated with respect to the traditional QCT value as the statistics of the reactive trajectories gets improved with respect to the non-reactive one. This is illustrated in Table 2, where the results from the $VEQMT_C$ and IEQMT methods are compared with those of traditional QCT. We emphasize that all trajectories not fulfilling the threshold conditions imposed by such methods are simply discarded, with no attempt being made to improve the statistics *a posteriori* [19]. As expected, the IEQMT results lie between QCT and $VEQMT_C$. To give reasonable lower and upper limits of reactivity one then needs to consider only the QCT and $VEQMT_C$ methods. Thus, we focus heretofore only on these two approaches. In the absence of a potential energy barrier, the tittle reaction should be controlled at low energies by long-range interactions associated to the permanent electric moments of the reactants. The reactive cross section may then be expressed by multiplying the capture cross section [22, 23] by a factor $F_{rec}(E_{\rm tr})$ that accounts for recrossing effects:

$$\sigma(E_{\rm tr}) = n\pi(n-2)^{(2-n)/n}\left(\frac{C_n}{2E_{\rm tr}}\right)^{2/n} F_{rec}(E_{\rm tr}) \qquad (4)$$

Note that F_{rec} depends on the translational energy, as opposed to Refs. 22, 23 where the correction for recrossing appears in the rate constant and hence is

Table 2. A summary of the trajectories calculations.

$E_{\rm tr}$	$E_{\rm tr}$	b_{max}	QCT				$\rm VEQMT_C$				IEQMT			
K	kcal mol^{-1}	Å	N_T	N_{com}	N_{rec}	N_r	N_T	N_{com}	N_{rec}	N_r	N_T	N_{com}	N_{rec}	N_r
100	0.199	8.8	1946	1656	83	1573	1444	1444	0	1444	1551	1551	0	1551
200	0.396	7.6	1862	1624	92	1532	1395	1395	0	1395	1511	1511	0	1511
300	0.596	7.0	1800	1518	81	1437	1301	1301	0	1301	1422	1422	0	1422
500	0.993	6.1	1742	1405	106	1299	1175	1175	0	1175	1287	1287	0	1287
1000	1.987	5.3	1672	1126	138	988	901	901	0	901	986	986	0	986
3000	5.962	3.7	1791	1097	499	598	570	561	18	543	648	624	28	596
5000	9.936	3.4	1903	1170	864	306	419	398	110	288	549	442	136	306
10000	19.872	2.6	2000	1275	1158	117	695	624	508	116	887	659	542	117

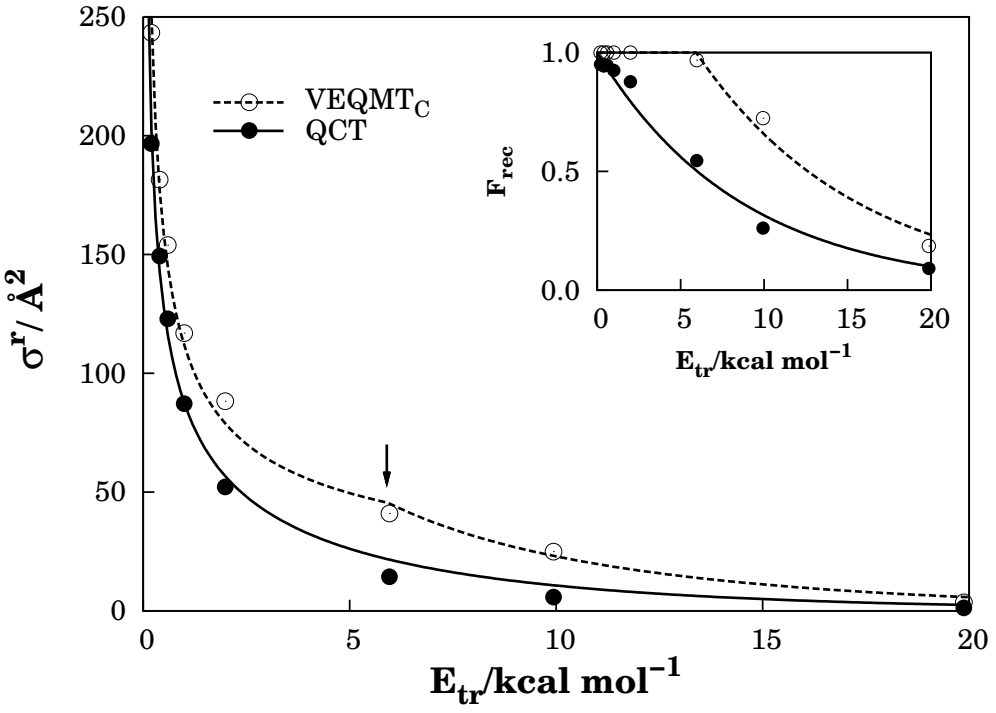

Figure 3. Reaction cross section *vs* translational energy for QCT and VEQMT$_C$ results. The arrow indicates the step introduced in the recrossing function in Eq. (5) at $E_{tr} = E_{tr}^{th}$, which is shown graphically in the insert.

written as a function of temperature. We have found convenient the form:

$$F_{rec}(E_{tr}) = \begin{cases} 1 & E_{tr} < E_{tr}^{th} \\ \exp\left[-\alpha(E_{tr} - E_{tr}^{th})\right] & E_{tr} \geq E_{tr}^{th} \end{cases} \quad (5)$$

as it mimics well the recrossing data shown in Table 2. Note that E_{tr}^{th} can be regarded as a threshold energy for recrossing under the requirements of a given method. As expected, E_{tr}^{th} vanishes (or lies close to zero) in the traditional QCT method. The calculated reactive cross sections are shown in Figure 3, jointly with the results of the fits based on Eqs. (4) and (5). Note the expected bump in the VEQMT$_C$ curve due to the use a non-vanishing threshold energy in Eq. (5). After substitution of Eq. (4) in Eq. (2) and integration, one gets:

$$k(T) = k_{cap}(T)\left[P\left(\frac{2(n-1)}{n}, \frac{E_{tr}^{th}}{k_B T}\right) + \exp\left(\frac{E_{tr}^{th}}{k_B T_0}\right)\left(\frac{T_0}{T_0+T}\right)^{\frac{2(n-1)}{n}} \times \right.$$
$$\left. \times Q\left(\frac{2(n-1)}{n}, \frac{E_{tr}^{th}}{k_B T}\right)\right] \quad (6)$$

Table 3. Rate constants for the title reaction.

$k(T)/10^{-11}\,\mathrm{cm^3\,s^{-1}}$	T/K	source
8.3 ± 1.7	298	literature review [10]
7.9 ± 1.6	295	discharge flow [8]
8.4 ± 1.5	298	electron spin resonance [6]
5.0 ± 3.0	298	literature review [5]
11.6 ± 3.2	300	literature review [4]
11.6 ± 5.0	298	chemiluminescence [3]
$10.4 - 15.4$	300	this work

where $T_0 = 1/\left(\alpha k_B\right)$,

$$k_{cap}(T) = 2n\pi g_e(T)(n-2)^{(2-n)/n}\left(\frac{2}{\pi\mu}\right)^{1/2}\left(\frac{C_n}{2}\right)^{2/n}\Gamma\left[\frac{2(n-1)}{n}\right](k_BT)^{(n-4)/2n} \quad (7)$$

and P and Q stand for the incomplete gamma function and its complement (respectively), while Γ is the Gamma function. Figure 4 shows a plot with rate constants reported in literature and both the lower and upper limits that have been calculated in this work. The two delimit a shaded area that should bound a realistic estimate of the quasi-classical rate constant. In turn, Table 3 compares the values calculated for room temperature. Note that we have used the high-temperature limit [24, 25] of the electronic degeneracy factor ($g_e = 1/6$) such as to get the 'pure' dependence of the rate constant on temperature [*i.e.*, without including the dependence due to $g_e(T)$]. Clearly, our results agree well with the limited experimental values reported in the literature [3–6, 10]. We now address the work by Blitz *et al.* [8]. Their rate constants were measured for OH + SO over the temperature range $295 - 703\,\mathrm{K}$, and measured at pressures of 100 Torr. Because it agrees at room temperature with the values reported by Jordain *et al.* [6] and Fair *et al.* [3] which have been obtained at low pressures ($\sim 1\,\mathrm{Torr}$), this led those authors [8] to suggest that the title reaction can be treated as pressure-independent. However, because pressure effects are likely to increase the complex lifetime due to the presence of third-bodies, we may argue that an increasing pressure will result on an increasing recrossing probability, thus diminishing reactivity as predicted from our calculations. In fact, for high

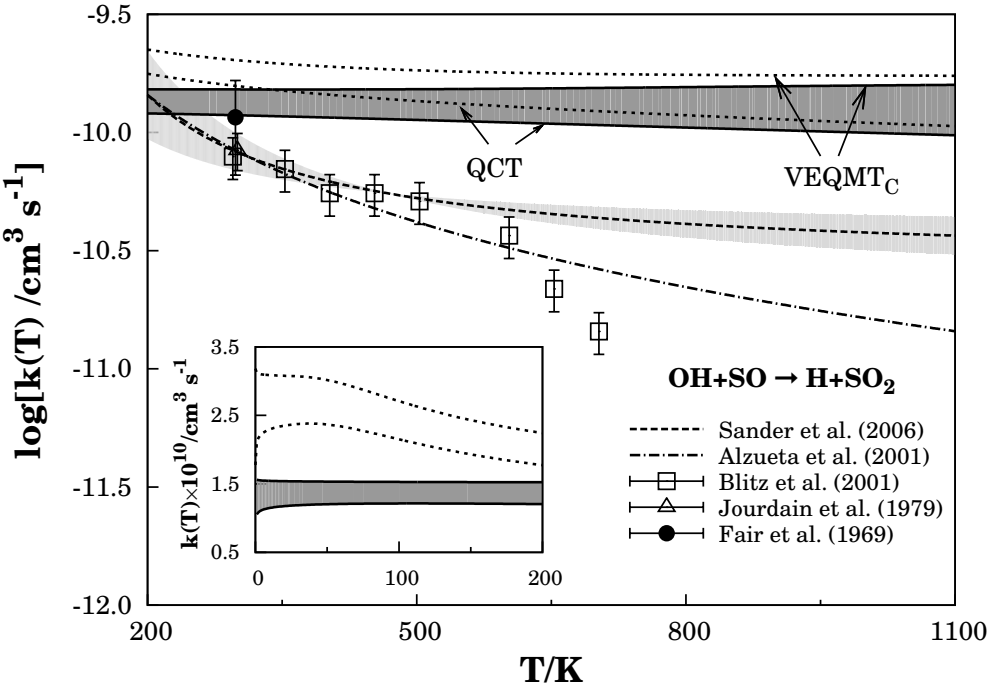

Figure 4. Temperature-dependence of the rate constant for the reaction OH + SO → H + SO_2. Shown by the two solid lines are the QCT and $VEQMT_C$ results from Eq. (6), with the dark shaded area delimiting the interval where the true classical value is likely to fall. The experimental values from the literature [3, 6, 8] are indicated by the symbols jointly with the associated error bars. Shown by the dotted line are the recommended values [10], together with the reported limits which are indicated by the light shaded area. An empirical fit from the literature [9] is also shown by the dash-dot line.

temperatures, our results show significant differences from those of Blitz *et al.* [8] which show a sudden drop with temperature. Such a "sudden-drop" in $k(T)$ has also been observed by Sander *et al.* [10], who have referred to it as 'a non-expected behavior for temperatures above 500 K'. We further remark that Blitz *et al.* [8] relied on the assumption [7] that isomerization HOSO → HSO_2 is needed for the title reaction to take place. As noted above, direct processes HO + SO → H + SO_2 without isomerization to HSO_2, are the only ones observed in the present study. Figure 4 depicts the temperature dependence recommended by Sander *et al.* [10] based on the temperature data of Blitz et al. [8] for the range 295 − 453 K, as well as their suggested error bars which are indicated by the shaded area. Also shown is the rate constant proposed by Alzueta *et al.* [9], which has been derived from a

fit to the Blitz *et al.* [8] data. The salient feature is the good agreement between the results from the present work and the measurement of Fair *et al.* [3] for room temperature, as well as with other experimental values or recommendations for the same temperature [4–6, 10]. They predict a small T-dependence which is best seen in a (non-logarithmic) plot of $k(T)$ vs T: a modest initial increase before stabilization at high temperatures. Thus, both the VEQMT$_{\rm C}$ and QCT curves show maxima, but they occur at higher temperatures (respectively ~ 1400 and $\sim 100\,{\rm K}$) than predicted by quantum capture rate constant calculations [24, 25]. In an attempt to clarify this behavior, we have fitted the energy along the minimum energy path (for diatom-diatom separations $2.4 \leq R/{\rm \AA} \leq 4.8$) to a simple isotropic long-range $C_n R^{-n}$ form and calculated the rate constant using classical capture theory [22]. We observe the following: a) the optimum power in the long-range potential is found to be $n = 5.9$ ($C_n = -7.3\,{\rm E_h \AA^n}$), which is due to probing various arrangements of the interacting permanent electrostatic (*i.e.*, dipole-dipole, dipole-quadrupole, and quadrupole-quadrupole) moments along such a path of the DMBE potential energy surface [11], as well as to having additional long-range contributions included in the latter; b) the calculated rate constant at room temperature is predicted to be $5.3 \times 10^{-11}\,{\rm cm^3\,s^{-1}}$, which is somewhat smaller than Clary's recommended [24] value of $8.0 \times 10^{-11}\,{\rm cm^3\,s^{-1}}$ obtained using the adiabatic capture global centrifugal sudden approximation, although it lies closer to their reported result of $6.5 \times 10^{-11}\,{\rm cm^3\,s^{-1}}$ obtained with the adiabatic capture infinite order sudden approximation [24]; c) no maximum arises in the classical capture rate constant, which is predicted to increase with temperature as expected for a power law larger than $n = 4$. This result suggests that the maximum arising in the curves of Ref. 25 at very low temperatures can be ascribed to changing from a fixed orientation of the permanent moments at low temperatures to a rotationally-averaged regime with increasing temperature. However, such a mechanism conflicts with the prediction from DMBE which shows significant angle-scrambling (besides dispersion interactions) in the minimum energy path itself. Such an averaging process becomes even more prominent if one recalls that OH in its ground state has already one quantum of rotational energy. Indeed, movies of OH($v_{\rm OH} = 0, j_{\rm OH} = 1$)+SO($v_{\rm SO} = 0, j_{\rm SO} = 0$) trajectories show a quick sampling of all diatom-diatom interaction angles. Finally, we emphasize

that a full comparison with experiment requires a thermalized distribution of initial reactant states. Although the above arguments suggest that the general trends are likely to be maintained, calculations are required to confirm such an assertion and to assess the role of excited vibrational states, especially at high temperatures.

5 Conclusions

The reaction $OH + SO \rightarrow H + SO_2$ has been theoretically studied over a range of translational energies. No formation of HSO_2 has occurred, thus predicting reaction to proceed via an HOSO intermediate. Cross sections have been calculated and fitted to a two-step model based on capture×recrossing. Such a model offers an analytic expression for the rate constant which, for the title reaction, predicts only a slight dependence on temperature. The calculated state-specific rate constant is predicted in fair agreement with experimental data reported in the literature for room temperature.

Acknowledgments

M.Y.B. thanks the Centro de Estudios Ambientales de Cienfuegos, Cuba, for leave of absence during his PhD studies. This work has been carried out under the auspices of Fundação para a Ciência e a Tecnologia, Portugal (contracts POCI/QUI/60501/2004, POCI/AMB/60261/2004, and REEQ/128/QUI/2005).

References

[1] P. Glarborg, D. Kubel, K. Dam-Johansen, H.-M. Chiang, and J. W. Bozzelli, Int. J. Chem. Kinet. **28**, 773 (1996).

[2] R. P. Wayne, *Chemistry of Atmospheres* (Oxford University Press, 2002).

[3] R. W. Fair and B. A. Thrush, Trans. Faraday Soc. **65**, 1557 (1969).

[4] J. W. E. Wilson, Phys. Chem. Ref. Data. **1**, 535 (1972).

[5] K. Schofield, J. Phys. Chem. Ref. Data **2**, 25 (1973).

[6] J. L. Jourdain, G. L. Bras, and J. Combourieu, Int. J. Chem Kinet. **11**, 569 (1979).

[7] A. J. Frank, M. Sadìlek, J. G. Ferrier, and J. Tureček, J. Am. Chem. Soc. **119**, 12343 (1997).

[8] M. A. Blitz, K. W. McKee, and M. J. Pilling, Proceedings of the Combustion Institute **28**, 2491 (2000).

[9] M. U. Alzueta, R. Bilbao, and P. Glarborg **127**, 2234 (2001).

[10] S. P. Sander, R. R. Friedl, D. M. Golden, M. J. Kurylo, G. K. Moorgat, P. H. Wine, A. R. Ravishankara, C. E. Kolb, M. J. Molina, B. J. Finlayson-Pitts, R. E. Huie, and V. L. Orkin, *Chemical kinetics and photochemical data for use in atmospheric modeling.*, Tech. rep., Jet Propulsion Laboratory, NASA (2006).

[11] M. Y. Ballester and A. J. C. Varandas, Phys. Chem. Chem. Phys. **7**, 2305 (2005).

[12] W. L. Hase, R. J. Duchovic, X. Hu, A. Komornicki, K. F. Lim, D. Lu, G. H. Peslherbe, K. N. Swamy, S. R. V. Linde, A. J. C. Varandas, H. Wang, and R. J. Wolf, QCPE Bull. **16**, 43 (1996).

[13] A. J. C. Varandas, J. Chem. Phys. **99**, 1076 (1993).

[14] J. M. C. Marques, W. Wang, A. A. C. C. Pais, and A. J. C. Varandas, J. Phys. Chem. **100**, 17513 (1996).

[15] D. G. Truhlar, J. Chem. Rev. **56**, 3189 (1972).

[16] J. T. Muckerman and M. D. Newton, J. Chem. Phys. **56**, 3191 (1972).

[17] K. P. Huber and G. Herzberg, *Constants of diatomics molecules* (Van Nostrand, Princeton, 1979).

[18] A. J. C. Varandas, Int. Rev. Phys. Chem. **19**, 199 (2000).

[19] A. J. C. Varandas and J. M. C. Marques, J. Chem. Phys. **100**, 1908 (1994).

[20] A. J. C. Varandas and L. Zhang, Chem. Phys. Lett. **340**, 62 (2001).

[21] A. J. C. Varandas, J. Brando, and M. R. Pastrana, J. Chem. Phys. **96**, 5137 (1992).

[22] A. J. C. Varandas, Faraday Discuss. Chem. Soc. **84**, 353 (1987).

[23] A. J. C. Varandas, in *Conferencias Plenarias de la XXIII Reunin Bienal de Química*, edited by A. S. Feliciano, M. Grande, and J. Casado (Universidad de Salamanca, Salamanca, 1991), p. 321.

[24] T. Stoecklin, C. E. Dateo, and D. C. Clary, J. Chem. Soc. Faraday Trans. **87**, 1667 (1991).

[25] D. C. Clary, T. S. Stoecklin, and A. G. Wickham, J. Chem. Soc. Faraday Trans. **89**, 2185 (1993).

Chapter 5

The reaction $\mathbf{H + SO_2 \rightarrow OH + SO}$

Chem. Phys. Lett. **439**, 301-307 (2007).

Dynamics and kinetics of the $H + SO_2$ reaction: A theoretical study

M.Y. Ballester, P.J.S.B. Caridade and A.J.C. Varandas

Departamento de Química, Universidade de Coimbra
P-3049 Coimbra Codex, Portugal.

(Received 23 February 2007; in final form 27 March 2007)

Abstract

We report a quasi-classical trajectory study of the title reaction using a double many-body expansion potential energy surface for ground state HSO_2. Calculations for specific low ro-vibrational states of the reactants, as well as thermalized reactants, have been performed. The calculated cross sections indicate a barrier-type mechanism, and nearly thermalized product distributions. Both HOSO and HSO_2 isomers are formed during the collisional process, although with quite different incidences. The rate constant is found to be enhanced by adding internal energy to the reactants, with the thermalized result being in good agreement with existing experimental data.

1 Introduction

Sulfur dioxide is well known as an important atmospheric pollutant [1], while catalytic recombination of H atoms in SO_2 doped flames is considered to be responsible for radical sink in fuel-rich flames [2]. Considerable work has been devoted to study the reaction of SO_2 with atomic hydrogen, both experimentally and theoretically. By measuring the thermal profiles of H atoms behind the reflected shock of $C_2H_5I/SO_2/Ar$ mixtures, Murakami *et al.* [3] have studied the reaction

$$H + SO_2 \rightarrow \text{products} \tag{1}$$

and reported for the rate constant the value $k = \exp(-66.1\,\mathrm{kJ\,mol^{-1}}/\mathrm{R}T) \times 10^{-11}\,\mathrm{cm^3\,s^{-1}}$. Such a result has been obtained under the assumption it yields only OH + SO above 1000 K, being therefore valid for the temperature range of $1400 \leq T/\mathrm{K} \leq 2200$. In turn, Goumri *et al.* [4] have employed RRKM theory to study the reaction (1) for formation of an adduct as well as the isomerization process. Additionally, Fair and Thrush [5] studied complex formation in an experimental frame using an Ar bath. More recently, Blitz *et al.* [6] reported a master equation for the $H+SO_2$ reaction, with the derived rate coefficients relying heavily on measurements of the reverse OH + SO reaction that had previously been analyzed [7]. Their reported low pressure limit rate constant for the title reaction is $k(T) = 4.51\,(T/300)^{-2.3}\exp(-15582/\mathrm{T}) \times 10^{-8}\,\mathrm{cm^3\,s^{-1}}$. In turn, Morris *et al.* [8] have carried out *ab initio* calculations on properties of the intermediate structures for the title reaction, while in another publication [9] they reported an observation of time-resolved IR emission from ro-vibrational excited OH that is produced when reacting 'hot' hydrogen atoms (58 kcal mol^{-1} of average effective initial translational energy) with vibrationally excited SO_2. A quasi-triatomic approximation has then been utilized to describe the HSO_2 potential energy surface where quasi-classical trajectory (QCT) calculations have been performed [9]. Their calculations have shown a "statistical but non-Boltzmann vibrational distribution of OH" when vibrational excitations as high as $v = 11-13$ are deposited into the non-frozen SO bond of SO_2. A rather more pronounced non-statistical behavior has been observed both experimentally [10–12] and theoretically [13–15] for the analogous reaction $H + O_3 \rightarrow OH(v) + O_2$, which is exothermic by about

81 kcal mol^{-1}. Although the reduced-dimensionality QCT results of Morris *et al.* [9] tend to support their experimental observations for the title reaction, they are clearly not definitive due to the simplistic nature of the employed potential energy surface. Recently, we have reported a full-dimensional single-sheeted potential energy surface [16] of the double many-body expansion [17] (DMBE) type for the ground electronic state of HSO_2, which will be here employed. The major aim of the present work will be to elucidate the mechanism the H + SO_2 reaction, and study the influence of the internal energy of the reactants (at moderate regimes of excitation) in the rate constant over a wide range of temperatures. Thus, we will not address the vibrational issue raised by Morris *et al.* [9] in the present work.

The paper is organized as follows. Section 2 addresses briefly the main aspects of the potential energy surface, while the details of the computational methods are presented in section 3. The results are reported and discussed in section 4, and the conclusions gathered in section 5.

2 Potential energy surface

All calculations reported in this work have employed the six-dimensional ($6D$) single-sheeted DMBE potential energy surface [16] for ground state HSO_2. It uses in its definition DMBE functions previously reported for the diatomic and triatomic fragments (Ref. 16, and references therein) and four-body energy terms that have been calibrated from correlated CASPT2/FVCAS/AVXZ ($X = 2, 3$) calculations. For brevity, only some major topographical features of interest for the title reaction are described, with the readers being referred to the original papers for details. Such a DMBE form has recently been employed [18] in a QCT study of the OH + SO $\rightarrow$ H + SO_2 reaction, with the results showing good agreement with the available experimental data. Figure 1 illustrates the minimum energy path for title reaction, assuming as intermediate the stable HOSO species. As shown, the reaction is endothermic by 27.6 kcal mol^{-1}, with a potential well of -3.1 kcal mol^{-1} and a barrier of 9.1 kcal mol^{-1} preceding the deep well (-49.2 kcal mol^{-1}) associated to the HOSO intermediate; all energies are measured with respect to the H + SO_2 asymptote. As it will be discussed,

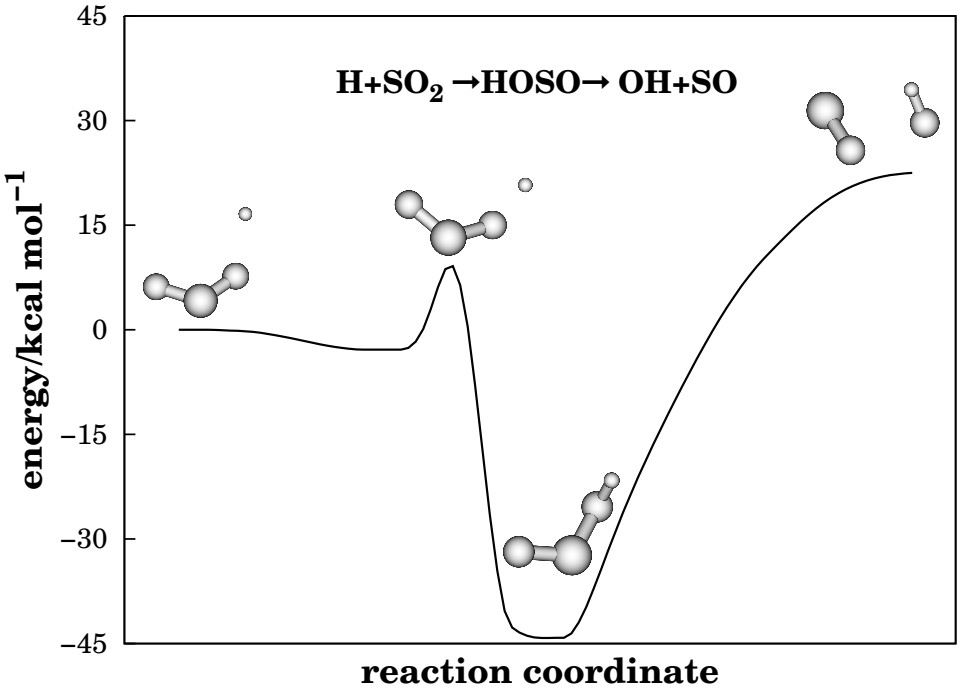

Figure 1. Minimum energy path of title reaction with the HOSO adduct as intermediate.

there is also a possibility of forming a HSO_2 intermediate, but its likelihood is rather small.

3 Computational procedures

All calculations used the QCT method as implemented in the VENUS96 [19] code, which have been suitably modified to accommodate the HSO_2 DMBE potential energy surface. For the numerical integrations, a step size of 2.5×10^{-16} s has been utilized, warranting the conservation of total energy to better than 1 part in 10^3. The procedure employed to assign the various reactive channels has been described elsewhere [20]. As for the OH + SO reaction [18], there will be 14 possible channels since we do not consider as distinct those corresponding to isomers of a given species.

Two types of calculations have been here performed. First, we have studied the role of the reactants internal energy by performing calculations for specific rovibrational combinations of the reactants (SO_2). To directly calculate the rate

constant, we have then carried out calculations using thermalized reactants. Details of both such studies are given in the following.

The specific ro-vibrational calculations have covered translational energies over the range $31.0 \leq E_{\rm tr}/{\rm kcal\ mol^{-1}} \leq 55.0$. In turn, the translational energies were selected such as to exceed the classical threshold for reaction as dictated by the energetics of the DMBE potential energy surface, but below the minimum energy required to open other channels [16]. Two specific cases have been considered. First, sulfur dioxide has been prepared in its ground vibrational state [21] ($v_1 = 0, v_2 = 0, v_3 = 0$), with the rotational energy around each principal axis of inertia [19] being $RT_{\rm rot}/2$. The rotational temperature has then been fixed at $T_{\rm rot} = 300\,{\rm K}$, as indicated heretofore by writing $SO_2(\mathbf{v} = \mathbf{0}, T_{\rm rot} = 300\,{\rm K})$, where $\mathbf{v} = \{v_1, v_2, v_3\}$ denotes the set of quantum numbers for the triatomic vibrational modes. Second, the triatomic molecule has been considered vibrationally excited, with one quantum of excitation in each normal mode ($\mathbf{v} = \mathbf{1}$ or $v_1 = 1, v_2 = 1, v_3 = 1$) and the rotational temperature set at 1800 K, as denoted by $SO_2(\mathbf{v} = \mathbf{1}, T_{\rm rot} = 1800\,{\rm K})$. Thus, the first case considers the title reaction without any extra internal energy, while in the latter we choose both the vibrational and rotational energies to have the same order of magnitude (the rotational and vibrational temperatures correspond to the average temperature for the range $1400 \leq T/{\rm K} \leq 2200$ here considered).

Batches of 100 trajectories per collisional energy have been run to determine the maximum impact parameter (b_{max}) that leads to reaction. For a given translational energy, the reactive cross section has been calculated by using $\sigma_r = \pi b_{max}^2 P_r$, with the associated 68 % uncertainties being $\Delta\sigma_r = \sigma_r[(N_T - N_r)/(N_T N_r)]^{1/2}$; N_r is the number of reactive trajectories in a total of N_T, and $P_r = N_r/N_T$ the reaction probability. From the reactive cross section and assuming a Maxwell-Boltzmann distribution over the translational energy, the specific thermal rate coefficient assumes the form

$$k(T;\mathbf{v},T_{\rm rot}) = g_e(T)\left(\frac{2}{k_B T}\right)^{3/2}\left(\frac{1}{\pi\mu}\right)^{1/2}\int_0^\infty E_{\rm tr}\sigma(E_{\rm tr};\mathbf{v},T_{\rm rot})\exp(-E_{\rm tr}/k_B T)dE_{\rm tr} \quad (2)$$

where T is the temperature, k_B the Boltzmann constant, μ the reactants reduced mass, and g_e a factor that accounts for the electronic degeneracy [22, 23]. Since H is a doublet (^2S), SO_2 is a singlet ($\tilde{X}^1A'$), and the tetratomic is a doublet, one

has $g_e = 1$.

To monitor complex formation, we have first studied in detail 100 trajectories at 32.0 and 55.0 kcal mol^{-1} of translational energy with $SO_2(\mathbf{v} = \mathbf{0}, T_{\rm rot} = 300\,{\rm K})$. Traditional 'distance vs time' plots have then been carefully examined for many reactive trajectories. From such plots, we have concluded that both HOSO and HSO_2 structures are formed during the collisional event. Since it is unpractical to examine all such plots, we require a definition of intermediate complex that may operate without being so time consuming. Following previous work, and taking into account the energetics of the HSO_2 DMBE potential energy surface [16], we have defined complex as any configuration of the four-body system in which the SH distance is smaller than 1.3 times its value at the HSO_2 equilibrium geometry. If any of the OH distances is smaller than $R_{\rm SH}$, the HOSO adduct is considered to have been formed, otherwise the complex will be considered to correspond to an HSO_2 configuration. To assess the merits of such a definition, we have then compared the lifetimes of a large set the intermediates so assigned with the results obtained by viewing the corresponding 'distance vs time' plots. In all cases, we have found our "blind" procedure to be sufficiently accurate to be used in the present calculations.

A well known problem in classical molecular dynamics is the so-called zero-point energy leakage (Ref. 24 and references therein). To approximately account for this problem, we have followed our previous work [18] by considering the VEQMT$_{\rm C}$ [25] method. According to this method, only the trajectories leading to total vibrational energies of the products larger than the sum of their separed ZPEs are considered for the final statistical analysis.

For the thermalized calculations, the collisional energy has been selected from a Maxwell-Boltzmann distribution by using the cumulative function

$$G(E_{\rm tr}) = \left(\frac{1}{k_B T}\right)^2 \int_0^{E_{\rm tr}} E'_{\rm tr} \exp(-E'_{\rm tr}/k_B T) dE'_{\rm tr} \tag{3}$$

where $E_{\rm tr}$ is chosen randomly for each trajectory by solving the equation $G(E_{\rm tr}) - \xi = 0; \xi$ is a random number. In turn, the vibrational quantum numbers $\mathbf{v}$ of SO_2 were sampled by using a cumulative distribution function of the form

$$C(E_{\mathbf{v}}) = \sum_{n=0}^{\mathbf{v}} P(n) \tag{4}$$

where the probability $P(n)$ is chosen from a Boltzmann distribution, and the dependence of the vibrational energy ($E_{\mathbf{v}'}$) on the vibrational quantum numbers of SO_2 has been reported elsewhere [21]. The selected vibrational states are obtained from the requirement that $C(E_{\mathbf{v}}) \geq \xi$. To complete the specification of the initial internal energy, the standard thermal distribution is assumed for the rotational energy [19] by considering the reactant triatomic as a symmetric top. With the maximum impact parameter being optimized as described above, the thermalized rate constant assumes now the form

$$k(T) = g_e(T) \left(\frac{8k_B T}{\pi \mu} \right)^{1/2} \pi b_{max}^2 \frac{N_r}{N_T} \tag{5}$$

where all symbols have the usual meaning (see above), and the associated uncertainty is given by the corresponding analog of the expression used for the cross section. Batches of 3×10^5 trajectories have then been run at temperatures of $T = 1400, 1800$, and 2200 K to cover the range of experimental values reported in literature for the title reaction. To save computer time, trajectories with total energies bellow the classical threshold ($E_T \leq 30.11\,\mathrm{kcal\,mol^{-1}}$) have not been integrated, although the original distributions have been preserved by counting such non-integrated trajectories as non-reactive.

4 Results and discussion

Tables 1 and 2 collect the results of the vibrationally-specific calculations carried out in the present work, both using the QCT and $\mathrm{VEQMT_C}$ methods. Average lifetimes of both complexes are also reported. As shown, the HSO_2 lifetimes are in all cases found to be much smaller than the HOSO ones: $\langle \tau_{\mathrm{HOSO}} \rangle \gg \langle \tau_{\mathrm{HSO_2}} \rangle$. Actually, most reactive trajectories do not form HSO_2 while, for the ones that form, the lifetime of the HOSO complex has a value larger than the average lifetime of all formed complexes. The title reaction is therefore more likely to occur by direct attack of the hydrogen atom to one of the terminal oxygen atoms in SO_2: formation of an HSO_2 intermediate may take place but it rapidly decomposes back to reactants or forms HOSO. Notice that the optimized maximum impact parameters have values around 2 Å, the value used by Morris *et al.* [9] in

their reduced-dimensionality QCT calculations. In fact, a similar value has been utilized in our thermalized calculations.

The calculated cross sections for specifically prepared reactants can be modeled by the following barrier-type excitation function [26]:

$$\sigma_r = C(E_{\rm tr} - E_{\rm tr}^{\rm th})^n \exp[-m(E_{\rm tr} - E_{\rm tr}^{\rm th})] \tag{6}$$

where C, n, and m are least-squares parameters and $E_{\rm tr}^{\rm th}$ is the translational energy threshold. As it has been pointed out elsewhere [24], the value of $E_{\rm tr}^{\rm th}$ dictates the slope of the calculated rate constant and is hard to determine at the QCT level due to ZPE leakage. Following Ref. 24, for $H + SO_2(\mathbf{v} = \mathbf{0}, T_{\rm rot} = 300\,{\rm K})$ we have then fixed its value at the energy difference between products and reactants once the zero-point energies are accounted for, yielding $E_{\rm tr}^{\rm th} = 30.11\,{\rm kcal\,mol^{-1}}$. As expected, such a value may decrease when internal energy is added to reactants; thus, for $H + SO_2(\mathbf{v} = \mathbf{1}, T_{\rm rot} = 1800\,{\rm K})$, the actual threshold energy has been obtained from a fit to the calculated cross sections by using the above mentioned estimate as starting guess. Figure 2 shows the fitted excitation functions so obtained. Also indicated in the plot is the classical energy threshold which, as expected, decreases slightly with increasing ro-vibrational excitation of the reactants. Cross sections for different vibrational excitations of SO_2 obtained by Morris *et al.* [9], when they use an entrance channel barrier of $13.6\,{\rm kcal\,mol^{-1}}$, are found to have the same order of magnitude of those here reported. Figure 3 shows the OH product vibrational and rotational distributions for the title reaction under the initial conditions considered in the present work. The general pattern is the formation of vibrationally cold OH radicals, as could be expected from nearly thermalized (at relatively low temperatures) vibrational-rotational distributions. This is observed even for the two state-specific cases that have been here considered. This is better illustrated by comparing the actual calculated distributions to the fitted Boltzmann distributions that are shown by the solid lines in Figure 3. From such fits, we obtain as rotational temperatures $T_{\rm rot} = 4332, 7444$, and $888\,{\rm K}$, respectively for $H + SO_2(\mathbf{v} = \mathbf{0}, T_{\rm rot} = 300\,{\rm K})$, $H + SO_2(\mathbf{v} = \mathbf{1}, T_{\rm rot} = 1800\,{\rm K})$, and thermalized $H + SO_2$. However, it is also seen that even a democratic vibrational

Table 1. Summary of trajectories calculations for the $H + SO_2(\mathbf{v}=\mathbf{0}, T_{rot}=300\,K)$ reaction.[a)]

E_{tr}	b_{max}	QCT						$VEQMT_C$					
		N_T	N_c	N_{rec}	N_r	$\langle\tau_{HOSO}\rangle$	$\langle\tau_{HSO_2}\rangle$	N_T	N_c	N_{rec}	N_r	$\langle\tau_{HOSO}\rangle$	$\langle\tau_{HSO_2}\rangle$
31.0	1.9	10000	9578	9422	156	40.7	1.1	6605	6257	6253	4	47.0	1.4
32.0	2.2	10000	9391	9242	149	33.4	1.1	6428	5976	5964	12	42.1	1.4
35.0	2.0	10000	9667	9413	254	21.6	1.0	6630	6363	6294	69	22.1	1.2
40.0	2.3	10000	9547	9300	247	11.3	0.9	6702	6382	6232	150	13.8	1.1
45.0	2.3	10000	9669	9421	248	7.8	0.9	6996	6767	6587	180	9.6	1.0
50.0	2.3	10000	9752	9496	256	6.3	1.0	7205	7034	6822	212	6.4	1.0
55.0	2.4	10000	9684	9459	225	3.9	0.8	7285	7058	6859	199	4.9	0.9

[a)] Energies are in kcal mol^{-1}, distances in Å, and times in units of 10^{-14} s.

Table 2. Summary of trajectories calculations for the $H + SO_2(\mathbf{v}=\mathbf{1}, T_{\rm rot}=1800\,K)$ reaction.[a)]

$E_{\rm tr}$	b_{max}	QCT						$VEQMT_C$					
		N_T	N_c	N_{rec}	N_r	$\langle\tau_{\rm HOSO}\rangle$	$\langle\tau_{\rm HSO_2}\rangle$	N_T	N_c	N_{rec}	N_r	$\langle\tau_{\rm HOSO}\rangle$	$\langle\tau_{\rm HSO_2}\rangle$
31.0	2.2	10000	9365	9113	252	10.6	1.2	9648	9029	8878	151	9.0	1.3
32.0	2.2	10000	9406	9136	270	9.5	1.2	9667	9092	8907	185	8.3	1.2
35.0	2.2	10000	9507	9167	340	8.0	1.2	9670	9191	8937	254	7.2	1.2
40.0	2.4	10000	9375	9078	297	5.8	1.0	9697	9092	8857	235	5.3	1.0
45.0	2.2	10000	9758	9423	335	4.8	1.0	9736	9500	9210	290	4.6	1.0
50.0	2.2	10000	9821	9466	355	3.9	1.0	9769	9593	9273	320	3.9	1.0
55.0	2.0	10000	9921	9545	376	3.3	0.9	9801	9723	9380	343	3.3	0.9

[a)] Energies are in kcal mol^{-1}, distances in Å, and times in units of 10^{-14} s.

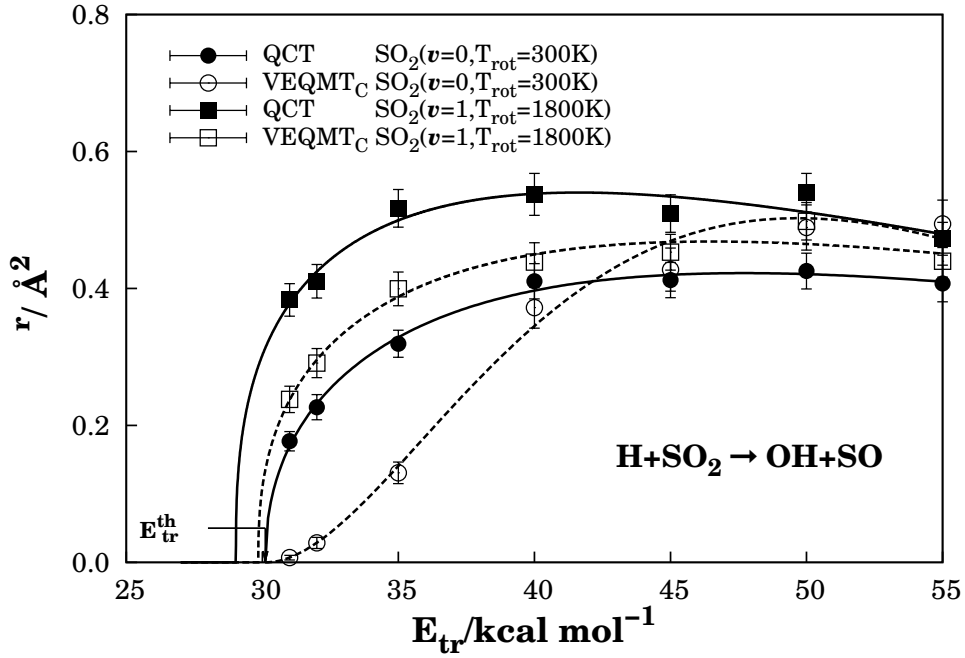

Figure 2. Cross section of title reaction as a function of translational energy for reactants prepared in specific vibrational states. $E_{\rm tr}^{\rm th}$ is the classical threshold energy.

excitation of the reactants with one quantum of vibrational excitation into each mode leads to significant deposition of vibrational energy into the newly formed OH bond. The above results may be rationalized from the fact that the reaction is endothermic and has a deep potential well due to the HOSO intermediate which is sampled by most reactive trajectories. Thus, some energy randomization is expected to occur before the products are formed. In fact, the fractions of energy released in the products is shown to vary little with the three sets of chosen initial conditions, although as shown by the fitted curves the distribution is somewhat closer to a Boltzmann one in the case of initially thermalized reactants. The above results contrast with those for the reaction $H + O_3 \rightarrow OH + O_2$ which is highly exothermic and has no deep potential well along the minimum energy path [10–15]. In this case, the formed OH is characterized by an inverted vibrational distribution, which some experiments suggest to peak at quantum numbers as high as $v_{\rm OH} = 9$. Of course, the results observed for the title reaction may change drastically if further vibrational excitation is put into one of the SO

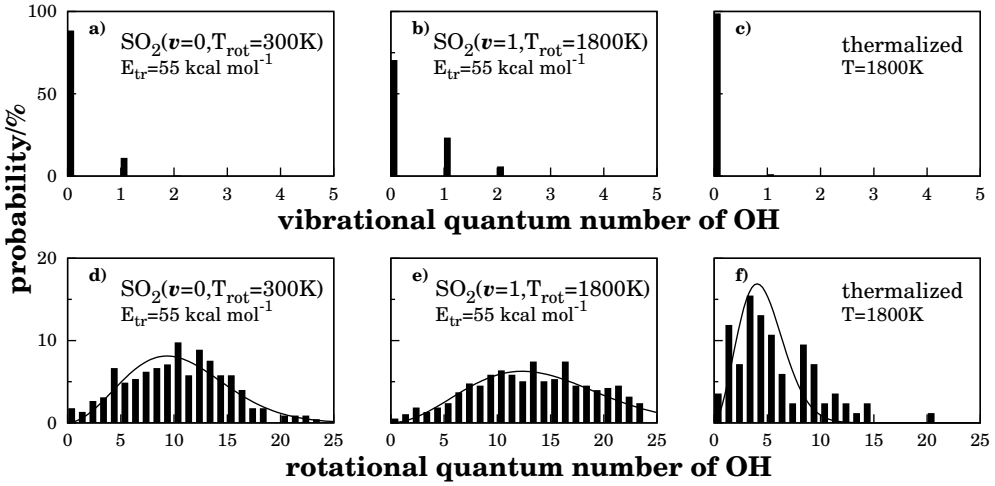

Figure 3. Vibrational and rotational distributions of OH for the reaction $H + SO_2 \rightarrow OH(v_{OH}, j_{OH}) + SO(v_{SO}, j_{SO})$.

bonds of SO_2. Such a study is currently in progress and will be hopefully reported elsewhere. By substituting Eq. (6) into Eq. (2) and integrating, one gets

$$k(T;\mathbf{v},T_{\rm rot}) = g_e(T)C\left(\frac{8k_BT}{\pi\mu}\right)^{1/2}\frac{(k_BT)^n\exp(-E_{\rm tr}^{\rm th}/k_BT)}{(1+mk_BT)^{n+2}}\times \\ \times\left[\Gamma(n+2)+\Gamma(n+1)\frac{(1+mk_BT)E_{\rm tr}^{\rm th}}{k_BT}\right] \quad (7)$$

where Γ is the Gamma function. Figure 4 shows the calculated rate constants for the title reaction. Indicated by the shaded areas are the intervals where the most likely values of the calculated specific rate constants should lie: following previous work [18, 24], the upper and lower limits are defined by QCT (solid line) and $VEQMT_C$ (dashed line) results. Note that the dark-filled area stands for $H + SO_2(\mathbf{v} = \mathbf{0}, T_{\rm rot} = 300\,{\rm K})$, while the light-filled one refers to $H + SO_2(\mathbf{v} = \mathbf{1}, T_{\rm rot} = 1800\,{\rm K})$. In turn, the hashed area indicates the region where the optimum thermalized QCT results are likely to fall, with the open rhombuses indicating the actually calculated QCT values (and corresponding error bars) and the solid line a linear fit to such points. Note further that, for the thermalized calculations, there was a number of trajectories that have not been integrated, and hence the $VEQMT_C$ rate constant could not be rigorously calculated. To obtain an estimate of it, we have assumed that the ratio of QCT and $VEQMT_C$ results

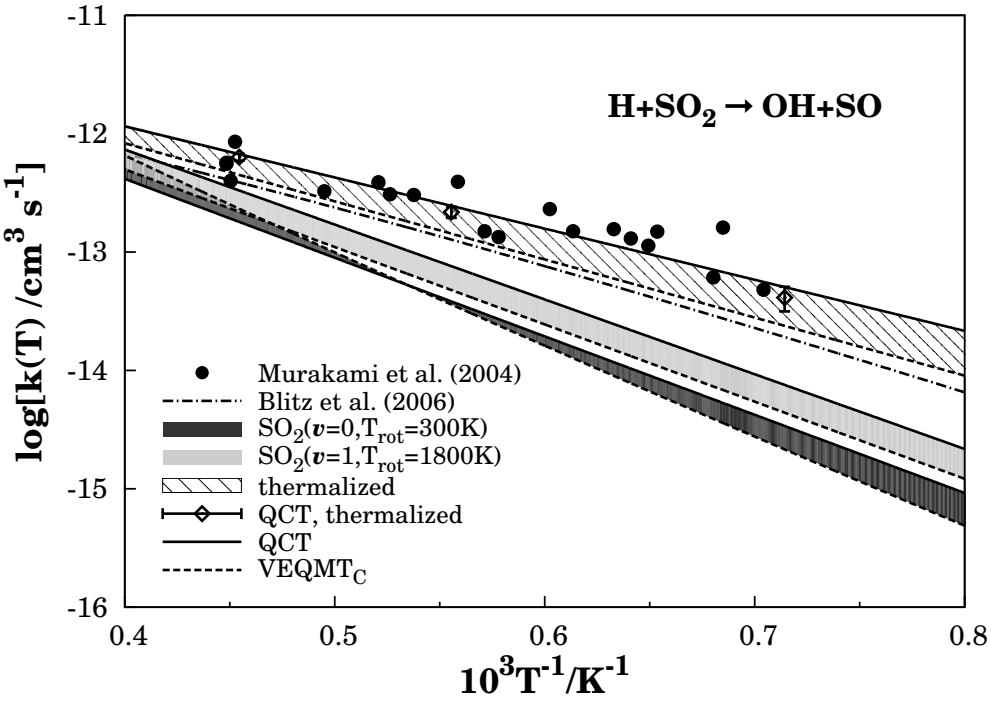

Figure 4. Rate constant as a function of temperature for the title reaction. The light shaded area denotes the specific rate coefficient for $H + SO_2(\mathbf{v} = \mathbf{0}, T_{rot} = 300\,K)$ reactants, while the dark shaded one is for $H + SO_2(\mathbf{v} = \mathbf{1}, T_{rot} = 1800\,K)$. The hashed area refers to the thermalized results, with the open rhombuses indicating the actually calculated values. The solid lines represent the QCT calculations, and the dashed line the $VEQMT_C$ ones. The solid dots indicate the experimental results of Murakami *et al.* [3], while the dotted line represents their recommended values. Shown by the dash-dot line is the low pressure limit of the rate constant given by Blitz *et al.* [6]

Table 3. Rate constants for the title reaction.

Method	$k(T) \times 10^{14}/\mathrm{cm^3 s^{-1}}$		
	1400 K	1800 K	2200 K
QCT/VEQMT$_C$, $SO_2(\mathbf{v}=\mathbf{0}, T_{rot}=300\,K)^{a)}$	$0.2-0.3$	$3.1-3.8$	$17.9-19.6$
QCT/VEQMT$_C$, $SO_2(\mathbf{v}=\mathbf{1}, T_{rot}=1800\,K)^{a)}$	$0.4-0.8$	$4.8-7.6$	$21.9-33.1$
QCT/VEQMT$_C$, thermalized$^{a)}$	$2.3-5.1$	$14.3-24.5$	$44.1-67.0$
Master equation [6]	1.9	12.7	38.7
exp. [3]	3.4	12.1	26.9

$^{a)}$This work.

should approximately mimic those obtained with $SO_2(\mathbf{v}=\mathbf{1}, T_{rot}=1800\,K)$. Finally, the circles indicate the results of Murakami *et al.* [3], while the dotted line is their reported fit to such points. In turn, the low pressure limit of the rate constant for the title reaction reported by Blitz *et al.* [6] is shown by the dash-dot line. As Figure 4 and Table 3 show, the specific rate constant calculations reported in this work underestimate reactivity when comparing with the existing experimental values. This suggests that the inclusion of internal energy into the reactants may play a significant role. This by no means implies that the near-Boltzmann distributions observed for both OH and SO will drastically change. A similar finding has been reported in the quasi-classical trajectory calculations by Morris *et al.* [9], although a more detailed study will be required to pinpoint the differences. Our calculations have also indicated that thermalization is essential to get a rate constant in good agreement with experiment: the thermalized rate coefficient shows significant differences with respect to the vibrationally-specific calculations carried out in the present work. Finally, we observe by extrapolating to the low temperature regimes that the rate coefficients become negligibly small for temperatures below 500 K, in qualitative agreement with previous findings [8, 27]. In summary, the present calculations show good agreement with those reported in the literature, as indeed have shown the ones [18] for the reaction $OH + SO \rightarrow H + SO_2$. Thus, both sets of results corroborate the reliability of the HSO_2 DMBE potential energy surface to describe the collision processes occurring in it.

5 Conclusion

We have reported a theoretical study of the $H + SO_2$ reaction. While both HSO_2 and HOSO complexes were predicted to be formed during the reaction process, the HOSO species is predicted to be by far the most likely intermediate to be formed. We have also shown from state-specific rate constant calculations that the addition of internal energy to the reactants may considerably enhance reactivity. Thermalized calculations of the rate constant have also been carried out, and shown to yield values in good agreement with the available experimental estimates.

Acknowledgments

M.Y.B. thanks the Centro de Estudios Ambientales de Cienfuegos, Cuba, for leave of absence during his PhD studies. This work has been carried out under the auspices of Fundação para a Ciência e a Tecnologia, Portugal (contracts POCI/QUI/60501/2004, POCI/AMB/60261/2004, and REEQ/128/QUI/2005).

References

[1] R. P. Wayne, *Chemistry of Atmospheres* (Oxford University Press, 2002).

[2] M. U. Alzueta, R. Bilbao, and P. Glarborg, Combust. Flame **127**, 2234 (2001).

[3] Y. Murakami, S. Onishi, and N. Fujii, J. Phys. Chem. A **108**, 8141 (2004).

[4] A. Goumri, J.-D. R. Rocha, D. Laakso, C. E. Smith, and P. Marshall, J. Phys. Chem. A **103**, 11328 (1999).

[5] R. W. Fair and B. A. Thrush, Trans. Faraday Soc. **65**, 1550 (1969).

[6] M. A. Blitz, K. J. Hughes, M. J. Pilling, and S. Robertson, J. Phys. Chem. A **110**, 2996 (2006).

[7] M. A. Blitz, K. W. McKee, and M. J. Pilling, Proceedings of the Combustion Institute **28**, 2491 (2000).

[8] V. R. Morris and W. M. Jackson, Chem. Phys. Lett. **223**, 445 (1994).

[9] V. R. Morris, K.-L. Han, and W. M. Jackson, J. Phys. Chem. **99**, 10086 (1995).

[10] J. C. Polanyi and J. J. Sloan, Int. J. Chem. Kin. Symp. **1**, 51 (1975).

[11] D. Klenerman and I. W. M. Smith, J. Chem. Soc., Faraday Trans. 2 **83**, 229 (1987).

[12] A. M. L. Irvine, I. W. M. Smith, and R. P. Tuckett, J. Chem. Phys. **93**, 3187 (1990).

[13] H. G. Yu and A. J. C. Varandas, J. Chem. Soc. Faraday Trans. **93**, 2651 (1997).

[14] H. Szichman and A. J. C. Varandas, J. Phys. Chem. **103**, 1967 (1999).

[15] A. J. C. Varandas, Int. Rev. Phys. Chem. **19**, 199 (2000).

[16] M. Y. Ballester and A. J. C. Varandas, Phys. Chem. Chem. Phys. **7**, 2305 (2005).

[17] A. J. C. Varandas, *Conical Intersections: Electronic Structure, Spectroscopy and Dynamics* (World Scientific Publishing, 2004), chap. 5, p. 91, Advanced Series in Physical Chemistry.

[18] M. Y. Ballester and A. J. C. Varandas, Chem. Phys. Lett. **433**, 253 (2007).

[19] W. L. Hase, R. J. Duchovic, X. Hu, A. Komornicki, K. F. Lim, D. Lu, G. H. Peslherbe, K. N. Swamy, S. R. V. Linde, A. J. C. Varandas, H. Wang, and R. J. Wolf, QCPE Bull. **16**, 43 (1996).

[20] A. J. C. Varandas, A. A. C. C. Pais, J. M. C. Marques, and W. Wang, Chem. Phys. Lett. **249**, 264 (1996).

[21] A. J. C. Varandas and S. P. J. Rodrigues, Spectrochim. Acta A **58**, 629 (2002).

[22] D. G. Truhlar, J. Chem. Phys. **56**, 3189 (1972).

[23] J. T. Muckerman and M. D. Newton, J. Chem. Phys. **56**, 3191 (1972).

[24] A. J. C. Varandas, P. J. S. B. Caridade, J. Z. H. Zhang, Q. Cui, and K. L. Han, J. Chem. Phys. **125**, 064312 (2006).

[25] A. J. C. Varandas and L. Zhang, Chem. Phys. Lett. **340**, 62 (2001).

[26] R. L. Le Roy, J. Chem. Phys. **73**, 4338 (1969).

[27] A. Hinchliffe, J. Mol. Struct. **71**, 349 (1981).

Chapter 6

The reaction $S + HO_2$

Intl. J. Chem. Kin. **000**, 000-000 (2008).

Dynamics and kinetics of the of the $S + HO_2$ reaction

M. Y. Ballester and A.J.C. Varandas

Departamento de Química, Universidade de Coimbra
P-3049 Coimbra Codex, Portugal.

(Received: 31 November 2007; *in press*)

Abstract

We report a quasi-classical trajectory study of the $S + HO_2$ reaction using a previously reported global potential energy surface for the ground electronic state of HSO_2. Zero-point energy leakage is approximately accounted for by using the vibrational energy quantum mechanical threshold method. Calculations are carried out both for specific ro-vibrational states of the reactants and thermalized ones, with rate constants being reported as a function of temperature. The results suggest that the title reaction is capture-type, with OH and SO showing as the most favorable products. The internal energy distribution of such products and the reaction mechanism are also investigated.

1 Introduction

Sulfur is an important element when studying atmospheric chemistry [1]. In turn, the mercapto radical (HS) has been observed in interstellar space [2], while sulfur compounds are also known to play an important role in combustion chemistry [3]. However, due to the large number of electrons involved, high level theoretical studies involving sulfur atoms are somewhat limited due to being computationally too expensive. In previous works of this series [4, 5], we have reported full dynamics studies involving the title sulfur-containing species by using a global double many-body expansion (DMBE [6, 7]) potential energy surface reported elsewhere [8]. All those studies have employed the quasi-classical trajectory (QCT) method, a technique that will be also adopted in the current study. In fact, the good agreement previously achieved when comparing our predictions with available experimental results suggests that both the HSO_2 DMBE potential energy surface and the dynamics approach should be reliable for our purposes in this work.

Although the title reaction should play a role whenever sulfur atoms (the ground electronic state of atomic sulfur is implied heretofore) are present in the atmosphere, no dynamics study of it has yet been reported in the open literature. Our aim in the present work is to extend the series of previous studies to the reaction

$$S + HO_2 \rightarrow \text{products} \tag{1}$$

by using the QCT and the above mentioned DMBE potential energy surface. Thus, we will ignore both quantum effects (except for those related with the reactant triatomic molecular whose initial state is mimicked as closely as possible) and non-adiabaticity. Given the large masses of the reactant species and the fact that the ground (^3P) and first-excited (^1D) electronic states are separated by more than $25\,\mathrm{kcal\,mol^{-1}}$ [9], we can hardly judge such effects to have any crucial role for the rate constant calculations carried out in the present work. The paper is organized as follows. Section 2 reviews the potential energy surface, while the utilized computational methods are described in section 3. The results will be presented and discussed in section 4, and the major conclusions gathered in section 5.

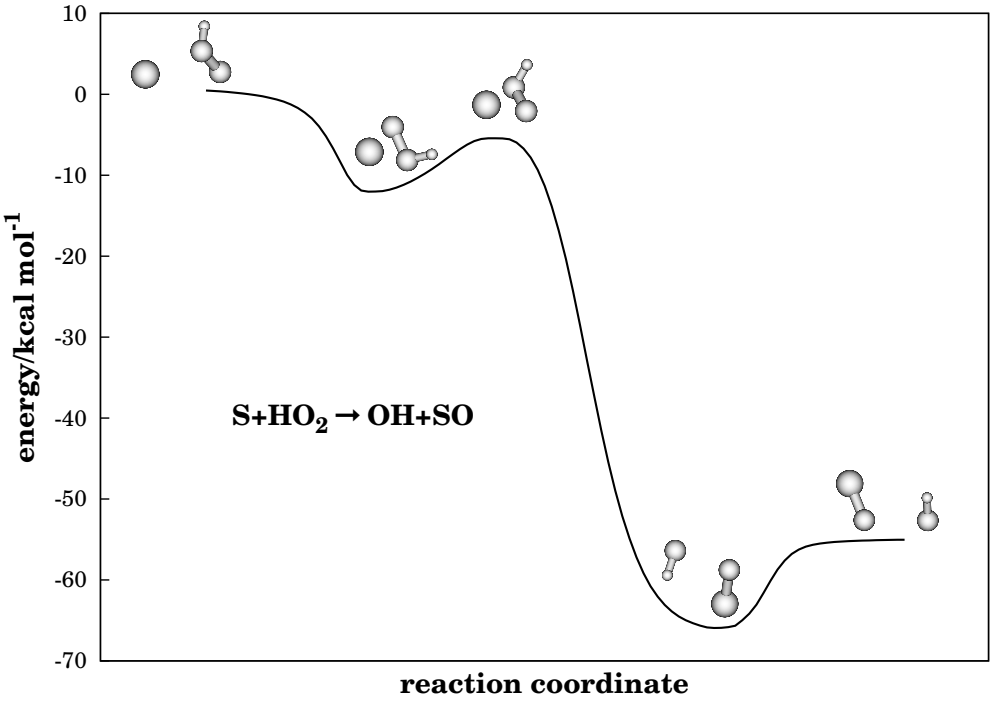

Figure 1. Minimum energy path for the reaction $S + HO_2 \rightarrow OH + SO$ according to the potential energy surface used in this work.

2 Potential energy surface

All calculations here performed have employed our six-dimensional DMBE potential energy surface published elsewhere [8] for the electronic ground state of HSO_2. It employs previously reported forms of the same type for the diatomic and triatomic fragments (Ref. 8, and references therein), and four-body energy terms that were parametrized to mimic CASPT2/FVCAS/AVXZ ($X = D, T$) calculations for the tetratomic system. In this section, we illustrate its major features that are of interest for the title reaction.

Figure 1 displays the minimum energy path (MEP) for the formation of OH+SO from $S+HO_2$, while Figure 2 represents the MEP for HOS formation. Other products are allowed for such reactants but the illustrated here are the most favored ones. According to energetics of the surface (see Table 1 and Figure 11 of the Ref. 8), the $H + SO_2$ channel lies 84.4 kcal mol^{-1} bellow the reactants[1].

[1]Energies in this paragraph do not include the zero-point energy (ZPE).

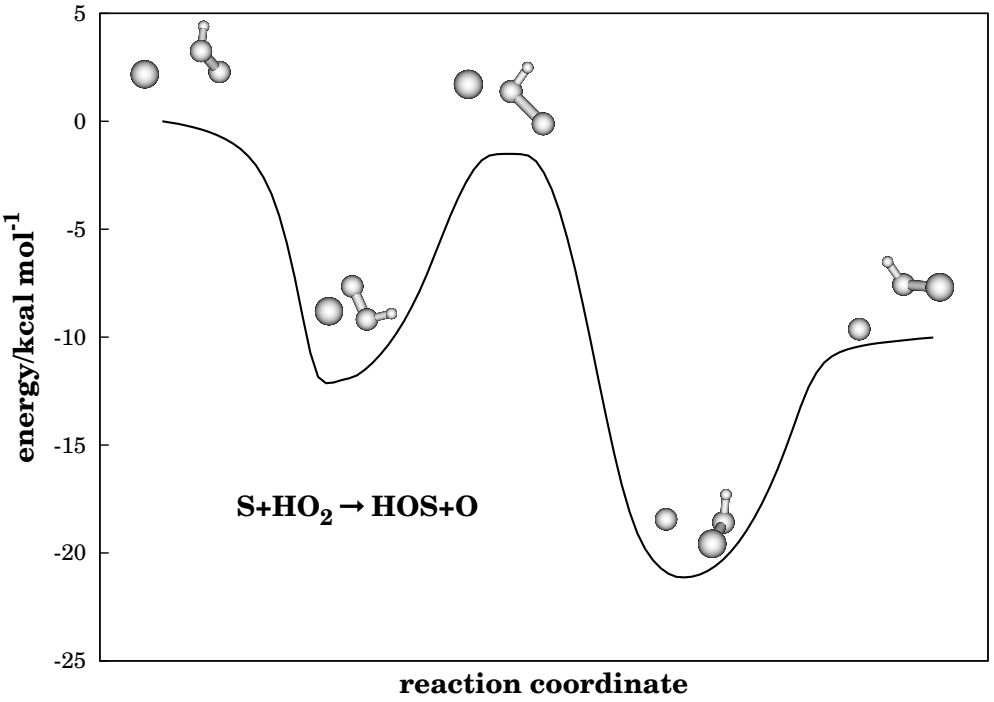

Figure 2. Minimum energy path for the reaction $S + HO_2 \rightarrow HOS + O$ according to the potential energy surface used in this work.

Figures 1 and 2 also show a common four-body intermediate structure, $HOO \cdots S$. The relative large well depth of this adduct (12.2 kcal mol^{-1}) is directly linked to the two attractive SO interactions (5.1 and 7.1 kcal mol^{-1}), since the repulsive three-body contributions involving the sulfur atom, as well as four-body ones, are irrelevant for such an arrangement. Although such a species could in principle be isolated, coming from $S + HO_2$ yields an extra energy of 5.6 kcal mol^{-1} that must be removed from the moiety such as to allow stabilization and avoid decaying into other species. To our knowledge, no evidence has yet been reported about its existence.

3 Computational procedures

To run the trajectories we have utilized an adapted version of the VENUS [10] code which accommodates the HSO_2 DMBE potential energy surface [8]. The step size used for the numerical integrations was 2.5×10^{-16} s, warranting a

conservation of the total energy to better than 2 parts in 10^4. Two types of calculations have been carried out. First, we have run trajectories for fixed ro-vibrational combinations of the reactants (HO_2) such as to provide a detailed understanding of the reaction mechanism. Then, thermalized calculations have been performed to directly assert the rate constant.

The calculations for specific ro-vibrational states have been carried out for translational energies over the range $0.2 \leq E_{\rm tr}/{\rm kcal\ mol}^{-1} \leq 10.0$, with the hydroperoxyl radical kept in its ground vibrational state [11] ($v_1 = 0, v_2 = 0, v_3 = 0$), and the rotational energy for each principal axis fixed at $RT/2$ with $T = 300$ K. Following the usual practice, batches of 100 trajectories per collisional energy have been run to determine the maximum impact parameter (b_{max}) that leads to reaction. For a given translational energy, reactive cross section were then calculated from $\sigma_r = \pi b_{\rm max}^2 P_r$ and the associated 68 % uncertainties from $\Delta\sigma_r = \sigma_r[(N_T - N_r)/(N_T N_r)]^{\frac{1}{2}}$, where N_r is the number of reactive trajectories in a total of N_T, $P_r = N_r/N_T$ is the reactive probability, and b_{max} the maximum impact parameter.

From the reactive cross section assuming a Maxwell-Boltzmann's distribution over the translational energy ($E_{\rm tr}$), the specific thermal rate coefficient is obtained as

$$k(T) = g_e(T) \left(\frac{2}{k_{\rm B}T}\right)^{3/2} \left(\frac{1}{\pi\mu}\right)^{1/2} \int_0^\infty E_{\rm tr}\sigma(E_{\rm tr}) \exp\left(-\frac{E_{\rm tr}}{k_{\rm B}T}\right) dE_{\rm tr} \qquad (2)$$

where T is the temperature, $k_{\rm B}$ is the Boltzmann constant, μ the reactants reduced mass, and

$$g_e(T) = 1/\left[5 + 3\exp(-570/T) + \exp(-825/T)\right] \qquad (3)$$

accounts in the usual way [12, 13] for the electronic degeneracies of the reactants [$S(^3P) + HO_2(^2A'')$] and the fact that DMBE potential energy surface refers to a doublet. The atomic levels of sulfur have been taken from the NIST database [14].

We now address the problem of ZPE leakage, which is well known in QCT theory. Both 'active' and 'non-active' methods have been suggested (Ref. 15, and references therein) to account for it in an approximate manner. In the non-active methods such as the one [16] here utilized, trajectories leading to aphysical products (with vibrational/internal energies below a given threshold) are thrown out

and eventually replaced [17] by running novel trajectories. The perturbed statistics may then be corrected *a posteriori* [18]. Thus, no trajectory calculations, besides those run in the traditional QCT method are required. Specifically, in VEQMT$_{\rm C}$ [16] we consider as physical only the outcomes where the total vibrational energy is larger than the sum of their ZPEs [16], an approach that has also been employed in previous work [4]. Clearly, VEQMT$_{\rm C}$ [16] and other similar methods (including active ones [15], where a constraint is introduced to prevent the trajectories from entering the region of phase space which allows vibrational modes to have less than its ZPE) will not be free from ambiguity, an issue that will not be addressed any further in the present work. Suffice it to say that accounting for ZPE tends to enhance reactivity for the title reaction (see later).
The second series of calculations refers to thermalized ones. The collisional energy is then selected from a Maxwell-Boltzmann distribution by using the cumulative function:

$$G(E_{\rm tr}) = \left(\frac{1}{k_{\rm B}T}\right)^2 \int_0^{E_{\rm tr}} E'_{\rm tr} \exp(-E'_{\rm tr}/k_B T) dE'_{\rm tr} \tag{4}$$

where $E_{\rm tr}$ is chosen randomly for each trajectory by solving the equation $G(E_{\rm tr})-\xi = 0$, where ξ $(0 \leq \xi \leq 1)$ is a random number. In turn, as in Ref. 5, the vibrational quantum numbers $v = v_1, v_2, v_3$ of the HO_2 were sampled by using the cumulative distribution function

$$C(E_v) = \sum_{n=0}^{v} P(n) \tag{5}$$

where $P(n)$ has been chosen to be the Boltzmann distribution. With the dependence of the vibrational energy (E_v) on the quantum number of HO_2 being reported elsewhere [19], the specification of the initial internal energy is completed by specifying a standard thermal distribution for the rotational energy [10] (for this, we considered the reactants triatom as a symmetric top). After optimizing the maximum impact parameter as described above, the thermalized rate constant is calculated from

$$k(T) = g_e(T) \left(\frac{8k_{\rm B}T}{\pi\mu}\right)^{1/2} \pi b_{max}^2 \frac{N_r}{N_T} \tag{6}$$

where all symbols have the meaning assigned in preceding paragraphs. Similarly, the associated uncertainty has been calculated using an analogue of the

expression used above for the cross section. For production, batches of 5000 trajectories were judged sufficient for the thermalized calculations (at $T = 300$, 1000 and 1500 K), while batches of 2000 trajectories were run at each translational energy for specific calculations.

The procedure used to assign the reaction products is the same as in previous studies [20]. Although there are 14 possible channels in an atom+triatom collisional process (the various isomers of a given species are assumed indistinguishable), we note that according to the energetics of the potential energy surface [8] there is no direct connection between the reactants and the HSO + O channel. This issue has been checked in detail by running two batches of 100 trajectories for specific calculations at translational energies of 0.2 and 10.0 kcal mol^{-1}. In both cases, formation of HSO has not been observed, with HOS being formed instead. Note that HOS refers to a structure with a central oxygen atom bonded to sulfur and hydrogen. This isomer differs therefore from HSO in that the central atom in the latter is sulfur: such a structure corresponds to the global minimum [21], with an energy difference of 0.9 kcal mol^{-1} separating those two species. Accordingly, we have modified the assignment of channels 5 and 6 used in our previous work [4] such as to identify the corresponding HOS + O ones.

4 Results and discussion

Table 1 collects the results of the specific calculations, both of pure QCT and VEQMT$_C$ types. All symbols have the meaning assigned above, with N_T indicating the total number of trajectories run in each method, and $N_r = \sum_x N_r^x$ the total number of reactive ones. Headings of other columns specify the number of reactive trajectories for the corresponding x products. As seen, the OH and SO products are by far the most formed ones, followed by HOS and O in a 5:1 ratio. For completeness, we show also SO_2 formation, even if being an almost negligible process.

The results for thermalized calculations are similarly presented in Table 2. There, the total number of trajectories for QCT is reported to recall that some of the

Table 1. Results of specific trajectories calculations for[a)] $S + HO_2$.

E_{tr}/	b_{max}/	QCT				VEQMT$_C$				
kcal mol^{-1}	Å	$\sum_x N_r^x$	$x = H + SO_2$	OH + SO	O + HOS	N_T	$\sum_x N_r^x$	$x = H + SO_2$	OH + SO	O + HOS
0.2	8.7	492	15	405	72	639	483	15	405	63
0.5	7.3	405	5	326	74	577	393	5	325	63
1.0	6.4	342	7	274	61	595	335	7	273	55
1.5	6.0	299	5	236	58	637	296	5	236	55
2.0	5.2	339	7	259	73	733	333	7	259	67
3.0	4.9	304	3	238	63	784	301	3	238	60
5.0	4.3	307	6	235	66	964	299	6	235	58
10.0	3.5	360	7	274	79	1144	355	7	274	74

[a)]The total number of trajectories in QCT is $N_T = 2000$ in for all translational energies.

5000 trajectories run did not converge, *i.e.*, have not led to any of the possible products after 4×10^5 iterations. This has also occurred in previous work [4], when some of the trajectories were captured into the deep well associated to the HOSO species and persisted there until a pre-specified maximum number of iterations were reached.

When the VEQMT$_C$ criterion is utilized, a considerable number of non-reactive trajectories is disregarded, leading to an increase of the reactive probability with respect to QCT. This may be explained as due to the relatively high value of the ZPE in HO_2. In fact, during the collisional process, the vibrational energy of the HO_2 is partially transferred to translation of the system and therefore many of the non-reactive HO_2 molecules will be left behind with a vibrational energy below its starting ZPE value.

The ro-vibrational distributions of the OH and SO products are shown in Figure 3. The left and central panels refer to the results of specific calculations for translational energies of $E_{\rm tr} = 0.2$ and $E_{\rm tr} = 10.0$ kcal mol^{-1}. In turn, the right-hand-side panels show the results obtained for the thermalized calculations at $T = 300$ K. Note that the bottom plots refer to rotational distributions, while the upper ones are for the vibrational populations. The notable feature from this Figure is, perhaps, the fact that a high rotational energy content is deposited in the newly formed SO. This has been rationalized from a detailed study of the atomic rearrangements along reactive trajectories. To produce OH and SO, we first observe that the sulfur atom attacks the terminal oxygen atom in HO_2. Once the sulfur atoms gets attached to the oxygen one, they start to describe a rotation-like motion around the axis defined by the OH bond. Such a process corresponds to falling into the minimum of the energy path illustrated in Figure 1. As the SO bond gets shorter and the two oxygen atoms get separated, the sulfur atom maintains this revolving motion with the SO pair separating away with a relatively high content of rotational excitation. Meanwhile, the OH bond remains almost as a spectator, keeping its ro-vibrational distribution as originally was in HO_2. Similar results have been observed for the reaction $O + HO_2$ when O_2 is formed [22] with a high rotational temperature.

Table 2. Results of thermalized calculations for the title reaction.

T/	$b_{\max}$/	QCT					VEQMT$_{\mathrm{C}}$				
K	Å	N_{T}	$\sum_x N_{\mathrm{r}}^x$	$x=\mathrm{H}+\mathrm{SO}_2$	OH + SO	O + HOS	N_{T}	$\sum_x N_{\mathrm{r}}^x$	$x=\mathrm{H}+\mathrm{SO}_2$	OH + SO	O + HOS
300	8.0	5000	953	18	785	160	2536	952	18	784	150
900	7.8	4999	627	9	507	111	3369	622	9	507	106
1500	7.5	4996	628	21	493	91	4001	624	21	492	88

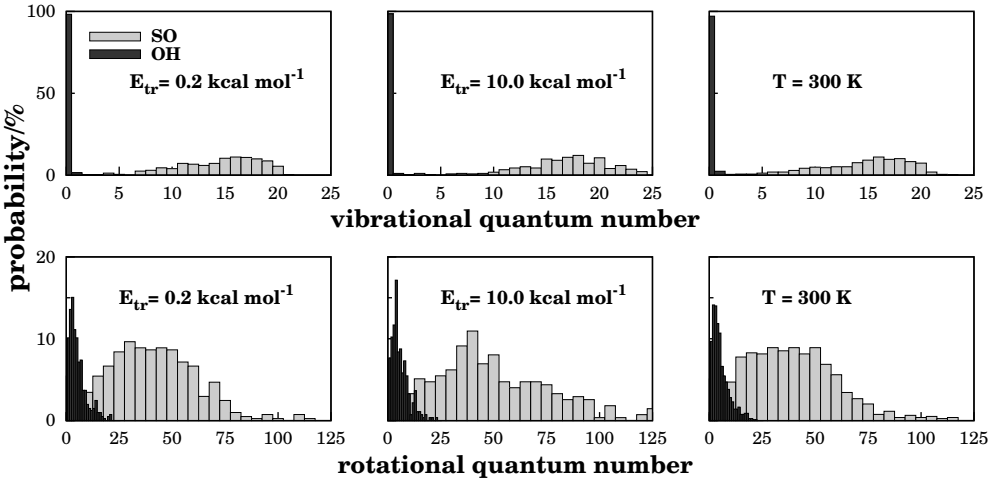

Figure 3. Ro-vibrational distributions of the OH and SO products. Left and central panels show quantum number populations for specific calculations at $E_{\rm tr} = 0.2$ and 10 kcal mol^{-1}, respectively. Panels on right-hand-side stand for thermalized calculations at $T = 300$ K.

For the thermalized calculations at $T = 1500$ K, part of the vibrational energy is initially deposited into the OH vibrational mode, with this bond showing no longer a spectator behavior. As a result, the HS + O_2 channel opens: 6 trajectories in a total of 4996. Such a process occurs via an isomerization of HOO into H $\cdots$ OO (see Table 5 of Ref. 8) and continues with the capture of the quasi-free hydrogen atom by the sulfur one. As expected from this analysis, the H + S + O_2 products are also obtained under such conditions, with almost three times more occurrences (17 trajectories) than the diatom-diatom process referred to above. Of course, both processes are statistically negligible when compared with formation of OH + SO (493 trajectories).

Figure 4 shows the predicted excitation functions for the specific calculations. Total reactive and OH + SO formation cross sections are displayed. In turn, the insert shows the corresponding reactive cross section for H + SO_2 formation. As already noted in previous paragraphs, the QCT results are smaller than the VEQMT$_{\rm C}$ ones, as the latter lead to a higher reactivity. According to the above results and the shape of the potential energy surface (a representative view is the minimum energy paths shown in Figures 1 and 2, the title reaction is largely controlled by long-range interactions, mainly associated to the permanent electric

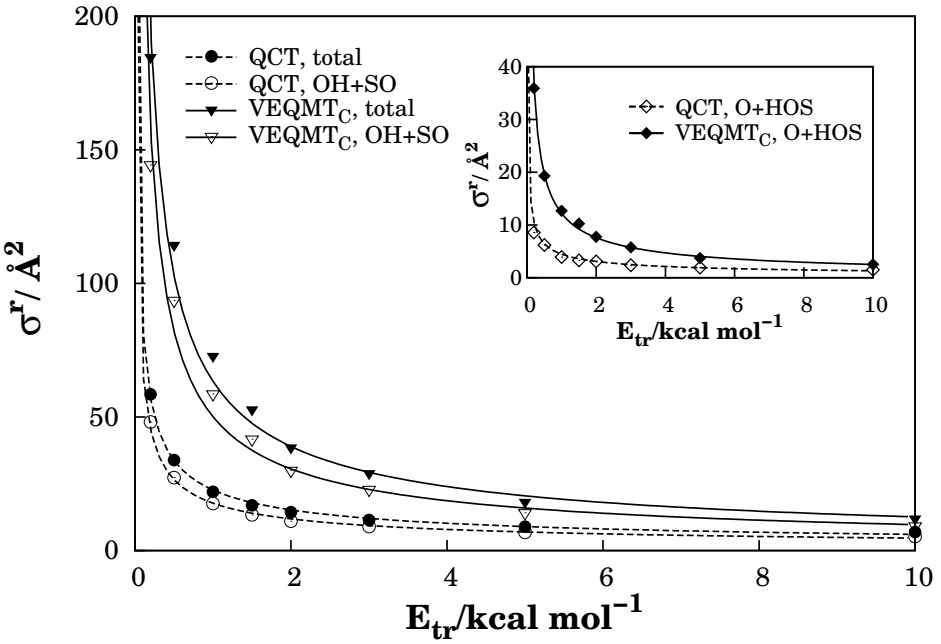

Figure 4. Reactive QCT and VEQMT$_C$ cross sections (total and OH + SO formation) for the title reaction. Also shown in the insert is the cross section for HOS + O formation.

quadrupole of sulfur and the multipoles of HO_2. Thus, the total reactive cross section and corresponding results for specific channel may be approximated by means of the capture cross section [23]

$$\sigma(E_{\rm tr}) = n\pi(n-2)^{(2-n)/n}\left(\frac{C_n}{2E_{\rm tr}}\right)^{2/n} \tag{7}$$

where C_n and n are coefficients to be fitted. The calculated values are shown in Figure 4, with the lines indicating the best fits obtained using Eq. (7). For QCT, $n = 3.432$ and $C_n = 6.083$, while $n = 2.805$ and $\mathrm{C_n} = 20.977$ for the VEQMT$_C$ results. Note that the dominant long-range energies arise from the permanent electric quadrupole moment of the S atom and the electric permanent dipole and quadrupole moments of HO_2. Thus, one would formally expect a $V \sim R^{-n}$ dependence. However, due to dispersion (from two- and three-body terms) as well as other attractive forces of short-range type, such a dependence turns out to be somewhat stronger as indicated above.

By substituting Eq. (7) in Eq. (2) and performing the integration, one gets

the following analytical expression for the specific rate constant as a function of temperature:

$$k(T) = 2n\pi g_e(T)(n-2)^{\frac{2-n}{n}} \left(\frac{2}{\pi\mu}\right)^{\frac{1}{2}} \left(\frac{C_n}{2}\right)^{\frac{2}{n}} \Gamma\left(\frac{2n-2}{n}\right) (k_B T)^{(n-4)/2n} \qquad (8)$$

where $\Gamma(\ldots)$ is the gamma function. Since OH + SO have already been identified to be the main products, only the rate constants accounting for its formation will be presented. In fact, other products have rate constants a few orders of magnitude smaller ($k^{\text{others}} \ll k^{\text{OH+SO}}$), with the total rate coefficient differing therefore very little from the one for OH + SO formation. Figure 5 shows the specific QCT and VEQMT$_C$ rate constants calculated in the present work. As expected from the corresponding cross sections in Figure 4, the VEQMT$_C$ curves lie above the QCT ones. The interval defined by the former curves is light shadowed, with the expected value of $k(T)$ resulting from them being expected to lie somewhere between the upper and lower limits so defined. The dark shadowed region identifies the corresponding results for the thermalized calculations, according to Eq. (6) and Table 2.

Circles and squares denote the actually calculated values, while solid line stands for the QCT results as fitted to the Arrhenius-type form $k(T) = AT^n \exp(-mT)$, and the dashed line to the corresponding fit for the VEQMT$_C$ results. Note that the temperature dependence is similar for both calculations. However, the thermalized rate constants are in average five times larger than the specific ones, with the discrepancy becoming more significant as the temperature rises. As noted above, this is due to the inclusion of vibrational excitation on the thermalized reactants, thus leading to an increase in reactivity. Because the rotational and vibrational energy of the reactants is properly sampled according to the temperature in the thermalized calculations, our recommended values lie inside the darker region.

Finally, we note that the rate constant obtained in this work for the reaction $S + HO_2 \rightarrow OH + O_2$ is $k(T) = 9.4 \times 10^{-11}$ cm^3 s^{-1} at $T = 300$ K, a value quite similar to the one reported [22] for the reaction $O + HO_2 \rightarrow OH + SO$, namely $k(T) = 7\text{–}8 \times 10^{-11}$ cm^3 s^{-1} at the same temperature. More specifically, our recommended value expressed in Arrhenius form lies between $k(T) = 41.47 T^{0.336} e^{(245.2/T)} \times 10^{-13}$ cm^{3}s^{-1} and $k(T) = 1045.85 T^{-0.069} e^{(172.1/T)} \times 10^{-13}$ cm^{3}s^{-1}, with T in kelvin.

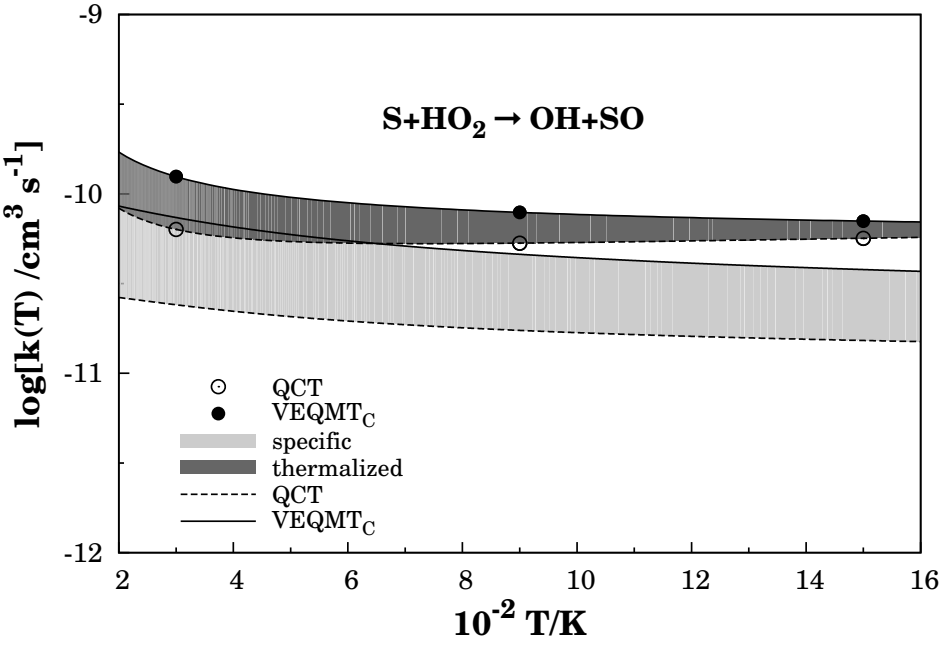

Figure 5. Rate constants for the $S + HO_2 \rightarrow OH + SO$ reaction. The light shaded region corresponds to specific ro-vibrational states of the reactants while dark shaded area represents the thermalized results. The dashed lines refer to the pure QCT results while the solid ones refer to the $VEQMT_C$ ones. For the thermalized results, the lines indicate Arrhenius-like functions fitted to rate coefficients obtained by QCT and $VEQMT_C$, whose actually calculated values are indicated by open circles and solid dots, respectively.

The above agreement should not be surprising as $O + HO_2$ and $S + HO_2$ have similar bonding characteristics, with a minimum energy path controlled by long range forces. Indeed, both reaction rate coefficients show a similar dependence on temperature.

5 Conclusions

The $S + HO_2$ reaction has been studied using two variants of the QCT method. To the best of our knowledge, this is the first study of the dynamics and kinetics of such a reaction. The process has been shown to be dominated by long range forces, thus manifesting a capture-type behavior. $OH + SO$ has been predicted to be the most formed products channel, although SO_2 and HOS were also formed but with significantly smaller occurrences. Formation of HSO has not been observed. When ZPE leakage is accounted for by the $VEQMT_C$ method, reactivity is favored leading to reactive rate constants larger than in the pure QCT calculations. Calculations using both reactants prepared in specific ro-vibrational states and thermalized ones have been carried out, with larger values of the rate constant predicted for the latter. This is attributed to the fact that vibrationally excited reactants are allowed to occur when preparing the reactants initial states. In both calculations, the formed SO is predicted to be vibrationally hot, similarly to what has been observed [22] for the reaction $O + HO_2 \rightarrow OH + O_2$. The calculated rate coefficient is predicted to assume a nearly constant value of $k(T) = 9.4 \times 10^{-11}$ cm^3 s^{-1} for temperatures in the range of $T = 200 - 1600$ K.

Acknowledgment

M.Y.B. thanks the Centro de Estudios Ambientales de Cienfuegos, Cuba, for leave of absence during his PhD studies. This work has the support of Fundação para a Ciência e a Tecnologia, Portugal, under POCI 2010 of Quadro Comunitário de Apoio III co-financed by FEDER.

References

[1] R. P. Wayne, *Chemistry of Atmospheres* (Oxford University Press, 2002).

[2] I. Yamamura, K. Kawaguchi, and S. T. Ridgway, Astrophys. J. **528**, L33 (2000).

[3] M. U. Alzueta, R. Bilbao, and P. Glarborg, Combust. Flame **127**, 2234 (2001).

[4] M. Y. Ballester and A. J. C. Varandas, Chem. Phys. Lett. **433**, 279 (2007).

[5] M. Y. Ballester, P. J. S. B. Caridade, and A. J. C. Varandas, Chem. Phys. Lett. **439**, 301 (2007).

[6] A. J. C. Varandas, Adv. Chem. Phys. **74**, 255 (1988).

[7] A. J. C. Varandas, *Conical Intersections: Electronic Structure, Spectroscopy and Dynamics* (World Scientific Publishing, 2004), chap. 5, p. 91, Advanced Series in Physical Chemistry.

[8] M. Y. Ballester and A. J. C. Varandas, Phys. Chem. Chem. Phys. **7**, 2305 (2005).

[9] C. Heinemann, W. Koch, G. G. Lindner and D. Reinen, Phys. Rev. A. **52**, 1024 (1995).

[10] W. L. Hase, R. J. Duchovic, X. Hu, A. Komornicki, K. F. Lim, D. Lu, G. H. Peslherbe, K. N. Swamy, S. R. V. Linde, A. J. C. Varandas, H. Wang, and R. J. Wolf, QCPE Bull. **16**, 43 (1996).

[11] A. J. C. Varandas, J. Brandão, and M. R. Pastrana, J. Chem. Phys. **96**, 5137 (1992).

[12] D. G. Truhlar, J. Chem. Phys. **56**, 3189 (1972).

[13] J. T. Muckerman and M. D. Newton, J. Chem. Phys. **56**, 3191 (1972).

[14] NIST Chemistry WebBook **69**, http://webbook.nist.gov/chemistry (2003).

[15] A. J. C. Varandas, Int. Rev. Phys. Chem. **19**, 199 (2000).

[16] A. J. C. Varandas and L. Zhang, Chem. Phys. Lett. **340**, 62 (2001).

[17] A. J. C. Varandas, J. Chem. Phys. **99**, 1076 (1993).

[18] A. J. C. Varandas, Chem. Phys. Lett. **225**, 18 (1994).

[19] D. H. Zhang and J. Z. H. Zhang, J. Chem. Phys. **101**, 3671 (1994).

[20] A. J. C. Varandas, A. A. C. C. Pais, J. M. C. Marques, and W. Wang, Chem. Phys. Lett. **249**, 264 (1996).

[21] E. Martínez-Núñez and A. J. C. Varandas, J. Phys. Chem. A **105**, 5923 (2001).

[22] D. M. Silveira, P. J. S. B. Caridade, and A. J. C. Varandas, J. Phys. Chem. A **108**, 8721 (2004).

[23] A. J. C. Varandas, in *Conferencias Plenarias de la XXIII Reunión Bienal de Química*, edited by A. S. Feliciano, M. Grande, and J. Casado, Universidad de Salamanca (1991), p. 321.

Final remarks

In this thesis a theoretical study on the HSO_2 molecular system was carried out. The first global single-valued potential energy surface for the ground electronic state of this radical was built an characterized in detail. Double many-body expansion (DMBE) has been used for this achievement. The properties obtained for minimum and transition state configurations agree with those reported in literature. Apart from this, this surface provides new insights in the topology of the interaction potential for the title four-body system.

Quasiclassical dynamical studies employing the six dimensional function constructed here, were also carried out. Three bi-molecular collisions, with relevance in atmospheric and combustion chemistry, have been examined in detail, yielding information on reaction mechanisms, cross sections, rate coefficients and product properties. There is a general agreement between the rate constants reported here and the available experimental data. Predictions have also been made for a reaction not studied before. The results obtained in this thesis can be used in models of the atmospheric sulfur cycle.

The new potential energy surface gives a good description of the HSO_2 molecular system. It can be further used to study other reactive processes and the possible effects of the ro-vibrational energies of the reactants. Finally it may enable the construction of larger polyatomic DMBE potential energy surfaces in which HSO_2 is contained, most importantly that of HSO_3 which would be used in modeling the reaction $HS + O_3$ with large interest in atmospheric chemistry.

Mathematical appendices

A Changing distances to bond coordinates

The potential energy surface of the title system is a function of the six distances between the four atoms $\{\mathrm{R_i}\}$, $\mathrm{i} = \overline{1,6}$. Numbering the atoms 1-4, the distances are labeled in the usual form: R_1 is the distance 1-2, R_2 the distance 1-3, R_3 1-4, R_4 2-3, R_5 2-4 and R_6 3-4 . However, in the PES reported in this thesis, we include four body energy terms which depends on the valence bond coordinates $\{r_j, \alpha, \beta, \gamma\}$. Thus a transformation from distances to bond coordinates is needed. This transformation must not contain singularities.

Firstly Cartesian coordinates $\{X_{ij}\}$ of the four atoms were calculated as a function of the $\{R_i\}$, in X_{ij} the i-index labels the atom, while $j = 1, 2, 3$ represents the Cartesian component. Then, bond coordinates $\{r_j, \alpha, \beta, \gamma\}$ are represented by means of the X_{ij} according to the given bonding connections. Cartesian coordinates were calculated as follows: the first atom (1) is placed at the origin, the second (2) is placed along the x axis, the third (3) is placed in the xy plane, the position of the remaining one will be uniquely determined by the distances to the previous three. Figure 1 illustrates this process; then, Cartesian coordinates are given by:

$$X_{11} = 0,\ X_{12} = 0,\ X_{13} = 0 \tag{A 1}$$

$$X_{21} = R_1,\ X_{22} = 0,\ X_{23} = 0 \tag{A 2}$$

$$X_{31} = R_2 \cos\rho,\ X_{32} = R_2 \sin\rho,\ X_{33} = 0 \tag{A 3}$$

$$X_{41} = \frac{R_3^2 - R_5^2 + R_1^2}{2R_1} \tag{A 4}$$

$$X_{42} = \frac{R_3^2 + R_2^2 - R_6^2 - 2X_{41}X_{31}}{2X_{32}} \tag{A 5}$$

$$X_{43} = \sqrt{R_3^2 - X_{41} - X_{42}} \tag{A 6}$$

being

$$\cos\rho = \frac{R_1^2 + R_2^2 - R_4^2}{2R_1R_2} \text{ and } \sin\rho = \sqrt{1 - \cos^2\rho} \tag{A 7}$$

We call bonding connectivity to the way atoms are connected one to each other, hence bonding coordinates for a given connectivity $\mathrm{I_1}$-$\mathrm{I_2}$-$\mathrm{I_3}$-$\mathrm{I_4}$ ($\mathrm{I}_k = \overline{1,4}\ \mathrm{I_i} \neq \mathrm{I_j}$ for

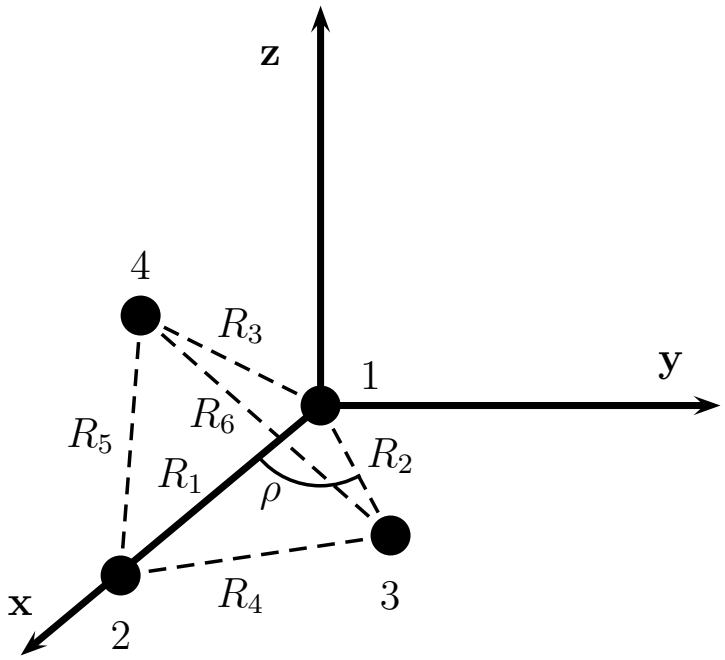

Figure 1. A simple way to calculate Cartesian coordinates as a function of distances

j $\neq$ i) are r_1=distance I_1-I_2, r_2=distance I_2-I_3, r_3=distance I_3-I_4, α=ang $I_1I_2I_3$, β=ang $I_2I_3I_4$ and γ=dihedral angle between planes $I_1I_2I_3$ and $I_2I_3I_4$. It may be illustrated by means of the Z-matrix:

$$
\begin{array}{lllllll}
\text{Zmat}= & \{\mathrm{I}_1; & & & & & \\
 & \mathrm{I}_2, & \mathrm{I}_1, & r_1; & & & \\
 & \mathrm{I}_3, & \mathrm{I}_2, & r_2, & \mathrm{I}_1, & \alpha; & \\
 & \mathrm{I}_4, & \mathrm{I}_3, & r_3, & \mathrm{I}_2, & \beta, & \mathrm{I}_1, \quad \gamma\}
\end{array}
$$

We consider a maximum of two connections per atom, which is the case we are interested in. The resulting valence bond coordinates will depend on such connectivity order. Let us represent the position vector of the i^{th} atom with $\overrightarrow{\mathcal{R}_i}$, $\overrightarrow{\mathcal{R}_i} = (\mathrm{X_{i1}}, \mathrm{X_{i2}}, \mathrm{X_{i3}})$; then, the valence bond coordinates can be calculated as follow:

$$r_1 = \sqrt{(\overrightarrow{\mathcal{R}_{I_1}} - \overrightarrow{\mathcal{R}_{I_2}}) \cdot (\overrightarrow{\mathcal{R}_{I_1}} - \overrightarrow{\mathcal{R}_{I_2}})} \qquad \text{(A 8)}$$

$$r_2 = \sqrt{(\overrightarrow{\mathcal{R}_{I_2}} - \overrightarrow{\mathcal{R}_{I_3}}) \cdot (\overrightarrow{\mathcal{R}_{I_2}} - \overrightarrow{\mathcal{R}_{I_3}})} \qquad \text{(A 9)}$$

$$r_2 = \sqrt{(\overrightarrow{\mathcal{R}_{I_3}} - \overrightarrow{\mathcal{R}_{I_4}}) \cdot (\overrightarrow{\mathcal{R}_{I_3}} - \overrightarrow{\mathcal{R}_{I_4}})} \tag{A 10}$$

and the angles:

$$\cos\alpha = \frac{(\overrightarrow{\mathcal{R}_{I_1}} - \overrightarrow{\mathcal{R}_{I_2}}) \cdot (\overrightarrow{\mathcal{R}_{I_3}} - \overrightarrow{\mathcal{R}_{I_2}})}{r_1 r_2} \tag{A 11}$$

$$\cos\beta = \frac{(\overrightarrow{\mathcal{R}'_2} - \overrightarrow{\mathcal{R}'_3}) \cdot (\overrightarrow{\mathcal{R}'_4} - \overrightarrow{\mathcal{R}'_3})}{r_2 r_3} \tag{A 12}$$

for the dihedral angle we first define two auxiliary vectors:

$$\overrightarrow{a_1} \equiv (\overrightarrow{\mathcal{R}_{I_1}} - \overrightarrow{\mathcal{R}_{I_2}}) \times (\overrightarrow{\mathcal{R}_{I_3}} - \overrightarrow{\mathcal{R}_{I_2}}) \tag{A 13}$$

and

$$\overrightarrow{a_2} \equiv (\overrightarrow{\mathcal{R}_{I_2}} - \overrightarrow{\mathcal{R}_{I_3}}) \times (\overrightarrow{\mathcal{R}_{I_4}} - \overrightarrow{\mathcal{R}_{I_3}}) \tag{A 14}$$

then

$$\cos\gamma = \frac{\overrightarrow{a_1} \cdot \overrightarrow{a_2}}{\mid \overrightarrow{a_1} \mid\mid \overrightarrow{a_2} \mid} \tag{A 15}$$

The above procedure is implemented in the HSO_2 potential energy surface code with some corrections to avoid numerical indeterminations.

B Changing bond coordinates to distances

Ab initio calculations carried in this thesis uses Z-matrix geometry representation, hence, bond coordinates were used. However in fitting process we need interatomic distances, thus a transformation from bond coordinates $\{r_j, \alpha, \beta, \gamma\}$ to distances $\{\mathrm{R_i}\}$ is needed. As in the previous appendix cartesian coordinates $\{X_{\mathrm{ij}}\}$ are used as intermediary set.

With a given bonding connectivity order $\mathrm{I_1I_2I_3I_4}$, the procedure is as follow: The atom $\mathrm{I_2}$ is placed in the origin, the atom $\mathrm{I_3}$ along the x axis, the $\mathrm{I_4}$ in the xy plane, while the $\mathrm{I_1}$ atom has a well defined cartesian coordinates as a function of the remaining three. Thus cartesian coordinates can be written:

$$X_{I_1 1} = r_1 \cos\alpha \tag{B 1}$$

$$X_{I_1 2} = r_1 \sin\alpha \cos\gamma \tag{B 2}$$

$$X_{I_1 3} = -r_1 \sin\alpha \sin\gamma \tag{B 3}$$

$$X_{I_2 1} = X_{I_2 2} = X_{I_2 3} = 0 \tag{B 4}$$

$$X_{I_3 1} = r_2 \tag{B 5}$$

$$X_{I_3 2} = X_{I_3 3} = X_{I_4 3} = 0 \tag{B 6}$$

$$X_{I_4 1} = r_2 - r_3 \cos\beta \tag{B 7}$$

$$X_{I_4 2} = r_3 \sin\beta \tag{B 8}$$

Once cartesian coordinates are obtained distances can be calculated according to the definition given in the previous appendix for $\{\mathrm{R_i}\}$.

C Gamma Function

The **Gamma function** is defined[2] by the integral

$$\Gamma(z) \equiv \int_0^\infty t^{z-1} e^{-t} dt \tag{C 1}$$

When the argument z is an integer, the Gamma function can be written in the form of a factorial function:

$$\Gamma(n+1) = n! \tag{C 2}$$

Gamma function satisfies recurrence relation:

$$\Gamma(z+1) = z\Gamma(z) \tag{C 3}$$

The natural logarithm of the Gamma function is implemented in the *gammln* function from Numerical recipes.
The **Incomplete Gamma Function**is defined by:

$$P(a,x) \equiv \frac{\gamma(a,x)}{\Gamma(a)} \equiv \frac{1}{\Gamma(a)} \int_0^x t^{a-1} e^{-t} dt, \ (a > 0) \tag{C 4}$$

It has the limiting values

$$P(a,0) = 0 \quad \text{and} \quad P(a,\infty) = 1 \tag{C 5}$$

The complement $Q(a,x)$ is:

$$Q(a,x) \equiv 1 - P(a,x) \equiv \frac{1}{\Gamma(a)} \int_x^\infty t^{a-1} e^{-t} dt, \ (a > 0) \tag{C 6}$$

Functions *gammp* and *gammq* from Numerical recipes provides P and Q functions respectively.

[2]All definitions and properties from "Numerical Recipes in Fortran '77"